The role of the exocyst member EXOC8 in the formation of cytoplasmic rods and rings

Submitted by Bethany Kerenza Dean to the University of Exeter

as a thesis for the degree of

Masters by Research in Biological Sciences

In September 2020

I certify that all material in this thesis which is not my own work has been identified and that no material has previously been submitted and approved for the award of a degree by this or any other University.

Signature: ……Bethany Dean……

Abstract

Inosine monophosphate dehydrogenase (IMPDH) and cytidine triphosphate synthase (CTPS) are two rate-limiting enzymes involved in the catalysis of GTP and CTP. In humans, these enzymes can form into filamentous structures termed cytoplasmic rods and rings. Although cytoplasmic rods and rings have been described in multiple cell types, neither their formation nor their composition are well understood. Here we identify a novel localisation for the exocyst complex subunit EXOC8 to cytoplasmic rod/ring structures. Upon closer inspection, these structures resemble beads on a string, similar to the structure of IMPDH2-containing cytoplasmic rods and rings previously observed by cryo-EM. We found that EXOC8 interacts physically with IMPDH2 and CTPS1. Although it is not required to form IMPDH2-containing rods and rings in non-stressed cells, when these structures are induced by changes to metabolic conditions, rod length and organisation is altered in the absence of EXOC8. Mutations in the closely related enzyme IMPDH1 are a cause of inherited retinal degeneration, and mutation in EXOC8 is a candidate for pleiotropic syndromes where retinal dystrophy is part of the clinical presentation. We found that rod and ring localisation was lost in a disease-linked EXOC8 variant, and interaction with IMPDH2 was lost. This is the first time that an exocyst subunit - and indeed any membrane trafficking complex - has been linked to cytoplasmic rods and rings. We propose that the exocyst plays a role in trafficking proteins required for IMPDH2 rod and ring maturation and/or turnover, thereby regulating cyclic nucleotide metabolism, and that dysregulation may contribute to the molecular pathology of retinal degeneration and phototransduction.

Acknowledgements

I would like to thank Dr Helen Dawe and Dr Joe Costello for being brilliant supervisors and constantly giving me support and guidance. A special mention must also go to Dr Isabelle Jourdain, for her encouragement and kind words.

Next, I would like to thank Lauren Adams and Connor Horton for all their continued help and advice. Thank you for continually listening to me talk about rods and rings. I could not have been welcomed into a better lab, and it has been a brilliant three years working alongside you both.

A big thank you must go to Dr Kate Heesom (University of Bristol, Proteomics Facility) for conducting the mass spectrometry on the GFP-Trap and to Tina Schrader for providing the cell lines used in this thesis.

I would also like to express my gratitude to the cytoplasmic rod and ring community. Thank you for welcoming me in. A special thank you must go to John Calise, whom I met at ASCB and who kindly suggested experiments for this thesis.

I would also like to like to thank Sharon Turner, Emma Doyle and Tilly Dixon for all their guidance in the lab and for forever answering my questions. Thank you for making sure the lab runs so smoothly.

To the people in Lab 211, past and present. Thank you for making Lab 211 such an enjoyable place to work. In particular I would like to thank, Lucy Witherall, Rachael Murray, Tilly Dixon, Shayma Al-Athari, Alexa Bishop and Andy Early. It has been a pleasure to get to know you all during my time in the lab. I will miss you all.

And lastly, this thesis would not have been possible without the constant support and encouragement from my wonderful family. Thank you for getting me through this year, I could not have done it without you.

Contents

List of Figures

Chapter 1. Introduction

Chapter 2. Materials and Methods

Chapter 3. Results

List of Tables

Chapter 1. Introduction

Chapter 2. Materials and Methods

Chapter 3. Results

Abbreviations

AC	Anchor cells
ACEC	Apical Ceramide Enriched Compartment
ACK1	Activated cdc42-associated kinase 1
AICAR	5-aminoimidazole-4-carboxamide ribonucleotide
AJ	Adherens Junctions
AMPK	Adenosine Monophosphate Protein Kinase
aPKC	atypical Protein Kinase C
ARL2	ARF-like 2
BEC	Bladder epithelial cells
BMMC	Bone marrow derived mast cells
CATCHR	Complexes associated with tethering containing helical rods
CDK	Cyclin Dependent Kinase
CDK1	Cyclin Dependent Kinase 1
CorEx	Core exocyst
CTP	Cytidine Triphosphate
CTPS	Cytidine Triphosphate Synthase
DAPI	4′,6-diamidino-2-phenylindole
DHFR-PCA	Dihydrofolate reductase protein-fragment complementation assay
DMEM	Dulbecco's Modified Eagle's Medium
DNP	Dinitrophenyl
DON	diazo-5-oxo-l-norleucine
EM	Electron Microscopy
ER	Endoplasmic Reticulum
ESC	Embyronic Stem Cells
GEC	Gingival Epithelial Cells
GTP	Guanine Nucleotide Synthesis
HCV	Hepatitis C Virus
HEK	Human Embryonic Kidney cells
IFN	Interferon

IMP	Inosine Monophosphate
IMPDH	Inosine Monophosphate Dehydrogenase
IPT	Ig-like, plexins, transcription factors domain
JBTS	Joubert Syndrome
JNK	c-Jun N-terminal kinases
kDa	kilodalton
MAP2	Microtubule Associated protein 2
MDCK	Madin-Darby Canine Kidney cells
MEF	Mouse Embryonic Fibroblasts
MEM	Minimal Essential Media
mIMCD3	mouse Inner medullary collecting duct cells
MMS	Methyl Methane Sulfonate
MPA	Mycophenolic Acid
MTC	Multisubunit Tethering Complex
nm	nanometre
NRK	Normal Rat Kidney Epithelial Cells
NSF	N–ethylmaleimide sensitive factor
PAR-3/PAR-6/aPKC	Partitioning-defective and atypical protein kinase C
PBS	Phosphate Buffered Saline
PCR	Polymerase Chain Reaction
PH	Pleckstrin Homology domain
PINS	Protein Interaction Network
PIP_2	Phosphatidylinositol 4,5-bisphosphate
PIP_3	Phosphatidylinositol (3,4,5)-trisphosphate
PLA	Proximity Ligation Assay
PM	Plasma Membrane
PPI	Protein-protein interactions
Ral	Ras-Like
RBV	Ribavarin
SH3BP1	SH3 domain-binding protein 1
SM	Sec1/Munc18

SNARE	Soluble N–ethylmaleimide sensitive factor (NSF) attachment protein receptor
TJ	Tight Junctions
UTP	Uridine Triphosphate
WCE	Whole Cell Extract
XMP	Xanthosine Monophosphate

1. Introduction

1.1. The exocyst complex

1.1.1. Overview of the exocyst complex

The exocyst complex is an evolutionary conserved protein complex composed of eight different subunits: Sec3, Sec5, Sec6, Sec8, Sec10, Sec15, Exo70 and Exo84 in yeast and EXOC1, EXOC2, EXOC3, EXOC4, EXOC5, EXOC7 and EXOC8 in mammalian cells (Figure 1.1). The exocyst complex plays a central role in exocytosis (Munson and Novick, 2006; Novick et al., 1980; TerBush and Novick, 1995; TerBush et al., 1996). It tethers post-Golgi secretory vesicles to the plasma membrane (PM), to facilitate the release of cellular material into the extracellular space (Heider and Munson, 2012; Wu and Guo, 2015). However, while the best understood role of the exocyst complex is exocytosis, it is also implicated in many other functions, including but not limited to cell polarity (Polgar and Fogelgren, 2018; Synek et al., 2014), cell morphogenesis (Finger and Novick, 1997; Zhao *et al.*, 2013), and cell division (Cascone et al., 2008; Guo et al., 2013; Martín-Cuadrado et al., 2005).

1.1.2. Discovery of the exocyst complex

The exocyst complex was originally discovered during a genetic screen in the budding yeast *Saccharomyces cerevisiae*. This screen identified 23 complementation groups of yeast mutants required for secretion (Novick and Schekman, 1979; Novick et al., 1980). Subsequent research showed that these 23 genes could be divided into two groups (Novick et al., 1981). One group consisting of 13 genes encoding proteins required for trafficking proteins from the endoplasmic reticulum to the Golgi-apparatus, and one group consisting of 10 genes encoding proteins required for trafficking proteins from the Golgi-apparatus to the PM (Novick et al., 1981). The latter group, which consists of 10 genes, are required in the later stages of exocytosis and are subsequently referred to as ‘late-acting’ secretory (sec) mutants: Sec1, Sec2, Sec3, Sec4, Sec5, Sec6, Sec8, Sec9, Sec10 and Sec15.

Analysis of Sec15 in yeast gave rise to the first possibility that ‘late-acting’ secretory proteins formed a complex, as Sec15 was found to associate with both PM and a soluble high molecular weight complex (Bowser and Novick, 1991). This high molecular weight complex localised to sites of polarised exocytosis in yeast and consisted of Sec15, Sec6 and Sec8 and five unknown proteins

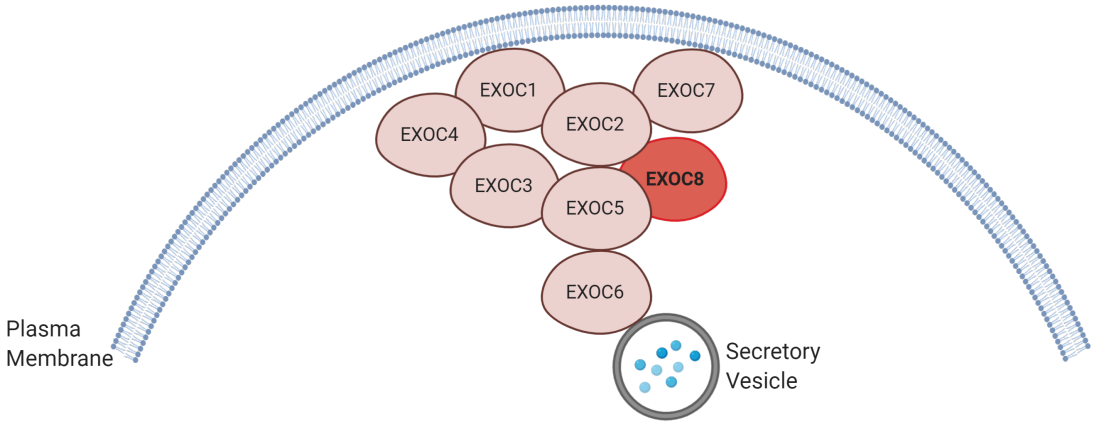

Figure 1.1. EXOC8 is a member of the octameric exocyst complex. The exocyst is an octameric protein complex that tethers post-Golgi secretory vesicles to the plasma membrane. EXOC8 is shown in red. Figure created with BioRender.com

(TerBush and Novick, 1995). The stability of such complex was disrupted in Sec3, Sec5 and Sec10 mutants, indicating that Sec3, Sec5 and, Sec10 are associated with Sec15, Sec6, and Sec8 in one large multiprotein complex (TerBush and Novick, 1995). Subsequent research confirmed that Sec3, Sec5 and Sec10 were part of this molecular weight complex along with the protein Exo70 (TerBush et al., 1996). This seven-protein complex was then termed 'the exocyst complex' because all its protein constituents are required for late stage exocytosis in yeast (TerBush et al., 1996).

Following the discovery of the exocyst complex in yeast, the search for mammalian homologues of the exocyst complex began. Using sequence analysis, Sec6 and Sec8 homologues were cloned from a rat brain cDNA library (Ting et al., 1995). Further analysis revealed that rat Sec6/Sec8 homologues were a component of a large molecular weight complex, similar to the large molecular weight complex obsereved in yeast. Purification of this Sec6/Sec8 complex in mammalian cells uncovered that it weighed 743 kilodalton (kDa) and was composed of eight proteins (Hsu et al., 1996). Cloning revealed that the mammalian exocyst complex contains yeast homologues of Sec3, Sec5, Sec10, Sec15 and Exo70 (Brymora et al., 2001; Guo et al., 1997; Hsu et al., 1996; Matern et al., 2001a). Cloning also revealed that the mammalian exocyst contained an 84 kDa protein with no yeast homologue (Hsu et al., 1996). It was not until 1999 that the yeast homologue of this 84 kDa protein was discovered and named Exo84 (Guo et al., 1999). In mammals, the yeast exocyst complex Sec3, Sec5, Sec6, Sec8 Sec10, Sec15, Exo70 and Exo84 are named EXOC1, EXOC2, EXOC3, EXOC4, EXOC5, EXOC6, EXOC7 and EXOC8 respectively. For simplicity, this report will here-on refer to the mammalian names of exocyst members.

1.1.3. Structure

Elucidating the structure and assembly of exocyst subunits is crucial to advance our understanding of the exocyst complex. However, structural studies of exocyst subunits have been hindered by preparations which result in poor yield, solubility and stability (Croteau et al., 2009; Heider et al., 2016). As a result, only the near full-length crystal structures of EXOC5 and EXOC7 have been resolved, with the near full-length crystal structure of EXOC7 being determined in three different organisms - mouse, yeast and plant (Chen et al., 2017; Dong et al., 2005; Moore

et al., 2007; Zhang et al., 2015). Partial structures of EXOC1, EXOC2, EXOC3, EXOC6 and EXOC8 have been resolved in different organisms (Table 1.1), but currently the crystal structure of EXOC4 remains unknown (Baek et al., 2010; Dong et al., 2005; Jin et al., 2005; Mott et al., 2003; Wu et al., 2005; Zhang et al., 2015).

Despite only a 10 % sequence identity between exocyst subunits, all subunits are predicted to be composed of 40-60 % α-helical repeats (Croteau et al., 2009). Crystallography of exocyst components has shown that components share characteristic helical bundle repeats that are packaged together into large rods (Munson and Novick, 2006). Recent studies have shown that exocyst members display elongated phenotypes consistent with the packing together of large rod structures (Ganesan et al., 2020). Furthermore, recent studies have shown that the exocyst complex resembles the characteristic ‘T’ or ‘Y’ shape. (Ganesan et al., 2020). Original studies showed that glutaraldehyde-fixed assembled exocyst complex resembles a uniform ‘T’ or ‘Y’ shape when observed using electron microscopy (EM) (Hsu et al., 1998). This is supported by Heider *et al.*, 2016, whose negative-stain EM of purified exocyst complexes, showed a roughly similar ‘T’ or ‘Y’ shape. However, the characteristic ‘arms’ of the ‘T’ or ‘Y’ shape were far shorter than in the EM images by Hsu *et al.*, 1998.

Given the dynamic nature of the exocyst, it is difficult to determine the shape and structure of the exocyst. Perhaps the uniform ‘T’ and ‘Y’ shapes are due to the exocyst being static at the PM, whereas the more elongated structures are due to the exocyst being unassembled. Future biochemical and structural analyses of the exocyst are needed to establish the conformation of the exocyst when both assembled and unassembled.

The structure of fully assembled exocyst complex was recently solved in *S. cerevisiae* using single-particle cryo-EM (Mei et al., 2018). This is the first time the structure of the assembled exocyst complex has been solved in a single organism, and sheds light on the formation and function of the exocyst. Cryo-EM often results in images having near-atomic resolution (Lepore et al., 2018). However, single particle cyro-EM enabled Mei *et al.*, 2018 to obtain high resolution yeast exocyst images, which showed that consistent with previous EM of negatively stained samples, the exocyst complex is ‘T’ or ‘Y’ shaped. This

Exocyst Member	**Structure Resolved**
EXOC1	N terminal domain of *S. cerevisiae* (Baek et al., 2010)
EXOC2	Ral-binding domain of *Rattus norvegicus* (Jin et al., 2005) Ral-binding domain of *Mus musculus* (Mott et al., 2003) Ral-binding domain of *Homosapiens* (Fukai et al., 2003)
EXOC3	C-terminal domain of *S. cerevisiae* (Sivaram et al., 2006)
EXOC4	Not yet resolved in any species
EXOC5	Near Full-length structure of *Danio rerio* (Chen et al., 2017)
EXOC6	C-terminal domain of *Drosophila melanogaster* (Wu et al., 2005)
EXOC7	Near Full-length structure of *S. cerevisiae* (Dong et al., 2005; Hamburger et al., 2006) Near Full-length structure of *Mus musculus* (Moore et al., 2007) Near C-terminal domain of *Arabidopsis* (Zhang et al., 2015)
EXOC8	C-terminal domain of *S. cerevisiae* (Dong et al., 2005) Ral-binding domain of *Rattus norvegicus* (Jin et al., 2005)

Table 1.1. Exocyst members and their association structural resolution. The full crystal structure of the exocyst complex has yet to be resolved. Details regarding resolved crystal structures are given for each exocyst member.

observation suggests that the ‘T’ or ‘Y’ shapes observed through EM, are not fixation artefacts, and instead represent the real shape of the exocyst complex in cells. Thus, supporting the idea that the exocyst complex is ‘T’ or ‘Y’ shaped with ‘arms’ that allow it to connect with different proteins to facilitate vesicle tethering.

Structural studies have revealed that different exocyst members contain different structural domains. For example, EXOC1 contains a pleckstrin homology (PH) domain at its N-terminal, allowing for its interaction with PIP_2 and GTPases (Baek et al., 2010; Yamashita et al., 2010). EXOC2 and EXOC8 have structural domains that allow them to compete for interaction of active Ral GTPases. Whereas EXOC8 interacts with Ral GTPases via its pH domain (Moskalenko et al., 2003) and EXOC2 interacts with Ral GTPases via its IPT (Ig-like, plexins, transcription factors) domain (Fukai et al., 2003; Mott et al., 2003). It is likely that additional structural domains exist in exocyst members, but until the full-length crystal structures of components have been resolved, these remain unknown.

Although there has been considerable progress in elucidating the structure of the exocyst complex, so far only 26 % of the crystal structure has been resolved (Picco et al., 2017). As a result, it is unknown if exocyst subunits contain additional, different subunit domains required for exocytosis. Therefore, until the structure of the exocyst complex is elucidated, the precise mechanisms of exocyst function in exocytosis remains undetermined.

1.1.4. Assembly of the exocyst complex

Precisely how the exocyst assembles is disputed. Previous studies proposed that EXOC1 and EXOC7 wait at the PM and tether a secretory vesicle by sequential interactions with the rest of the complex (Boyd et al., 2004; Finger et al., 1998). This model proposed that EXOC1 and EXOC7 reside at the PM where they interact directly with PIP_2, and only when the remaining exocyst members arrive by travelling with a secretory vesicle, the whole complex assembles (Boyd et al., 2004). However, this model has been questioned. Both EXOC1 and EXOC7 have been found to localise in the cytoplasm and not at the PM (Ma et al., 2016; Matern et al., 2001). In addition, other members of the exocyst have also been found to localise at the PM, independently to EXOC1 and EXOC7 (Songer and Munson, 2009). Taken together this suggests that exocyst assembly is not as simple as PM associated exocyst members binding with secretory vesicle associated exocyst members, and subsequently calls this model into question.

More recent studies have proposed that individual exocyst members form dimers which pair with another dimer to form a hetero-tetrameric complex. Cryo-electron microscopy has revealed that all eight subunits contain a conserved core exocyst 'CorEx' motif composed of an extended coiled-coil near the N-terminus (Mei et al., 2018). Mei *et al.*, 2018, discovered that the hierarchical assembly of the exocyst complex is dependent on binding of CorEx motifs. Here, four pairs of the exocyst (EXOC1–EXOC2, EXOC3–EXOC4, EXOC5–EXOC6 and EXOC7–EXOC8), assemble through the interactions of their respective CorEx motifs (Figure 1.2). These exocyst dimers further assemble into two four helix bundles through CorEx motifs: EXOC1–EXOC2-EXOC3-EXOC4 form into CorEx I (subcomplex I) and EXOC5–EXOC6-EXOC7–EXOC8 form into CorEx II (subcomplex II) (Mei et al., 2018). These four helix bundles are then able to bind to form the exocyst holo-complex.

In support of the exocyst assembling through interaction of two separate bundles, Heider *et al.*, 2016, developed a protocol that allowed the isolation of an endogenously intact exocyst complex from *S. cerevisiae.* Here, it was found that intact exocyst complex is stable under varying pH, salt and detergent conditions and consists of two-four subunit modules that comprise the octameric structure; EXOC1–EXOC2-EXOC3-EXOC4 comprises subcomplex I whereas EXOC5–EXOC6-EXOC7–EXOC8 comprises subcomplex II. Loss of EXOC2, EXOC3, EXOC4, EXOC5, EXOC7 or EXOC8 resulted in the octameric exocyst splitting into its two-four subunit modules, indicating that most subunits are required for maintaining the full octameric complex (Heider et al., 2016).

If the exocyst assembles hierarchically through subunit interaction, one question remains. What promotes and regulates exocyst assembly? As discussed in section 1.13 EXOC2 and EXOC8 compete for binding with active Ral GTPases and Ral-exocyst interactions are important for exocyst assembly (Jin et al., 2005; Moskalenko et al., 2002; Moskalenko et al., 2003; Mott et al., 2003). Inhibition of EXOC8 or RalA partially disrupted exocyst assembly by preventing the binding of EXOC3 and EXOC5 (Moskalenko et al., 2003). As previously discussed, it is proposed that EXOC3 is in subcomplex I and EXOC5 is in subcomplex II (Heider et al., 2016). It is therefore possible that through the formation of EXOC3-EXOC5 complexes, EXOC8 and RalA promote binding of subcomplex I and II to facilitate the assembly of the holo-exocyst complex. However, what initially promotes

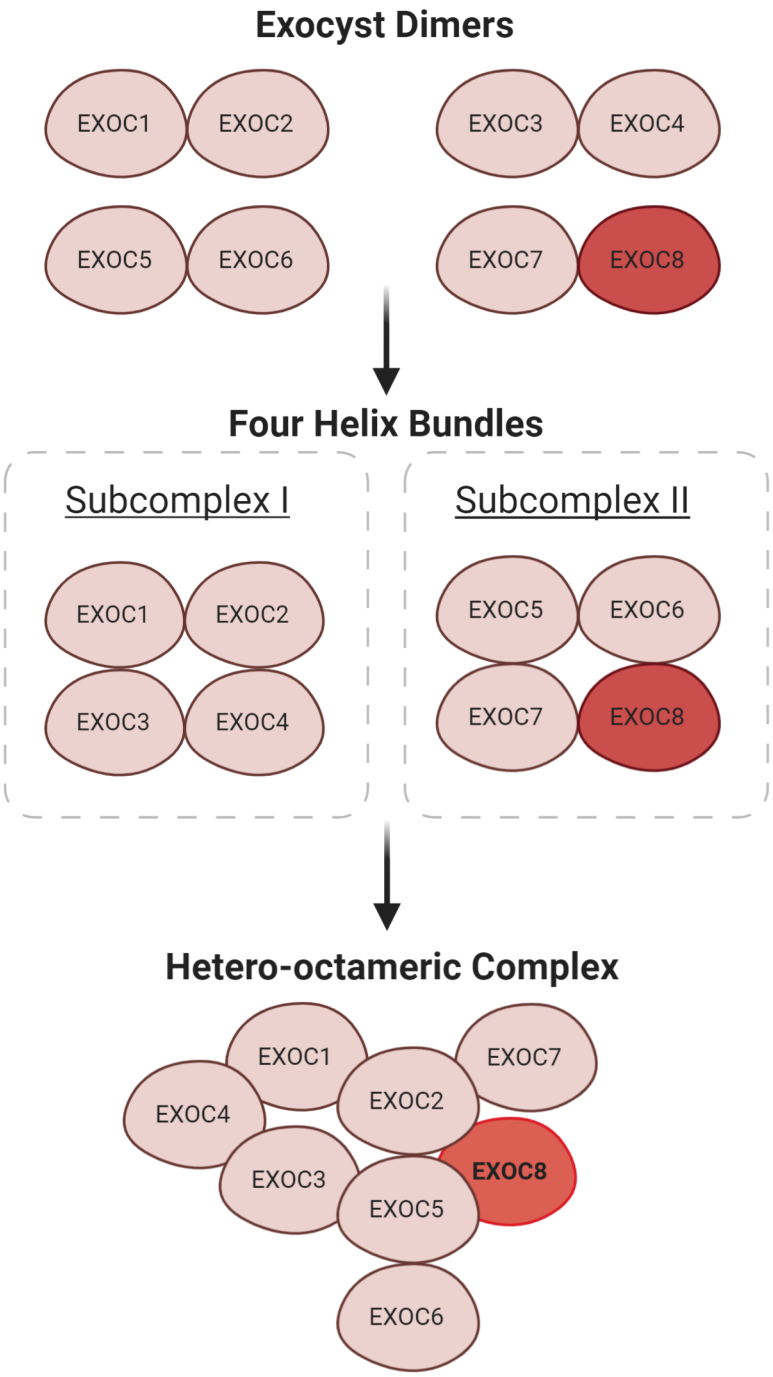

Figure 1.2. Proposed assembly of the exocyst complex. The assembly of the exocyst complex is thought to be hierarchical. Here, four pairs of the exocyst (EXOC1–EXOC2, EXOC3–EXOC4, EXOC5–EXOC6 and EXOC7–EXOC8), assemble. These exocyst dimers further assemble into two four helix bundles, to eventually form the octameric exocyst complex. Figure created using BioRender.com

exocyst assembly and the specific role GTPases play in assembly remains unclear.

1.2. Exocytosis

1.2.1. Exocytosis is an evolutionary conserved process

Exocytosis is an evolutionarily conserved process that mediates the secretion of intracellular proteins and is fundamental to membrane trafficking (Gerber and Südhof, 2002; Jahn and Südhof, 1999). It is the process in which cargo-filled intracellular secretory vesicles fuse to appropriate sites of the PM, to release cellular material into the extracellular space. Exocytosis is essential for a multitude of biological processes. For example, exocytosis is required for cell surface expansion, to facilitate cell growth, cell polarity and cell division (Boucrot and Kirchhausen, 2007; McCusker and Kellogg, 2012; Spiliotis and Nelson, 2003). In addition, exocytosis is required for cell-cell communication, cell migration and the excretion of cellular waste (Letinic et al., 2009; Liu and Guo, 2012; Pickett and Edwardson, 2006; Serini et al., 2012).

Exocytosis is a multi-step process (Figure 1.3). In brief, secretory vesicles are firstly trafficked to the vicinity of the PM. Then, secretory vesicles present at the appropriate sites of the PM and become tethered to the PM. Finally, interaction between the secretory vesicle and PM proteins facilitates the fusion of the secretory vesicles to the PM.

Trafficking of Golgi-derived secretory vesicles to the cell periphery prior to fusion with the PM, is predominantly controlled by the actin and microtubule network (Porat-Shliom et al., 2013; Schmoranzer and Simon, 2003). Initially, kinesin and dynein motors are recruited to vesicles during vesicle biogenesis. Here, the microtubule network supports the long-distance transport of secretory vesicles from sites of biogenesis at the Golgi to the cell periphery (Bloom and Goldstein, 1998). Once vesicles are in close proximity to the cell periphery, vesicles associate with myosin motors and the actin cytoskeleton, to begin the process of tethering and docking (Porat-Shliom et al., 2013).

Once secretory vesicles are near the PM, tethering and/or docking occurs (Whyte and Munro, 2002; Yu and Hughson, 2010). Membrane tethering mediates the docking of secretory vesicles to the target membrane prior to fusion of the two lipid bilayers. Tethering proteins bring vesicles into close contact with the PM by

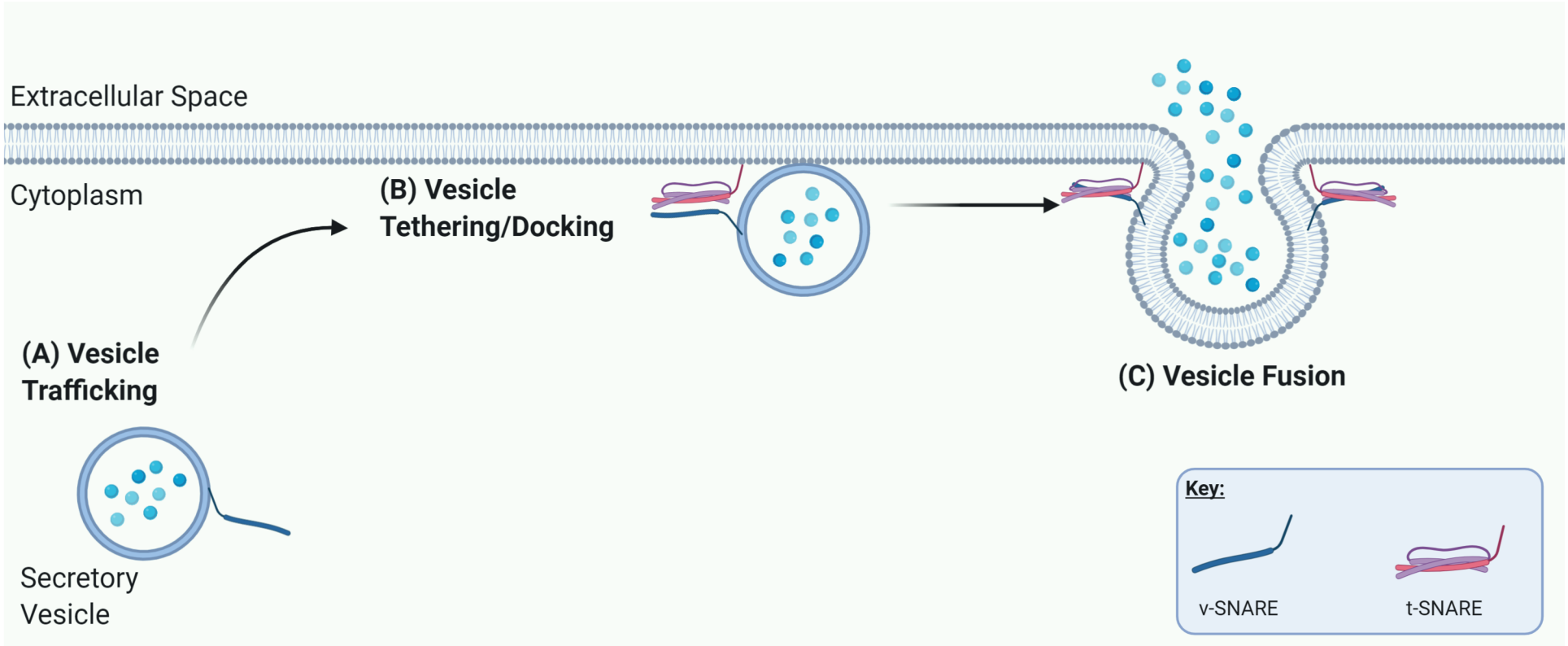

Figure 1.3. Process of Exocytosis. Exocytosis is a multi-step process. **(A)** Secretory vesicles are trafficked to the vicinity of the plasma membrane. **(B)** Secretory vesicles present at the appropriate sites of the plasma membrane and become tethered and docked. **(C)** Interaction between the secretory vesicle and plasma membrane proteins facilitates the fusion of the secretory vesicles to the PM. Figure created using BioRender.com

recognising specific proteins present on a secretory vesicle. This allows the membranes of the vesicle and PM to come within a bilayer's distance of one another, to facilitate vesicle docking and subsequent membrane fusion (Pfeffer, 1999). It is worth noting that there are varying definitions of the word "docked". Some authors believe that vesicles within 30 nanometres (nm) of the PM are "docked" (Verhage and Sørensen, 2008). On the other hand, other authors define "docked" as the presence of a "contact patch", where vesicles are in visible contact with the PM (Verhage and Sørensen, 2008). Regardless, vesicle tethering plays a fundamental role in facilitating vesicle docking and membrane fusion.

Loss of tethering proteins impairs exocytosis and therefore play a fundamental role in membrane trafficking. There are two main classes of tethering molecules: large multi-subunit tethering complexes (MTCs) and long coiled coil proteins (Bröcker et al., 2010; Gillingham and Munro, 2003). Long coiled coil proteins are large hydrophilic tethering complexes that span distances over 200 nm. Owing to their large size long coiled coil proteins and can can tether vesicles that are up to 200 nm from the target membrane. Long coiled coil proteins therefore bridge large distances potentially through anchoring at the membrane and searching for nearby vesicles (Gillingham and Munro, 2003). On the other hand, MTCs are composed of 3-8 subunits and have a molecular weight between 250 and 800 kDa. Unlike coiled coil proteins which tethers secretory vesicles over long distances, MTCs interact and tethers vesicles up to 30 nm from the target membrane (Bröcker et al., 2010). Both coiled coil protein and MTC tethering molecules function to promote vesicle fusion at correct membrane locations and are central for exocytosis and membrane trafficking.

The last stage of exocytosis is membrane fusion (Chen and Scheller, 2001; Han et al., 2017; Jahn and Scheller, 2006). Once a secretory vesicle has been tethered at appropriate sites of the target membrane, fusion of the two lipid bilayers can occur. Fusion is predominantly mediated by Soluble N–ethylmaleimide sensitive factor (NSF) attachment protein receptor (SNARE) proteins which reside on both on secretory vesicles (vSNAREs) and target membranes (tSNAREs) (Chen and Scheller, 2001; Han et al., 2017). vSNAREs and tSNAREs on separate membranes assemble into tight, four-helix bundles called "trans"-SNARE complexes (Han et al., 2017). Formation of this "trans"-

SNARE complex, pulls the vesicle and target membranes together, to overcome the energy barrier and allow membrane fusion to occur. This then marks the release of secretory vesicular content into the extracellular space. "Trans"-SNARE complexes are regulated by Sec1/Munc18 (SM), Rab and tethering proteins, to ensure that vesicular fusion occurs at appropriates sites of the PM (Jahn and Scheller, 2006).

1.2.2. Role of the exocyst in exocytosis

The exocyst complex has been implicated in exocytosis where it is thought to tether secretory vesicles to the PM prior to SNARE mediated fusion. Owing to its helical structure, the exocyst is part of the MTC CATCHR family (complexes associated with tethering containing helical rods) (Brunet and Sacher, 2014; Yu and Hughson, 2010). As previously discussed MTCs are large multisubunit complexes which during exocytosis, tether vesicles up to 30 nm from the target membrane. During exocytosis, the exocyst is concentrated in subdomains at the plasma membrane in sites that are active of exocytosis, suggesting that the exocyst is a fundamental protein for this process. Furthermore, cells with exocyst mutations display defects in exocytosis and accumulate secretory vesicles at the cell periphery and plasma membrane (Grote et al., 2000; Songer and Munson, 2009). This suggests that secretory vesicles are trafficked to the vicinity of the PM but are then hindered by a defect in either vesicle tethering or fusion. However, the fundamental mechanism of exocyst function in tethering remains unelucidated, owing to difficulties in *in vitro* reconstitution of the exocyst complex.

Besides its possible role as a membrane tether, the exocyst complex has also been implicated in the formation and regulation of SNARE-complexes. Sec3 has been shown to promote the formation of the initial SNARE complex (Sec9–Sso1/2–Snc2 SNAREpin) (Yue et al., 2017). Here, EXOC1 interacts with the tSNARE Sso2, and this interaction promotes the formation of a Sso2-Sec9 t-SNARE complex. This Sso2-Sec9 complex then stimulates membrane fusion as it is the rate limiting step in SNARE complex assembly (Yue et al., 2017). Loss of interaction between EXOC1 and Sso2, blocks exocytosis and suggests that in addition to its role as a membrane tether EXOC1 is also required for initiation of SNARE complex machinery. Other exocyst members have also been shown to play a role in SNARE assembly and fusion. EXOC7 is thought to aid SNARE complex assembly by binding to SNAP23, which serves as a binding site for

fusion machinery (Ahmed et al., 2018). As a result, fusion machinery is present at the tethering sites and exocytosis can occur. EXOC3 has been shown to bind to SM proteins, which regulates SNARE fusion by ensuring that vesicular fusion occurs at appropriates sites of the PM (Morgera et al., 2012). Finally, EXOC8 has been found to bind to Sro7, to regulate the formation and assembly of SNAREs through interaction with Sec9 (Zhang et al., 2005). Taken together, this data suggests that the interactions between PM, exocyst and SNARE complexes are crucial for successful exocytosis with future studies disentangling such complex interactions.

1.3. Non-conventional roles of the exocyst complex

In addition to the fundamental role the exocyst plays in exocytosis, the exocyst complex has been implicated in a variety of other cellular processes. For example, the exocyst complex is involved in cell-cell contact, apoptosis, and nanotube formation (Morin et al., 2010; Tanaka et al., 2014; Tanaka et al., 2016). It is therefore possible that the exocyst complex functions in processes besides or alongside exocytosis. However, it is hard to disentangle if such cellular processes occur due to the exocyst complex having distinct functions from exocytosis, or if such cellular processes are the result of exocytosis itself.

Moreover, individual components of the exocyst complex have been shown to have distinct functions. EXOC4 plays a role in synaptic plasticity, transcytosis, and DNA repair (Fölsch et al., 2003; Grindstaff et al., 1998; Riefler et al., 2003). EXOC1 plays a role in nanotube formation and mucin 5AC secretion (Li et al., 2015; Morin et al., 2010), and EXOC7 plays a role in tubulin polymerisation, transferrin recycling and pre-mRNA splicing (Dellago et al., 2011; Fölsch et al., 2003; Takahashi et al., 2012; Wang et al., 2004). This therefore begs the question; does the exocyst complex function as a complex or as single subunits? This makes the identification of specific roles of exocyst components difficult.

1.4. Cellular roles of EXOC8

EXOC8 is one of the least characterised members of the exocyst complex. Therefore, there is limited published information on EXOC8 function, and its cellular roles distinct from exocytosis are not necessarily limited to those below - there may be EXOC8-linked processes yet to be described. Furthermore, although EXOC8 has known roles in many cellular processes, the underlying

mechanisms of many of these processes remains unclear (Figure 1.4). This MbyRes thesis focuses on the function and role of EXOC8, since it is the least characterised member of the exocyst complex. Therefore, the following section explores what is known and what is yet to be understood about EXOC8 in a variety of cellular contexts.

1.4.1. EXOC8 is best characterised for its roles in cell migration and E-Cadherin recycling

Cell Migration

Perhaps the most well documented function of EXOC8 is its role in migration, with knockdown of different exocyst components perturbing cell migration (Spiczka and Yeaman, 2008; Thapa et al., 2012; Zuo et al., 2006).

SH3-domain Binding Protein 1 (SH3BP1) is a RhoGAP that binds and localises with EXOC4 and EXOC8, at the leading edge of motile cells (Parrini et al., 2011). Knockdown of EXOC4 and EXOC8 by RNAi reduced recruitment of SH3BP1 to the leading edge of motile cells. Conversely, knockdown of SH3BP1 reduced recruitment of EXOC4 to the leading edge (Parrini et al., 2011). The effect of knockdown of SH3BP1 on EXOC8 localisation was not examined. This suggests that EXOC4-SH3BP1 localisation to the leading edge of migrating cells is mutually dependent. SH3BP1 is important for cell migration; knockdown of SH3BP1 inhibited cell migration in both wound healing assays and Boyden chamber assays (Parrini et al., 2011). Furthermore, SH3BP1 depleted cells, displayed migration defects owing to unstable and disordered cellular protrusions. SH3BP1 is therefore required for cell migration by localising to the front of migrating cells. The exocyst members EXOC4 and EXOC8 may therefore contribute to transporting SH3BP1 to the leading edge of motile cells, for effective cell migration.

In support of the exocyst transporting SH3BP1 to the leading edge of motile cells, Hazelett and Yeaman discovered SH3BP1 localisation is dependent on RalA-exocyst binding (Hazelett and Yeaman, 2012). In cells expressing endogenous RalA, SH3BP1 localised to the cell periphery at the leading edge. In contrast, cells expressing RalA (47E) uncoupled from EXOC8, SH3BP1 had diffuse cytoplasmic localisation. RalA- EXOC8 binding therefore facilitates SH3BP1 at the leading edge of motile cells for regulation of lamellipodia (Hazelett and Yeaman, 2012).

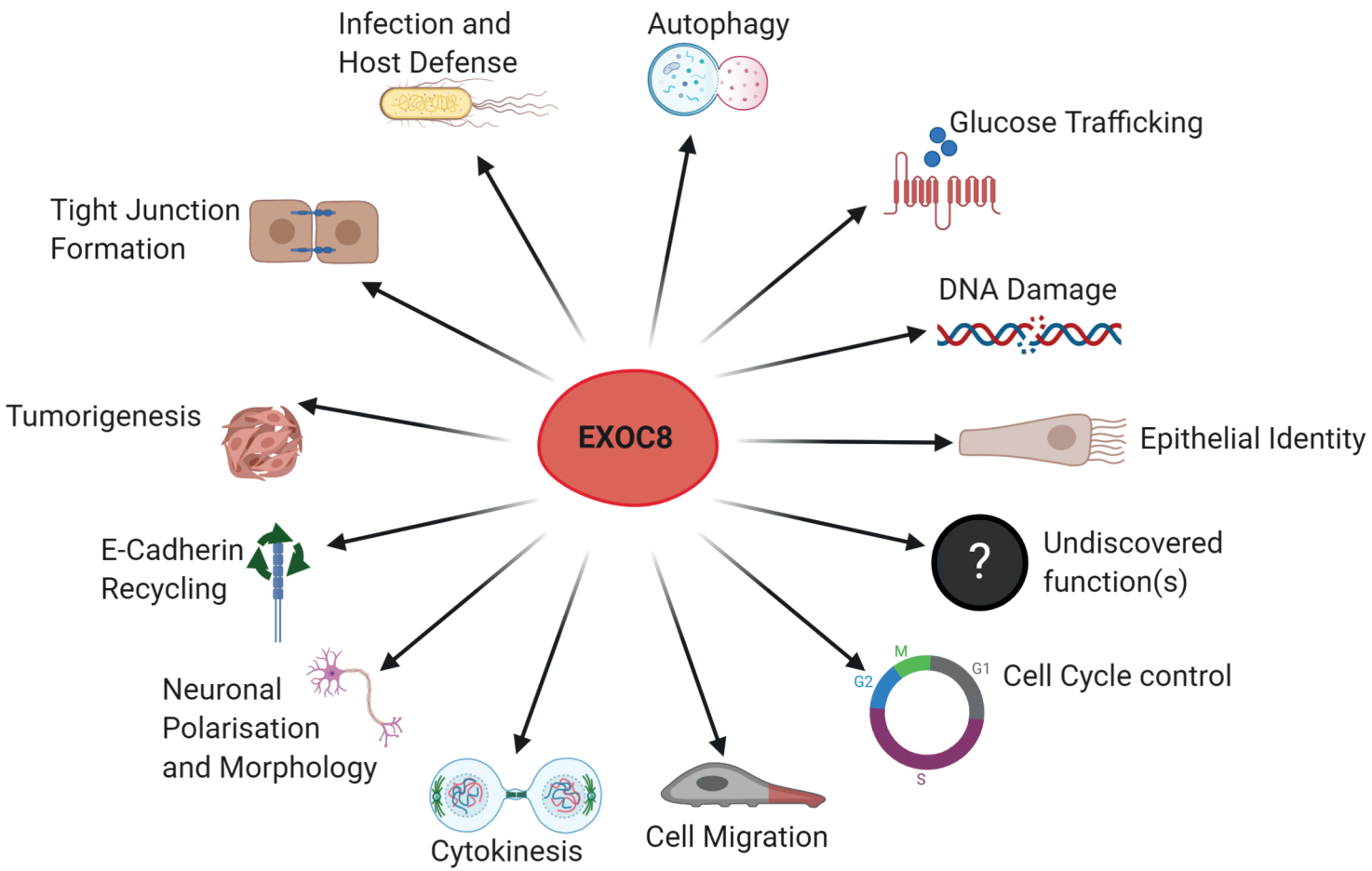

Figure 1.4. Overview of the cellular roles of EXOC8. EXOC8 is required for a multitude of cellular processes. Figure created using BioRender.com

The exocyst has been shown to interact with RalA to form membrane protrusions (Hazelett and Yeaman, 2012; Zago et al., 2019). Constitutively active RalA, induces the formation of filopodia (cellular actin-rich protusions that sense the environment in migrating cells) (Ohta et al., 1999; Sugihara et al., 2002). As mentioned in section 1.13, RalA interacts with both EXOC2 and EXOC8 to carry out a variety of cellular processes. Loss of interaction between RalA and EXOC2 prevents filopodia formation in migrating cells (Sugihara et al., 2002). Although the authors did not examine if the loss of interaction between RalA and EXOC8 prevented filopodia formation, it is possible that given the known association between the two proteins, EXOC8 could also function in filopodia formation. However, this has yet to be examined.

Atypical protein kinase C (aPKC) has been shown to play a role in cell migration (Wang et al., 2018). aPKC accumulates at the leading edge of migrating cells and interacts with many signalling proteins. In migrating cells, the exocyst and aPKC form a complex at the leading edge (Rosse et al., 2009). This complex activates the c-Jun N-terminal protein kinase JNK1, which is involved in regulating the phosphorylation of Paxillin. Paxillin is a focal adhesion protein that upon phosphorylation is involved in cell movement and migration (López-Colomé et al., 2017). Knockdown of EXOC8 inhibited cell migration by 60 %. Loss of EXOC8 prevents aPKC localising and activating JNK at the leading edge of cells, causing Paxillin to accumulate in large static focal adhesions. EXOC8 is therefore required for cell migration by forming a complex with aPKC, to activate JNK which in turn controls the phosphorylation and dynamics of Paxillin.

Precisely how EXOC8 localises to the leading edge of migrating cells to interact with aPKC is unknown. However, it is possible that RalB has a role in this process. In its active GTP bound state, RalB binds to both EXOC8 and EXOC2 (Moskalenko et al., 2002; Moskalenko et al., 2003). RalB lysine fatty acid acetylation promotes RalB activation and its localisation to the leading edge of migrating cells (Spiegelman et al., 2019). Lysine fatty acid acetylated RalB, is able to bind to its effector, EXOC8, promoting EXOC8 to localise to the leading edge of migrating cells. RalB lysine fatty acid acetylation promotes cell migration in cancer cells (Spiegelman et al., 2019). The authors hypothesise that RalB lysine fatty acid acetylation, promotes RalB activation and localisation to the leading edge of migrating cells, where it can recruit EXOC8 to promote cell

migration. However, the authors did not examine the effect of EXOC8 depletion on cell migration in cells where RalB was lysine fatty acid acetylated. It is therefore possible that RalB lysine fatty acid acetylation promotes cell migration independent of EXOC8 and the exocyst complex.

E-Cadherin Recycling

E-Cadherin is a calcium-dependent cell-cell adhesion glycoprotein that is the main constituent of at adherens junctions (AJs) (Collinet and Lecuit, 2013). The exocyst is known to play a role in cadherin delivery to AJs; Cholera toxin blocks this delivery, thus disrupting epithelial barrier function and leading to the water leakages in the gut that constitute the main symptom of cholera (Guichard et al., 2013). Similarly, in Drosophila EXOC8 mutants, E-cadherin is mis-localised from AJ and instead accumulates in recycling endosomes (Blankenship, Fuller and Zallen, 2007).

RalA is a tumour suppressor, that plays a key role in the suppression of the early stages of Ras-induced squamous cell carcinoma by stabilising E-cadherin (Sowalsky et al., 2011). Decreased expression of E-Cadherin induces Ras-expressing keratinocytes from a premalignant to malignant state (Sowalsky et al., 2011). Knockdown of both RalA and EXOC8 decreased expression of E-cadherin facilitating tumorigenesis. RalA and its effector EXOC8, stabilises E-cadherin by recycling E-cadherin to the PM. Decreased expression of RalA, prevents E-cadherin recycling to the PM by EXOC8, enhancing E-cadherin degradation in the cytoplasm and facilitating tumorigenesis (Jeanes, Gottardi and Yap, 2008; Sowalsky et al., 2010). In line with this, a RalA72L49E mutant which is unable to bind to EXOC8, failed to deliver E-cadherin to the basolateral surface of MDCK cells (Shipitsin and Feig, 2004). This further suggests that EXOC8 is required by RalA for E-cadherin recycling to the PM.

1.4.2. Through its role in exocytosis, EXOC8 facilitates glucose trafficking and the induction and maintenance of neuronal polarity, epithelial identity and cell cycle regulation

Given that the exocyst's classical role is membrane trafficking, it is unsurprising that the exocyst is required in processes where cellular material and proteins needs to be delivered to specific sites in a cell. As a result of EXOC8's role in exocytosis, EXOC8 facilitates glucose trafficking and the induction and maintenance of neuronal polarity, epithelial identity and cell cycle regulation.

Glucose trafficking

GLUT4 is a glucose transporter predominantly found in adipocytes and muscle cells (Huang and Czech, 2007; Stöckli, Fazakerley and James, 2011). Upon insulin secretion from the pancreas, GLUT4 facilitates the uptake of glucose into adipocytes and muscle cells. GLUT4 has widespread cellular distribution; it is present throughout the PM, the Golgi and in GLUT4 containing storage vesicles. The exocyst along with the GTPase RalA tethers GLUT4 containing storage vesicles to the PM, to facilitate insulin-stimulated glucose uptake (Chen et al., 2007). Upon release of insulin, RalA (which is present in GLUT4 storage vesicles) becomes activated, allowing it to bind to both EXOC2 and EXOC8. The exocyst complex then traffics and tethers GLUT4 storage vesicles to the PM, where GLUT4 can fuse with the PM (Chen et al., 2007; Uhm et al., 2017). TBK1 then phosphorylates EXOC8, allowing the exocyst to disengage from RalA and GLUT4 storage vesicles, in order to facilitate fusion and further GLUT4 trafficking to the PM (Uhm et al., 2017).

Further studies have shown that knockdown of EXOC8 inhibited glucose uptake in response to insulin, demonstrating that EXOC8 is important in transporting GLUT4 to the plasma membrane following insulin secretion (Chen et al., 2007).

Neuronal polarisation and morphology

Neuronal polarity is dependent on rearrangement of the actin and microtubule cytoskeleton and directed membrane trafficking (Da Silva and Dotti, 2002; Foletti et al., 1999). The partitioning-defective and atypical protein kinase C (PAR-3/PAR-6/aPKC) complex is fundamental in these processes and is therefore a major regulator of polarity in mammalian cells (Chen and Zhang, 2013). In hippocampal neurons, proper localisation of the PAR-3/PAR-6/aPKC complex to the growing tip of single axons establishes neuronal polarity and allows neural outgrowth (Lalli, 2009; Shi et al., 2003). The exocyst is essential for neuronal polarisation; neurons depleted of EXOC8 were unpolarised and had decreased neurite and axon branch density (Lalli, 2009). EXOC8 associated with PAR-3 and aPKC by immunoprecipitation and both EXOC8-PAR-3 and EXOC8-aPKC interaction increased over time. In neurons depleted of EXOC8, PAR-3 did not accumulate in any neurites, suggesting that EXOC8 is required for localising PAR-3 (Lalli, 2009). EXOC8 is essential for neuronal polarisation by interacting

with and correctly localising PAR-3 and aPKC to the growing tip of single axons, potentially through their trafficking.

Similarly, EXOC8 is required for neuronal polarity in neuroblasts, through its interaction with PAR-6 (Das et al., 2014). PAR-6 is a cell polarity protein which contains a PDZ protein interaction domain that recognises short amino acid motifs of target proteins (Das et al., 2014; Joberty et al., 2000; Lin et al., 2000). When RalA is active, EXOC8 directly interacts with PAR-6-PDZ via the PDZ-binding motif of EXOC8 (Das et al., 2014). In the absence of RalA, EXOC8-PAR-6-PDZ interaction is reduced. The absence of EXOC8-PAR-6-PDZ interaction, impaired polarity, migration and morphology in postnatal migratory neuroblasts and embryonic neurons (Das et al., 2014). This suggests that EXOC8 plays a role in establishing neuronal polarisation through interacting with PAR-6 in neuroblasts.

Schwann cells are the main cell of the peripheral nervous system, aiding the conduction of action potentials by producing myelin (Salzer, 2015). Myelin forms a sheath around sensory and motor neurons, which increases the conduction velocity of action potentials by saltatory conduction (Salzer, 2015). For effective myelination to occur, Schwann cells undergo radial sorting to “choose” which axon to myelinate; a process that requires Schwann cell extension by Ral GTPases (Feltri et al., 2016; Ommer et al., 2019). Loss of both RalA and RalB results in radial sorting defects, with Ral-deficient double mutant Schwann cells displaying extension defects (Ommer et al., 2019). RalA72L D49E is a constitutively active RalA unable to bind to EXOC2 and EXOC8. Expression of RalA72L D49E in double mutant Schwann cells did not rescue the length Schwann cell process extensions. However, expression of a constitutively active RalA (RalA72L), was able to rescue deficits in process extension length of double mutant Schwann cells (Ommer et al., 2019). Thus, indicating that the interaction of RalA with EXOC2 and EXOC8 is an important process for Schwann cell process extension.

Epithelial identity

The *Drosophila* homolog of EXOC8 is required for epithelial polarity in Drosophila embryos (Blankenship et al., 2007). Crumbs is a transmembrane protein found in *Drosophila* that is a key regulator of epithelial cell polarity through organising adherens junctions (Bulgakova and Knust, 2009). EXOC8 mutants resulted in the

mislocalisation of apical adherens junctions' proteins such as DE-Cadherin and Armadillo due to the loss of crumbs from the apical cell surface (Blankenship et al., 2007). In line with this, other apical proteins including Bazooka were mislocalised from the apical cell surface. Furthermore, in EXOC8 mutants the localisation of the recycling endosome protein Rab11 was perturbed. In EXOC8 mutants, Rab11 positive vesicles were aggregated in large clusters whereas in WT-embryos such vesicles had a punctate distribution (Blankenship et al., 2007). This suggests that EXOC8 is required for endosomal vesicle trafficking and that EXOC8 is required for trafficking Crumbs to the apical cell surface to regulate epithelial cell polarity.

Cell growth and cell cycle progression

Eukaryotic cell growth is tightly regulated to maintain cell size homeostasis (Amodeo and Skotheim, 2016; Jorgensen and Tyers, 2004). Endo- and exocytosis play a key role in the regulation of cell size through controlling cell surface growth (McCusker and Kellogg, 2012). Prior to mitosis, cell growth is inhibited before the metaphase to anaphase transition, for cells to preserve energy and reorganise their structures (Goranov et al., 2009; Miettinen et al., 2019). In the budding yeast, *S. cerevisiae,* exocytosis in inhibited in metaphase arrested cells (Guo et al., 2013). Phosphorylation of EXOC8 induces the disassembly of the exocyst complex (Duan et al., 2020). In *S. cerevisiae*, EXOC8 is phosphorylated by the cell cycle regulator, cyclin dependent kinase 1 (CDK1). Phosphorylation of EXOC8 by CDK1, results in disassembly of the exocyst complex halting exocytosis and cell surface expansion (Guo et al., 2013). Cell size homeostasis is therefore controlled by exocytosis and cell cycle progression.

In *S. cerevisiae,* phosphorylation of EXOC8 by CDK1 during mitosis, prevents exocytosis and subsequent cell surface expansion (Guo et al., 2013). However, in the fungal pathogen *Candida albicans,* phosphorylation of EXOC8 by CDK1 is essential for hyphal extension to continue in mitosis (Caballero-Lima and Sudbery, 2014). So why does phosphorylation of EXOC8 by CDK1 promote growth in one organism but inhibit it in another? EXOC8 contains CDK1 target sites, which CDK1 recognise and subsequently phosphorylate (Guo et al., 2013). In *S. cerevisiae* EXOC8, the CDK1 target site is present in the C-terminal interaction domain and its phosphorylation would induce loss of interaction with other exocyst subunits (Duan et al., 2020; Guo et al., 2013). On the other hand,

in *C. albicans* the CDK1 target site is present in the PH domain and its phosphorylation does not affect exocyst complex disassembly, meaning exocytosis and cell surface growth can continue (Caballero-Lima and Sudbery, 2014). EXOC8 has therefore evolved to allow phosphoregulation for control of cell growth in different organisms.

1.4.3. EXOC8 interacts with RalA to facilitate numerous cellular processes

As discussed in section 1.1.3. EXOC8 contains a pH domain, which binds to RalA. RalA is a multifunctional GTPase, that has functions in a variety of cellular processes, by cycling between its active-GTP and inactive GDP-bound state (Fukai et al., 2003). The exocyst is a major Ral effector and the interaction between RalA and EXOC8 is required for numerous cellular processes, including neuronal polarisation and cell migration (discussed above) and cytokinesis and tight junction formation (discussed below).

Cytokinesis

Cytokinesis is the division of the cytoplasm in eukaryotic cells after chromosome segregation which produces two distinct daughter cells (Guertin et al., 2002). It is reliant on cytoskeleton remodelling and membrane trafficking (Schiel and Prekeris, 2013). The exocyst is required for cytokinesis (Neto et al., 2013). Knockdown of individual exocyst subunit perturbs cytokinesis and results in increased proportions of binucleate cells (Fielding et al., 2005; Giansanti et al., 2015; Gromley et al., 2005; Kumar et al., 2019; Neto et al., 2013). Similarly, in EXOC8 mutant cells, cytokinetic ring ingression is impaired which perturbs cytokinesis (Chen et al., 2006; Giansanti et al., 2015). Addition of WT-EXOC8 to EXOC8 mutant cells rescued this cytokinesis defect suggesting that EXOC8 acts an effector for cytokinesis (Giansanti et al., 2015). This is supported by results that show that RalA mobilises EXOC8 for it to act as an effector for cytokinesis (Cascone et al., 2008). RalA localises at the cleavage furrow of mitotic cells and its depletion results in increased proportions of binucleate cells. Introduction of EXOC8 uncoupled RalA (A48W) in RalA depleted cells did not rescue cytokinesis defects caused by RalA, suggesting that it is EXOC8 that acts as an effector for cytokinesis (Cascone et al., 2008). This is consistent with EXOC8s localisation during mitosis; as similarly, to RalA, EXOC8 localises at the cleavage furrow of mitotic cells (Gromley et al., 2005). Together, this suggests that through its interaction with RalA, EXOC8 is required for successful cytokinesis.

Tight junction formation and function

Tight junctions (TJ) are fundamental cell junctions in epithelial cells required for cell adhesion, permeability and polarisation (Zihni et al., 2016). TJ integrity and maintenance is dependent on Ral-GTPases and the Par/aPKC cell polarity complex, both of which associate with the exocyst (Lalli, 2009). Knockdown of RalA and RalB directly impacts TJ formation and composition (Hazelett et al., 2011). To elucidate if RalA contributes to TJ formation and function through the exocyst complex, RalA mutants unable to bind to EXOC8 were generated. The RalA-A48W mutant, which is unable to bind to EXOC8, perturbed TJ biogenesis and function in MDCK cells (Hazelett et al., 2011). Therefore, EXOC8 engagement with RalA is required for TJ formation and subsequent TJ function.

1.4.4. Other emerging roles for EXOC8

Asides a role in exocytosis and vesicle tethering, EXOC8 also functions in other cellular processes. The evidence for EXOC8 participating in other cellular roles will be discussed below.

Autophagy

Autophagy is a self-degradative process that is critical for tissue homeostasis (Glick et al., 2010). EXOC8 plays a role in autophagy, where it is required for nutrient-starvation induced autophagocytosis (Bodemann et al., 2011). The RAS GTPase, RalB, localises to nascent autophagosomes whereby it becomes active in its GTP-bound state under nutrient deprivation. In response to this activation, the RalB effector EXOC8 directly binds to RalB. This binding subsequently causes the recruitment and assembly of the ULK1-Beclin1-VPS34 complex on EXOC8, which triggers vesicle nucleation and autophagosome biogenesis (Bodemann et al., 2011). EXOC8 therefore plays a role in activating autophagy in nutrient deprived conditions, through engagement of core autophagy activation machinery. Recent studies have supported the role of EXOC8 in autophagy, by showing that the protein kinase, STK38 is required for the assembly of both EXOC8-RalB and EXOC8-Beclin1 complexes (Joffre et al., 2015). Depletion of STK38, prevented the assembly of the ULK1-Beclin1-VPS34 complex on EXOC8 and subsequently resulted in reduced autophagosome production (Joffre et al., 2015). EXOC8 therefore plays a critical role in promoting autophagosome biogenesis through the binding and assembly of the ULK1-Beclin1-VPS34 complex.

The role of EXOC8 in autophagy is further supported by Simicek *et al.*, 2013. Ubiquitination of RalB at Lys47 prevents RalB binding to EXOC8 (Simicek et al., 2013). However, upon nutrient starvation, RalB becomes deubiquinated, because nutrient starvation results in the deubiquitylase USP33, becoming redistributed to RalB-positive vesicles. Upon this deubiquination, RalB can re-bind with EXOC8 allowing Beclin1 to be recruited, which in turn facilitates the formation of autophagosomes (Simicek et al., 2013).

DNA damage

In line with the function of other exocyst components, EXOC8 is also involved in the cellular response to DNA damage (Rochette et al., 2014; Torres et al., 2015). In response to detrimental perturbation, cells can re-organise their protein-protein interaction networks (PINs) in order to adapt to conditions and subsequently survive (Rochette et al., 2014). Using a dihydrofolate reductase protein-fragment complementation assay (DHFR-PCA), the modulation of protein-protein interactions (PPIs) was examined between standard and Methyl Methane Sulfonate (MMS) inducing DNA damage conditions. This identified 156 PPIs that were modulated in response to DNA damage and that modulated PPIs involve EXOC8 (Rochette et al., 2014). Temperature sensitive mutants of EXOC8 showed that depletion of EXOC8, resulted in modulated PPIs having increased susceptibility to MMS induced DNA damage. This suggests that EXOC8 plays a pivotal role in the DNA damage response, potentially through trafficking proteins and affecting protein localisation, therefore modulating PPIs.

1.4.5. Role of EXOC8 in infection and disease

Tumorigenesis

In nearly a third of cancers the oncogene Ras, is mutated to be constitutively activate in its GTP-bound state. Oncogenic Ras binds and activates Ral-GEFs, which in turn activates the GTPases RalA and RalB into their active GTP-bound state. Given that the exocyst components EXOC2 and EXOC8 are two downstream effectors of RalA and that RalA is implicated in tumorigenesis, Issaq *et al* 2010 wanted to explore if the exocyst contributes to transformation and tumorigenesis. Knockdown of both EXOC2 and EXOC8 reduced Ral-GEF mediated transformation of HEK cells, with EXOC8 knockdown resulting in 86% less transformed cells than in the control (Issaq et al., 2010). Similarly, knockdown of both EXOC2 and EXOC8 reduced oncogenic Ras mediated

tumourgenesis of HEK cells (Issaq et al., 2010). This is supported by a RalA mutant, which has decreased binding to EXOC2 and EXOC8, and a significant decrease in the proportion of transformed cells. (Lim et al., 2005). This suggests that EXOC2 and EXOC8 play a role in Ras-mediated tumourgenesis by acting as effector proteins for RalA.

Cell invasion

Cell invasion is required for many processes including leukocyte migration, neural crest formation and blastocyst implantation (Bronner, 2012; Gomez-Lopez et al., 2010; Kim and Kim, 2017). However, misregulated cell invasion contributes to many pathologies, such as metastatic cancer. In *Caenorhabditis elegans,* cell invasion plays a critical role in the development of the reproductive system (Sherwood and Plastino, 2018). In *C. elegans,* anchor cells (ACs) invade the basement membrane to initiate uterine-vulval contact (a connection required for both mating and laying embryos). Knockdown of different exocyst components in *C. elegans*, resulted in anchor cell invasion defects and aberrant uterine-vulval contact (Naegeli et al., 2017). In a null mutant of EXOC8, ACs breached the basement membrane but had significantly reduced rates of protrusion growth (Naegeli et al., 2017). This suggests that the exocyst complex and EXOC8 is required for AC invasive protrusion and plays a role in initiating uterine-vulval contact through exocytosis.

Infection and host defence

The exocyst complex plays a key role in facilitating pathogen infection. Pathogens use the exocyst complex to exit the cells that they have infected in order to colonise and infect neighbouring cells and tissues. One such example is the bacterial pathogen *Porphyromonas gingivalis, which* enters gingival epithelial cells (GEC) by endocytosis and passes through epithelial barriers to infect cells (Takeuchi et al., 2011). RNAi knockdown of the exocyst complex subunits (EXOC2, EXOC3 and EXOC8) significantly disrupted the exit of *P. gingivalis* from the host cell (Takeuchi et al., 2011). The exocyst complex therefore facilitates *P. gingivalis* infection, by allowing its exit from the host cell and its spread to neighbouring cells and tissues.

However, contrary to the exocyst complex facilitating pathogen infection, the exocyst complex is also involved in host defence. Knockdown of the exocyst and EXOC8 promotes an increase of intracellular bacteria in cells, suggesting that the

exocyst expels pathogens through exocytosis (Tanaka et al., 2017). Similarly, in bladder epithelial cells (BEC), uropathogenic *E.coli* are expulsed from cells by the exocyst complex (Miao et al., 2016). Expulsed, *E.coli* are either cleared by immune cells or are eliminated through body fluids such as urine. Knockdown of EXOC8 in BECs resulted in defective expulsion of *E.coli* from cells, allowing *E.coli* to colonise in BECs (Miao et al., 2016). EXOC8 is therefore important for maintaining exocytosis and the subsequent expulsion of intracellular bacteria from cells.

1.4.6. Undiscovered functions of EXOC8

As section 1.4. has shown, the precise role of EXOC8 in different cellular functions is unknown and the mechanisms of such processes are not clear. At this point it is not possible to precisely predict what other cellular processes EXOC8 is involved in. Given the widespread localisation of EXOC8 in the cell, it is likely that EXOC8 is multifunctional. It is known that other exocyst components play a crucial role in cell adhesion (Andersen and Yeaman, 2010; Xiong et al., 2012), nanotube formation (Lachambre et al., 2014; Morin et al., 2010; Mukerji et al., 2012) and apoptosis (Tanaka et al., 2014; Tanaka et al., 2016).It is plausible that EXOC8 also functions in these processes . However, without further studies, there is currently not enough evidence to state what other processes EXOC8 is involved in, and whether EXOC8 plays a direct or indirect role.

1.5. Exocyst and disease

Given the wide range of cellular roles of the exocyst it is not surprising that the exocyst complex is implicated in disease. Full knockout of exocyst members in mice is embryonically lethal and conditional or heterozygous mutant mice display varying developmental defects. As a result, recent studies have implicated the exocyst complex in a variety of diseases, including kidney disease, cancer, diabetes and neurodevelopmental disorders.

1.5.1. EXOC8 and disease

Ciliopathy

Most mammalian cells form a primary cilium; a sensory organelle projecting from the cell surface that receives and transmits diverse signalling cues (Satir et al., 2010; Wheway et al., 2018). Primary cilia are essential in humans and play important roles in many tissues and organs, including the kidney, skeleton, liver,

and brain (Gerdes et al., 2009). Ciliopathies are genetic disorders resulting from mutations that impair ciliary function or formation (Badano et al., 2006; Reiter and Leroux, 2017). Joubert syndrome (JBTS) is predominantly an autosomal recessive ciliopathy characterised by symptoms including hypotonia, hyperpnea, ataxia, polydactyly and polycystic kidneys. The most predominant symptom is hypoplasia of the cerebellar vermis, causing cerebellum and brainstem malformation: magnetic resonance imaging of JBTS patient brains reveals a diagnostic “molar tooth” sign (Nag et al., 2013).

Recently, a previously undescribed mutation in the exocyst component EXOC8 was found in a male with clinical features consistent with JBTS (Dixon-Salazar et al., 2012). Sequencing revealed that EXOC8 contained a point mutation that leads to the substitution of glycine instead of glutamic acid at position 265 (E265G). The exocyst complex therefore plays a role in either cilium formation or function.

Cancer

Given the wide-reaching cellular roles of EXOC8, it is unsurprising that EXOC8 is implicated in cancer and tumour formation. Knockdown of EXOC8 has been shown to decrease the proliferation of Ras transformed cells (Issaq et al., 2010). In colorectal cancer, EXOC8 interacts with RalA to support anchorage independent growth of colorectal cancer cells, thus contributing to its metastatic potential (Martin et al., 2011). Similarly, in prostate cancer, EXOC8 interacts with RalA which contributes to cancer cell motility, and invasion and inhibition of this EXOC8-RalA interaction reduces invasion in PC3 cells (Hazelett and Yeaman, 2012). As a result, the function of EXOC8 must be tightly regulated to maintain normal cellular homeostasis and prevent pathological processes such as cancer.

1.5.2. Future perspectives

There are undoubtedly many other diseases that are caused by dysfunction of EXOC8 and the exocyst complex. The fact that the exocyst is an essential gene in animals and that conditional or heterozygous mutant mice display developmental defects, demonstrates the importance of the exocyst in health and disease. The essential nature of the exocyst complex means that many mutations are probably early embryonic lethal and have therefore not been observed in human genetic disease. Mutations that have a milder effect might be extremely rare, as in the case of the sole JBTS patient, and therefore are yet to be

uncovered. Thus, it is vitally important that future studies investigate the mechanism and regulation of the exocyst complex at a cellular and pathological level.

1.6. EXOC8 localises to rod and ring structures

EXOC8 localises to organelles not associated with the late secretory pathway suggesting that it may function in a multitude of cellular roles distinct from exocytosis (Wang et al., 2004). During my undergraduate studies, I discovered that EXOC8 localises to previously unrecognised rod and ring like structures in the cytoplasm. This MbyRes thesis looks to elucidate what these EXOC8 rod and ring structures are and what cellular function they have. Based on the literature, there are four existing possibilities for what these EXOC8 rods and rings could be: 1) cytoplasmic rods and rings, 2) cytoophidia, 3) Loukoumasomes or 4) Apical Ceramide Enriched Compartments (ACECs). All are poorly characterised structures whose functions in the cell remain to be understood, but are linked to metabolic regulation, particularly purine and pyrimidine synthesis. Below, each structure will be discussed in turn.

1.7. Cytoplasmic rods and rings

1.7.1. Discovery of cytoplasmic rods and rings

Cytoplasmic rods (~3–10 μm in length) and cytoplasmic rings (~2–5 μm in diameter) were initially discovered in chronic hepatitis C virus (HCV) patients, treated with interferon-α/ribavirin combination therapy (IFN/RBV). Here, examination of patients' sera by indirect immunofluorescence using the Hep-2 cell assay, revealed human autoantibodies against cytoplasmic rods and rings (Covini et al., 2012). Subsequent studies revealed that cytoplasmic rods and rings were highly enriched in two rate-limiting enzymes involved in the catalysis of guanosine triphosphate (GTP) and cytidine triphosphate (CTP).

1.7.2. Components of cytoplasmic rods and rings

Inosine monophosphate dehydrogenase (IMPDH) and cytidine triphosphate synthase (CTPS) are key enzymes in the nucleotide synthetic pathway. IMPDH catalyses the conversion of inosine monophosphate (IMP) to xanthosine monophosphate (XMP) which is the rate limiting step in *de novo* guanine nucleotide synthesis (GTP) (Hedstrom, 2009). IMPDH plays an important role in cell proliferation and transformation and is therefore a common target for

immunosuppressive and cancer treatment (Hedstrom, 2009). In mammals there are two IMPDH isoforms: IMPDH1 and IMPDH2. IMPDH1 and IMPDH2 are encoded on separate genes and share 84% sequence homology (Carr et al., 1993). Whereas IMPDH2 is upregulated in proliferating tissues, IMPDH1 is constitutively expressed at low levels in multiple tissues (Hedstrom, 2009). Furthermore, knockout of IMPDH2 is embryonically lethal in mice, suggesting that it is required to maintain guanine nucleotide pools needed for cellular proliferation (Gu et al., 2000). On the other hand, CTPS catalyses the conversion of uridine triphosphate (UTP) into cytidine triphosphate (CTP) which is the rate limiting step in de novo cytidine nucleotide synthesis (CTP, Figure 1.5) (Long and Pardee, 1967; Weng and Zalkin, 1987). Similarly, to IMPDH, CTPS has two mammalian isoforms: CTPS1 and CTPS2 which share 74% sequence homology (Van Kuilenburg et al., 2000). Again, similarly to IMPDH enzymes, CTPS enzymes are the target of antiparasitic therapy and cancer treatment (Hofer et al., 2001; Kursula et al., 2006). Given that cytoplasmic rods and rings are enriched in enzymes required for nucleotide metabolism, it is believed that they are structures that have a role in cellular metabolism and metabolic regulation. However, the precise role of such structures remains unknown.

IMPDH2 is the major constituent of cytoplasmic rods and rings. IMPDH2 reacted with all sera containing anti-cytoplasmic rods and rings positive autoantibodies (Probst et al., 2013). Furthermore, patient sera containing anti-cytoplasmic rods and rings positive autoantibodies immunoprecipitated with a 55 kDa doublet which corresponds to IMPDH1/2 (Cam et al., 1993; Carcamo et al., 2011). However, there is varying evidence as to whether CTPS1 is a component of cytoplasmic rods and rings. CTPS1 did not react with any sera containing anti-cytoplasmic rods and rings positive autoantibodies (Probst et al., 2013). As a result, Probst et al., 2013 stated that CTPS1 is an unlikely target of cytoplasmic rod and ring autoantibodies.

It should be noted that there is a large overlap between CTPS1-containing cytoplasmic rods and rings and cytoophidia (discussed below). As a result, it is hard to disentangle whether the above mentioned CTPS1-containing structures are cytoplasmic rods and rings or cytoophidia. It is apparent that the terms “cytoplasmic rods and rings” and “cytoophidia” are used interchangeably. It is therefore possible that CTPS1-containing structures are “cytoophidia”. This could

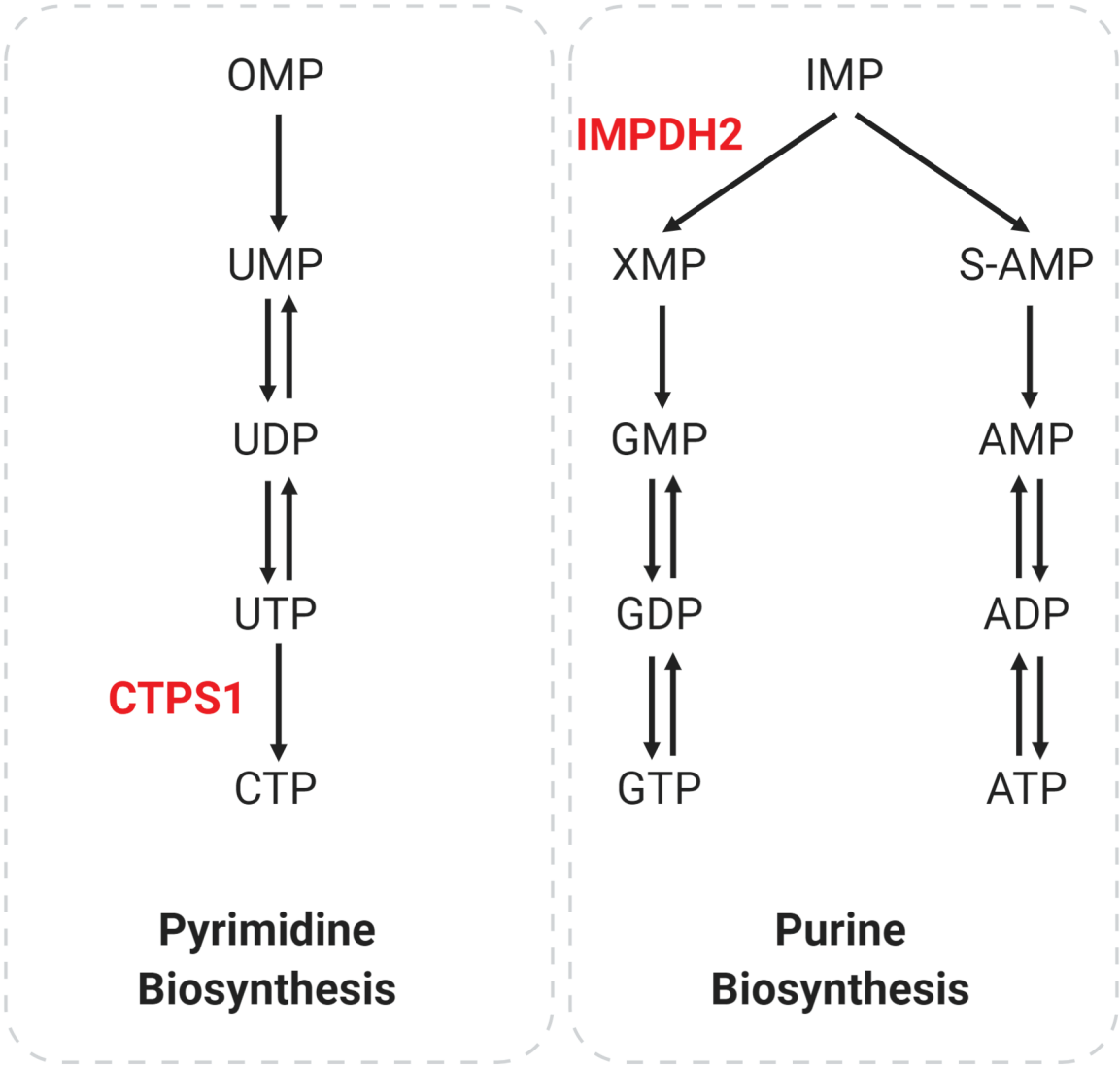

Figure 1.5. Role of IMPDH2 and CTPS1 in nucleotide synthesis. Both IMPDH2 and CTPS1 are key enzymes in the nucleotide biosynthetic pathway. Figure created with BioRender.com

explain the lack of evidence supporting CTPS1 as a component of cytoplasmic rods and rings. This section (1.7) will therefore describe IMPDH2 containing cytoplasmic rods and rings. CTPS1 containing rods and rings or cytoophidia will be discussed below in section 1.8.

Until recently it was unknown if cytoplasmic rods and rings were enriched in other proteins aside from CTPS and IMPDH. Given that cytoplasmic rods and rings are non-membranous structures it seemed likely that other protein constituents are present that act as a tether. Furthermore, given the large size of cytoplasmic rods and rings, it is plausible that rods and rings are composed of other proteins or enzymes. However, analysis of cytoplasmic rods and ring structures has shown that rods and rings are not enriched in actin, α- and β-tubulin or vimentin (Carcamo et al., 2011). In addition, cytoplasmic rods and rings did not associate with the Golgi, processing-bodies (P-bodies), the centrosome, cilia, mitochondria or autophagosomes (Carcamo et al., 2011; Schiavon et al., 2018). This begged the question: are there other components of cytoplasmic rods and rings? In 2018, Schiavon *et al.*, discovered that ARF-like 2 (ARL2), a regulatory GTPase localised to IMPDH2 positive cytoplasmic rods and rings. This was confirmed using three different monoclonal antibodies raised against ARL2 which localised to both endogenous and induced IMPDH2 cytoplasmic rods and rings. ARL2 did not co-localise with CTPS1 containing cytoplasmic rods and rings, further supporting the idea that CTPS1 containing structures are cytoophidia (Schiavon et al., 2018). The ARL2 binding partners, cofactor D, and ELMOD2 also localised to IMPDH2 rods and rings suggesting that cytoplasmic rods and rings are enriched in a multitude of proteins not necessarily related to nucleotide metabolism (Schiavon et al., 2018).

Until 2018, the general consensus was that cytoplasmic rods and rings are non-membranous structures (Calise et al., 2016; Carcamo et al., 2011). Cytoplasmic rods and rings have since been shown to associate with an ER-derived membrane (Schiavon et al., 2018). IMPDH2 and ARL2 containing rods and rings co-localise with Calnexin, a chaperone which resides in ER-derived membrane and Glucose-regulated protein-78 (GRP78), a chaperone which regulates ER homeostasis (Schiavon et al., 2018). However, the ER protein, calreticulin, did not localise with cytoplasmic rods and rings, demonstrating that only a subset of ER proteins co-localise with such structures (Schiavon et al., 2018). It is therefore

possible that only a specific domain or membrane of the ER interacts with cytoplasmic rods and rings, thus making cytoplasmic rods and rings membrane-associated.

1.7.3. Characteristics of cytoplasmic rods and rings

Morphologically, cytoplasmic rods are ~3–10 µm in length whereas cytoplasmic rings are ~2–5 µm in diameter (Carcamo et al., 2011; Thomas et al., 2012). On average there are one to two cytoplasmic rods and/or rings per cell (Carcamo et al., 2011; Thomas et al., 2012). As suggested by their name, rods and rings localise in the cytoplasm of cells. Specifically, cytoplasmic rods and rings are perinuclear with Carcamo *et al.*, 2011 stating that 40 % of rods localise adjacent to the nucleus (Thomas et al., 2012). However, smaller rods and rings have been observed in the nucleus when the formation of these structures are induced (Juda et al., 2014). Cytoplasmic rods and rings have differing conformations. For example, they have been observed as twisted and elongated rings, rods with pin loops and large figure of eight structures (Carcamo et al., 2011). It is unknown if the conformation is related to function, but it is possible that rods transition to rings via these intermediate conformations, although this has yet to be explored in detail.

1.7.4. Induction of cytoplasmic rods and rings

Inhibition of IMPDH2 has been found to induce the assembly of cytoplasmic rods and rings in immortalised cell lines, primary cell lines and untreated embryonic stem cells. Cytoplasmic rod and ring induction can be achieved using the IMPDH2 inhibitors mycophenolic acid (MPA) or ribavirin (Carcamo et al., 2011; Ji et al., 2006; Keppeke et al., 2015; Keppeke et al., 2019; Schiavon et al., 2018). Such inhibition increases both the frequency and size of cytoplasmic rods and rings although there is a more robust increase in cytoplasmic rods than rings. Inhibition of IMPDH2 does not induce the formation of CTPS1 containing rods and rings, providing evidence that CTPS1 and IMPDH2 rods and rings are distinct structures (Carcamo et al., 2011). However, given that some cytoplasmic rods and rings co-stain for both CTPS1 and IMPDH2 it is possible there is some overlap in structures as a result of being evolutionarily related (Chang et al., 2015; Keppeke et al., 2015).

In addition to inhibition, induction of cytoplasmic rods and rings can occur by depriving cells of different metabolites. Cells grown in culture medium deprived

of glucose for 48 hours, had increased numbers of IMPDH2 containing cytoplasmic rods and rings. However, the increase in cytoplasmic rods and rings was slower and not as substantial when compared to other induction methods such as IMPDH2 inhibition by MPA. Furthermore, whereas inhibiting IMPDH2 with MPA induced rods and rings in all cell lines (with the exception of NRK cells which had near to no difference in proportion of cytoplasmic rods and rings after MPA treatment), glucose starvation only induced rods and rings in specific cells lines. Glucose starvation induced rod and ring formation in IMCD3, NRK, MDCK, and NIH-3T3 cells but had no effect on the numbers of rods and rings in HeLa, COS7, G361 and human fibroblasts.

Glutamine starvation has also been shown to induce the formation of cytoplasmic rods and rings (Calise et al., 2014). Glutamine is an important amino acid that is a required substrate for *de novo* nucleotide synthesis. Cells deprived of glutamine formed cytoplasmic rods and rings after two days (Calise et al., 2014). Re-addition of glutamine to glutamine deprived cells, resulted in disassembly of induced cytoplasmic rods and rings. Similarly, supplementing glutamine deprived cells with guanosine resulted in the disassembly of induced cytoplasmic rods and rings (Calise et al., 2014).

As discussed, glutamine deprivation induces cells to form cytoplasmic rods and rings. Cells grown in glutamine deprived Dulbecco's modified Eagle's medium (DMEM) induced cytoplasmic rods and ring formation. However, cells grown in Minimum Essential Medium (MEM), induced cytoplasmic rod and ring formation, even in the presence of 2 mM glutamine (Calise et al., 2016). Comparison of the formulations of MEM and DMEM, showed that their compositions differed; unlike DMEM, MEM contains no Iron (III) nitrate ($Fe(NO_3)_3 \bullet 9H2O$), glycine or L-serine. As a result, Calise *et al.*, 2016, examined the effect of MEM on the induction of cytoplasmic rods and rings in HeLa cells. Cytoplasmic rods and rings are endogenously present in HeLa cells but can be induced using MPA (Carcamo et al., 2011). MEM induced the formation of cytoplasmic rods and rings in HeLa cells, suggetsing that the absence of glycine and L-serine can induce rod and ring formation (Calise et al., 2016). However further analysis showed that whereas L-serine deprivation promotes the formation of cytoplasmic rods and rings, glycine supplementation promoted their formation (Calise et al., 2016).

Cytoplasmic rods and rings can also be induced by treating cells with 5-aminoimidazole-4-carboxamide ribonucleotide (AICAR) (Schiavon et al., 2018). AICAR is a selective activator of adenosine monophosphate protein kinase (AMPK) which plays a role modulating cellular energy through the regulation of glucose and lipid metabolism. In addition, AICAR is an intermediate protein in the IMP pathway of *de novo* guanine nucleotide synthesis. Within 2 hours of treatment with AICAR, HeLa, MEF, NRK and IMCD3 cells all displayed at least one cytoplasmic rod and/or ring that stained positive for IMPDH2. Apart from NRK cells, induced cytoplasmic rods and rings were larger than their endogenous counterparts. However, all AICAR induced rods and rings were smaller than MPA induced rods and rings (Schiavon et al., 2018).

1.7.5. Rods and rings are cell line specific

As aforementioned cytoplasmic rods and rings are present in a variety of cell lines both endogenously and induced. Cytoplasmic rods and rings are present in immortalised cell lines, primary cell lines and untreated embryonic stem cells (Table 1.2).

1.7.6. Structure of cytoplasmic rods and rings

IMPDH predominantly exist as stable homotetramers that weigh 55 kDa (Carr et al., 1993). IMPDH tetramers can reversibly assemble into linearly stacked octamers when ATP or GTP binds IMPDHs canonical sites (Keppeke et al., 2018). Octamers of human IMPDH1 are then able to stack head-to head to form IMPDH fibres (Labesse et al., 2013). It is then thought that these IMPDH fibres assemble into higher order filamentous structures such as cytoplasmic rods and rings (Labesse et al., 2013).

This is supported by studies which show that IMPDH2 cytoplasmic rods and rings share a similar filamentous ultrastructure. Both are composed of long interwoven fibres that are not enclosed by a membrane (Juda et al., 2014). Individual fibres are arranged in parallel, with each fibre approximately 8.5 nm in diameter and 11 nm in length. Fibres are arranged in bundles composed of regulatory repeating parallel subunits (Juda et al., 2014). This is similar to Aughey *et al.*, 2014 who reported that cytoplasmic rods and rings were composed of linear elements with regular striations approximately 10 nm spacing (Aughey et al., 2014).

Type of cell line	Cell Line	Endogenous cytoplasmic rods and rings	Induced cytoplasmic rods and rings	Reference(s)
Immortalised cell Lines	Human epithelial type 2 (HEp-2) cells			(Carcamo et al., 2011; Juda et al., 2014; Magerl et al., 2019)
	Human cervical (HeLa) cells			(Calise et al., 2014; Carcamo et al., 2011; Chang et al., 2018; Gou et al., 2014; Keppeke et al., 2015b; Schiavon et al., 2018)
	African Green Monkey (COS-7) fibroblast cells			(Keppeke et al., 2015a; Keppeke et al., 2015b; Schiavon et al., 2018)
	Centre Antoine Lacassagne-27 (CAL-27) cells			(Carcamo et al., 2011; Covini et al., 2012)
	Human colorectal carcinoma (HCT116) cells			(Carcamo et al., 2011; Covini et al., 2012)
	Human monocytic (ITHP-1) cells			(Carcamo et al., 2011)
	Mouse (NIH-3T3) fibroblast cells			(Carcamo et al., 2011; Carcamo et al., 2014; Juda et al., 2014; Schiavon et al., 2018; Willingham et al., 1987)
	Chinese Hamster Ovary (CHO)			(Gunter et al., 2008; Stinton et al., 2013)
	Mouse embryonic fibroblasts (MEF) cells			(Schiavon et al., 2018)
	Normal Rat Kidney Epithelial (NRK) cells			(Carcamo et al., 2011; Carcamo et al., 2014; Schiavon et al., 2018)
	Human Embryonic Kidney (HEK-293T) cells			(Chang et al., 2015)
	Mouse Inner Medullary Collecting Duct cells (mIMCD3) cells			Carcamo et al., 2011; Schiavon et al., 2018)
	Madin-Darby Canine Kidney (MDCK) cells			(Schiavon et al., 2018)
Primary cell lines	Mouse primary cardiomyocytes			(Carcamo et al., 2011)
Other cell lines	Untreated Embryonic Stem Cells			(Carcamo et al., 2011)
	Human malignant melanoma (G361) cells			(Schiavon et al., 2018)
	Human fibroblast (hFB) cells			(Schiavon et al., 2018)
	Male Rat kangaroo kidney epithelial (Ptk2) cells			(Carcamo et al., 2014)
	Mouse leukemic monocyte/macrophage cells (RAW264.7)			(Carcamo et al., 2014)

Table 1.2. Presence of either endogenous or induced cytoplasmic rods and rings in multiple different cell lines. Green denotes cytoplasmic rods and rings were detected, pink denotes cytoplasmic rods and rings were not detected and white denotes no available information. N.B. Split green- pink boxes denote the presence of cytoplasmic rods and rings in one study but the absence of cytoplasmic rods and rings in another.

1.7.7. Biological function of cytoplasmic rods and rings

The function of cytoplasmic rods and rings is poorly understood. However, it is believed that they are formed as a result of decreased intracellular levels of CTP or GTP. For example, the highly proliferative embryonic stem cell (ESC), forms high numbers of cytoplasmic rods and rings without induction. As a result, it is speculated that due to the metabolism of ESCs, there are low levels of CTP and GTP which induces the formation of cytoplasmic rods and rings. This is consistent with data that shows that depleting the intracellular pool of CTP and GTP by drugs, induces the formation of cytoplasmic rods and rings. It is therefore possible that cytoplasmic rods and rings act as a homeostatic control for nucleotide metabolism. The structure of cytoplasmic rods and rings could increase the proportion of active IMPDH/CTPS1 enzymes, which in turn increases the *de novo* synthesis of CTP and GTP, to restore intracellular nucleotide levels for DNA/RNA synthesis.

As aforementioned, hyperproliferative cells such as T cells, B cells, stem cells and thymocytes contain a high proportion of spontaneously formed IMPDH2 rod and ring filaments (Calise et al., 2018; Carr et al., 1993; Thomas et al., 2012). This therefore begs the question, why are there high proportions of IMPDH2 rods and rings in proliferating cells? One possibility is the role of IMPDH2 rod and ring filaments in maintaining guanine nucleotide levels. For example, in hyperproliferating cells such as T cells and B cells, IMPDH2 assembles into rod and ring filaments to increase guanine nucleotide levels required for proliferation. Recent studies have suggested that filamentous IMPDH2 functions *in vitro* to resist allosteric inhibition of IMPDH2 by guanine nucleotides, to allow a steady production of guanine nucleotides (Buey et al., 2015; Johnson and Kollman, 2020). Buey et al., 2015 showed *in vitro* that whilst both momomeric IMPDH2 and reconstituted IMPDH2 filaments had similar enzymatic activity, filamentous IMPDH2 was significantly more resistant to inhibition by allosteric binding of either GTP or GDP (Buey et al., 2015). This is supported by recent work of Johnson and Kollman, 2020 who demonstrated *in vitro* that IMPDH2 filament assembly was dependent on low guanine nucleotide levels and high IMP levels. Using cryo-EM, Johnson and Kollman, 2020, showed that under physiologically high IMP levels, IMPDH2 assembled into rod and ring filaments, which resist an inactive state, even at high GTP levels (Johnson and Kollman, 2020). Therefore, IMPDH2 filamentation could serve to confer resistance to feedback inhibition, thus

promoting the expansion of guanine nucleotide pools in cells that require atypically high levels of guanine nucleotides.

1.8. Cytoophidia

As previously discussed, the terms “cytoplasmic rods and rings” and “cytoophidia” are used interchangeably. This section will focus on CTPS1 containing cytoplasmic rods and rings termed cytoophidia (Greek for “cellular snakes”). In 2010, three independent research groups discovered that CTPS1 compartmentalised into filaments known as cytoophidia (Ingerson-Mahar et al., 2010; Liu, 2010; Noree et al., 2010). CTPS catalyses the conversion of uridine triphosphate (UTP) into cytidine triphosphate (CTP) which is the rate limiting step in *de novo* cytidine nucleotide synthesis (CTP) (Long and Pardee, 1967; Weng and Zalkin, 1987).

1.8.1. Components of cytoophidia

CTPS1 is the major component of cytoophidia in both eukaryotes, *D. melanogaster, D. virilis, D. pseudoobscura, E. coli*, *S. pombe*, *S. cerevisiae* and *Rattus norvegicus* and the prokaryote *Caulobacter crescentus.* However, mixed cytoophidia containing both CTPS1 and IMPDH2 have been reported in mammalian cells (Chang et al., 2018; Keppeke et al., 2015). Unlike cytoplasmic rods and rings which colocalise with ARL2, ARL2 rarely colocalises with mammalian cytoophidia, further suggesting that cytoplasmic rods and rings and cytoophidia are distinct structures (Schiavon et al., 2018).

Interestingly, cytoophidia in *Drosophila,* have been found to associate with a variety of proteins. Cytoophidia present in *Drosophila* follicle cells associate with the microtubule network but not centrioles (Liu, 2010). Furthermore, micro-cytoophidia in follicle cells can couple to Golgi particles (Liu, 2010). Here, each micro-cytoophidia is capable of coupling to one or two Golgi particles via one or both of its ends. In germline nurse cells, cytoophidia colocalise with non-receptor tyrosine kinase DA ck (the homologue of mammalian activated cdc42-associated kinase 1 (ACK1)) (Strochlic et al., 2014). *Drosophila* lacking DA ck, had abnormal cytoophidia that appeared fragmented (Strochlic et al., 2014). This suggests that DA ck, has a role in regulating the morphology of cytoophidia.

1.8.2. Characteristics of cytoophidia

There is a large amount of morphological variation between cytoophidia of different species. In mammalian cells cytoophidia are characteristically similar to cytoplasmic rods; in its linear form, cytoophidia are ~ 3–10 μm in length (Liu, 2011). Like, cytoplasmic rods and rings, cytoophidia are predominantly cytoplasmic based, but cytoophidia have also been observed in the nucleus in both mammalian and *S. pombe* cells (Gou et al., 2014). Toroidal cytoophidia also exist, however these are rare and mammalian cytoophidia are predominantly linear and elongated (Noree et al., 2010). To this, Schiavon *et al.*, 2018, described mammalian cytoophidia as short, thick filaments lacking ring morphology (Schiavon et al., 2018).

Cytoophidia have been observed in *Drosophila* germline cells, follicle cells and in larval lymph glands, and it is only in larval lymph glands that cytoophidia are ring or C-shaped. In the *Drosophila* female germline, two variants of linear cytoophidia exist. As a result many papers subdivide cytoophidia into either marco- or micro-cytoophidia (Azzam and Liu, 2013). Macro-cytoophidia are large filamentous structures comprised of CTPS polymers. Macro-cytoophidia can break apart to form micro-cytoophidia and conversely micro-cytoophidia can undergo several rounds of fusion to form macro-cytoophidia. In *Drosophila* female germline cells, macro-cytoophidia are thick, often exceeding 30 μm in length, while micro-cytoophidia are small and short at 1-3 μm (Liu, 2010). In the germline, hundreds of thousands of micro-cytoophidia exist, whereas follicle cells contain just one cytoophidia.

Owing to their small cell size, cytoophidia in both yeast and the bacterium *Caulobacter crescentus* are considerably smaller than their mammalian and *Drosophila* counterparts. It is therefore possible that given the structural differences between mammalian and bacterial cytoophidia, cytoophidia have arisen independently in different lineages, hence offering an explanation for their differing functions (section 1.8.6). The presence of cytoophidia in bacteria, indicate that cytoophidia have evolved exceptionally early and have a fundamental role in the cell. Cytoophidia are ~ 500 nm in *C. crescentus* and exist towards the cell surface at sites of membrane curvature (Ingerson-Mahar et al., 2010). In the budding yeast *S. Cerevisiae*, cytoophidia are referred to as “stubby” and are ~ 2 μm in length (Noree et al., 2010).

1.8.3. Induction of cytoophidia

Inhibition of CTPS1 has been found to induce the assembly of cytoophidia in human cells. HEp-2 cells treated with the CTPS1 inhibitor -diazo-5-oxo-l-norleucine (DON) or the CTPS1 inhibitor acivicin, had increased numbers of cytoophidia, with cells predominantly displaying two cytoophidia (Carcamo et al., 2011). The CTPS1 inhibitor DON was also found to induce cytoophidia formation in other mammalian cell lines such as HEK-293 and COS-7 cells (Keppeke et al., 2015; Sun and Liu, 2019). Similarly, DON induces the formation of cytoophidia in *Drosophila* tissues (Chen et al., 2011). However, in the bacteria *C. crescentus,* the addition of DON was found to cause the dissociation of cytoophidia (Ingerson-Mahar et al., 2010). This suggests that the regulation and formation of cytoophidia differs between organisms.

Interestingly, cells treated with the IMPDH2 inhibitor MPA also displayed increased numbers of cytoophidia (Chang et al., 2015). This suggests that there is a functional overlap between cytoplasmic rods and rings and cytoophidia.

Similarly to cytoplasmic rods and rings, glutamine deprivation also promotes the formation cytoophidia in HeLa cells (Gou et al., 2014). HeLa cells cultured in glutamine deprived medium formed cytoophidia in both the cytoplasm and the nucleus. In contrast, Calise *et al.*, 2014, found that depriving HeLa cells of glutamine, increased CTPS1 mRNA levels but had little effect on increasing CTPS1 protein levels (Calise et al., 2014). Finally, unlike cytoplasmic rods and rings, neither AICAR or glucose starvation induced the formation of cytoophdia in HeLa cells (Schiavon et al., 2018).

On the other hand, media lacking glucose was found to strongly induce cytoophidia formation in *S. cerevisiae* (Noree et al., 2010). Furthermore, the addition of CTP to yeast cells increased the amount of cytoophidia in *S. cerevisiae* (Noree et al., 2010). This suggests that the formation of cytoophidia in yeast is dependent on nutrient availability.

1.8.4. Cytoophidia are present in multiple organisms

Unlike IMPDH containing cytoplasmic rods and rings, cytoophidia have been discovered in a multitude of organisms. Both budding and fission yeast form cytoophidia, with cytoophidia particularly prominent in yeast undergoing nutrient starvation (Noree et al., 2010; Shen et al., 2016; Zhang et al., 2014). Cytoophdia

have also been observed in *E. coli,* the bacteria *C. crescentus, and Drosophila Melanogaster* (Liu, 2010; Tastan and Liu, 2015).

Similarly, to cytoplasmic rods and rings, cytoophidia are present in a variety of cell lines both endogenously and induced (Table 1.3).

1.8.5. Structure of cytoophidia

Cytoophidia are long membraneless filamentous bundles composed of stacked CTPS tetramers (Lynch et al., 2017). This homo-tetrameric structure of CTPS is conserved across organisms. In *Drosophila,* it has been observed that CTPS1 does not distribute evenly in macro-cytoophidia bundles. Instead, CTPS1 is discontinuous and is absent from intermittent gaps along the filaments (Liu, 2010). It is speculated that these gaps contain additional components that are involved in cytoophidia assembly and formation.

1.8.6. Function of cytoophidia

Given that cytoophidia are conserved between prokaryotes and eukaryotes, it is likely that cytoophidia have an important biological function. Cytoophidia are thought to be involved in metabolic regulation. In bacteria, the formation of cytoophidia inhibits its enzymatic activity (Aughey et al., 2014; Barry et al., 2014). Here, the presence of CTP induces the formation of cytoophidia and inhibits the activity of CTPS, preventing further build up of CTP in the cytoplasm. Cytoophidia therefore act as a switch that respond to CTP levels, in order to maintain nucleotide homeostasis. In contrast, some studies have shown that human cytoophidia have increased enzymatic activity (Lynch et al., 2017; Sun and Liu, 2019). However, it is unclear, why a catalytically active cytoophidia is formed in response to increased CTP levels. Lynch *et al.*, 2017, speculate that stabilising CTPS in the cytoophidia keeps CTPS active and primed for activity if nucleotide levels change. Other studies state that the formation of cytoophidia sequesters CTPS activity, but increases its half-life (Sun and Liu, 2019). Here it is speculated that cytoophidia act as a CTPS storage pool that prevents ubiquitin-proteasome CTPS degradation. Ubiquitination of a protein leads to its degradation by the proteosome. CTPS contains 18 potential ubiquitination sites, and is therefore a target of the ubiquitin-proteosome system (Noree et al., 2014; Sun and Liu, 2019). However, when multiple CTPS tetramers bundle together to form the cytoophidium, CTPS ubiquitnation sites are no longer acessible. This suggests

Type of cell line	Cell Line	Endogenous cytoophidia	Induced cytoophidia	Reference(s)
Immortalised cell Lines	Human epithelial type 2 (HEp-2) cells			(Carcamo et al., 2011; Keppeke et al., 2015)
	Human cervical (HeLa) cells			(Carcamo et al., 2011; Keppeke et al., 2015; Chang et al., 2018; Sun and Liu, 2019)
	African Green Monkey (COS-7) fibroblast cells			(Keppeke et al., 2015)
	Normal Rat Kidney Epithelial (NRK) cells			(Schiavon et al., 2018)
	Mouse Inner Medullary Collecting Duct cells (mIMCD3) cells			(Schiavon et al., 2018)
Other cell lines	Mouse hepatocellular carcinoma (BNL 1ME A. 7R. 1) cells			(Guo et al., 2014)

Table 1.3. Presence of either endogenous or induced cytoophidia in multiple different cell lines. Green denotes cytoophidia were detected, pink denotes cytoophidia were not detected and white denotes no available information. N.B. Split green- pink boxes denote the presence of ccytoophidia in one study but the absence of cytoplasmic rods and rings in another.

that the formation of cytoophidia prevents CTPS ubiquitination and subsequent degradation, allowing cells to store CTPS until required.

Cytoophidia in *C. crescentus* are bi-functional (Ingerson-Mahar et al., 2010). Alongside the enzymatic function, cytoophidia act as a filament that regulates membrane curvature in conjunction with intermediate filaments (Ingerson-Mahar et al., 2010). Furthermore, given that cytoophidia associate with the microtubule network, it is possible that alongside their metabolic function they have cytoskeletal properties. However, this has yet to be explored in detail in other organisms.

The precise function of the cytoophidia has yet to be elucidated and research into cytoophidia is in its infancy. As a result, many questions remain. Why are cytoophidia present in both eukaryotic and prokaryotic lineages? How are cytoophidia formed? Why does a metabolic enzyme form into filaments? Answering these questions are crucial if we are to gain an understanding of the significance of cytoophidia.

1.9. Loukoumasomes

In 2010, a large organelle termed the loukoumasome or “doughnut-body” (*Loukoumades* = doughnut, *soma* = body (Greek)) was identified in a subset of rat adrenergic sympathetic neurons (Ramer et al., 2010). Loukoumasomes are similarly shaped to both cytoplasmic rods and rings and cytoophidia and exist as both linear and toroidal structures. Furthermore, loukoumasome size is consistent with the size of cytoplasmic rods and rings ~ 6 μm (Ramer et al., 2010). However, unlike cytoplasmic rods and rings, which are restricted to the cytoplasm, loukoumasomes are present in the initial axon segment, the cell body cytoplasm and at perinuclear regions within nuclear envelope folds, only appearing once per neuron. Moreover, whereas cytoplasmic rods and rings are distinct cellular structures, the loukoumasome interacts with other organelles including the primary cilium and the nucleolus like-organelle the nematosome (Ramer et al., 2010).

Unlike cytoplasmic rods and rings and cytoophidia, loukoumasomes are not enriched in either CTP or GTP synthase but are highly enriched in tubulins. Known components of loukoumasomes include myosin IIb, and cenexin. βIII tubulin (SDL. 3D10) is also thought to be a component of loukoumasomes.

However, not all monoclonal βIII tubulins antibodies localise to loukoumasomes suggesting that loukoumasomes contain a specific βIII tubulin isotype (Ramer et al., 2010).

Since loukoumasomes contain non-muscle heavy chain myosin, it was hypothesised that loukoumasomes are dynamic organelles that are motile (Ramer et al., 2010). Here, Ramer *et al.*, 2010 hypothesised that loukoumasomes are intracellular transport machines responsible for trafficking proteins between the axon, the primary cilium and the nematosome. Given that loukoumasomes are known to contain γ-tubulin, a key protein of the centrosome, it is possible that the loukoumasome maintains centrosome function by supplying the proteins it needs (Ramer et al., 2010). Similarly, loukomasomes also contain the protein cenexin, which is required for centrosome positioning and ciliogenesis (Chang et al., 2013; Ramer et al., 2010). It is therefore possible that loukoumasomes play a role in the maintenance of the centrosome and primary cilium, through the shuttling of proteins. However, the link between the primary cilium, the axon and the nematosome remains unknown, as does the mechanisms behind loukoumasome motility.

More recently, loukoumasomes have been identified in human retinoblastoma tissue (Noble et al., 2016). Similarly, to neuronal-loukoumasomes, retinal-loukoumasomes were enriched in tubulins, specifically α- and βIII tubulin. The presence of βIII tubulin in loukomasomes was confirmed by an in-situ proximity ligation assay (PLA) which showed that βIII tubulin colocalised with detyrosinated tubulin present in loukoumasomes and microtubule associated protein 2 (MAP2) (Noble et al., 2016). MAP2 is a microtubule associated protein that stabilises MT and prevent MT depolymerisation (Dehmelt and Halpain, 2005). MAP2 has also been shown to be involved in cargo transport through the control of motor proteins (Gumy et al., 2017). It is therefore possible that the interaction between loukoumasomes and MAP2 facilitates the loukoumasome motility observed by Ramer et al., 2010.

1.10. Apical Ceramide enriched compartments

The sphingolipid ceramide has been shown to be important for the formation and regulation of cilia (Wang et al., 2009). Polarised Madin–Darby canine kidney (MDCK) cells, contain a ceramide-enriched compartment at the base of the cilium

termed the Apical Ceramide Enriched Compartments (ACECs) (He et al., 2012). ACECs colocalise with Rab11a, a small Rab GTPase that regulates endocytic trafficking. Interestingly, ACECs enriched in Rab11a were found to colocalise and interact with the exocyst member EXOC4 (He et al., 2012). Furthermore, Rab11a has been shown to interact with EXOC6, suggesting that the ACEC acts as a hub for trafficking proteins (Oztan et al., 2007). Research into ACECs is in its infancy and the role of the exocyst here is unknown. However, the authors speculate that the exocyst mediates the association between ACECs and Rab GTPases, which are required for cilium formation.

1.11. Rods and rings and disease

Rod and ring structures have been observed in multiple cancers including human hepatocellular carcinoma, acral lentiginous melanoma and clear cell renal cell carcinoma (Chang et al., 2017; Keppeke et al., 2020; Ruan et al., 2020). Furthermore, in hepatoma patients CTPS1 activity is upregulated (Kizaki et al., 1980). However, the link between rods and rings and cancer has yet to be explored in detail. It is possible that due to cancer cells being highly proliferative, rod and ring structures form to regulate nucleotide metabolism. Further studies are required to examine the relationship between rod and ring structures and cancers and determine if rods and rings are a prognostic or therapeutic target.

1.12. Aims of this thesis

The overall aim of this master's project is to characterise the role of EXOC8 containing cytoplasmic rods and rings. Although other similar rods and ring structures have previously been described, the specific functions of such enigmatic structures have yet to be identified. Given the link between presence of rods and rings and disease, we sought to better understand the role of EXOC8 rods and rings. This study therefore asked:

- What are the physical, biochemical and kinetic parameters of EXOC8 rods and rings?
- Identify what proteins or cellular structures EXOC8 rods and rings associate with. Are EXOC8 rods and rings a component of previously described rod and rings structures?

- Assess how a disease related mutation in EXOC8 affects the physical, biochemical and kinetic parameters of EXOC8 rods and rings

2. Materials and Methods

Unless stated otherwise, all reagents were from Sigma-Aldrich.

2.1. Cell Culture

mIMCD3 cells (ATCC #CRL-2123), HepG2 cells (ATCC #HB-8065) COS-7 cells (ECACC #87021302) and HeLa cells (ECACC #93021013) were all cultured in Dulbecco's Modified Eagle's Medium (DMEM), high glucose + GlutaMAX (Thermo Fisher, Catalogue number : 61965026) supplemented with 10 % Foetal Bovine Serum (FBS, Thermo Fisher, Catalogue Number : 10270106) NIH-3T3 cells (ATCC #CRL-1658), were cultured in DMEM supplemented with 10 % Bovine Calf Serum (BCS, Merck from Sigma-Aldrich, Catalogue Number : 12138C). All cells were cultured at 37°C and 5% CO_2, and were routinely passaged at 60-70 % confluency using TrypLE Express (Gibco, Catalogue Number : 12604013). For all experiments, cells were between passage 9 and 22.

For transfection, mIMCD3 cells at 60-70 % confluency were transfected with 100 pmol of siRNA and/or 1000 ng of plasmid using Lipofectamine 3000 (Invitrogen) according to the manufacturer's instructions.

2.1.1. Induction of cytoplasmic rods and ring by glucose deprivation

For glucose starvation experiments, mIMCD3 cells were cultured in DMEM in 4 well plates and allowed to attach for a minimum of 6 hours. Following attachment, cells were washed twice in PBS and media was exchanged for Dulbecco's Modified Eagle's Medium, no glucose (DMEM, no glucose; Thermo Fisher, Catalogue number: 11966025) containing 10 % Foetal Bovine Serum and were incubated at 37°C and 5% CO_2 for 24 hours.

2.1.2. Induction of cytoplasmic rods and ring by IMPDH2 and CTPS1 inhibitors

Ribavirin (Sigma-Aldrich, R9644) was solubilised in water to a stock concentration of 50 mM. 6-diazo-5-oxo-L-norleucine (DON, Sigma-Aldrich; D2141) was solubilised in DMEM to a stock concentration of 100 mM. mIMCD3 cells were seeded and allowed to attach for a minimum of 12 hours. Ribavirin or DON were then added to cells at final concentrations of 1 mM were incubated at 37°C and 5% CO_2 for times ranging between 5 minutes to 24 hours.

2.2. siRNA

For EXOC8 knockdown, an *exoc8* siRNA pool was obtained from Invitrogen (Stealth siRNA). Target sequences were: 5'-CCAUGGGCAUGUUCGUGGAUGCUUU, 5' GACUGCUGGGUGAACUUGAGCUACA, 5'-GAGAGAGUUUGAGACGGACUUUGCA.

For IMPDH2 knockdown, an *impdh2* siRNA pool was obtained from Qiagen (Flexitube siRNA). Target sequences were: 5'- AACTAAGAAGATTACACTAAA, 5'- CAGGTCATTGGAGGCAATGTA

Medium GC non-targeting scrambled siRNA (Invitrogen) were used as the negative control for all knockdowns. Cells were processed 72-96 hours post-transfection.

2.3. Immunofluorescence and imaging

For immunofluorescence, cells lines were seeded at $8x10^4$ cells per 13 mm glass coverslip in 4 well plates (Nunc) and fixed in methanol (10 minutes at-20°c) or 2-4 % formaldehyde in phosphate buffered saline (PBS; 20 minutes at room temperature). Cells were permeabilised for 5 minutes with 0.5 % Triton-X100/PBS, blocked with 2 % Bovine Serum Albumin/0.1 % Triton-X/PBS and incubated with primary and secondary antibodies (Table 2.1). Cells were stained with DAPI (4′,6-diamidino-2-phenylindole; 1µg/ml) before being mounted using Vectashield® mounting media (Vector Laboratories).

Fluorescence microscopy was performed with a Zeiss AxioObserver Z1 epifluorescence microscope (Carl Zeiss) equipped with a motorised stage and using a PlanApo40x or PlanApo100x, 1.3NA oil immersion objective. Images were acquired using a CCD camera (Coolsnap HQ2, Photometrics) controlled by Axiovison software (Universal Imaging). Confocal microscopy was performed with a Zeiss LSM510 confocal microscope equipped with Airyscan (Carl Zeiss). Images from both microscopes were analysed and adjusted for contrast and brightness using FIJI (Image J) and Photoshop (Adobe).

Antibody	Supplier catalogue number	Species	Dilution (IF)	Dilution (WB)
PRIMARY ANTIBODIES				
Anti-alpha Tubulin (acetyl K40) [6-11B-1] antibody	abcam #ab24610	Mouse	1:500	-
Anti-CTPS1 antibody	ProteinTech # 15914-1-AP	Rabbit	1:500	-
Anti-EXOC8 antibody	Sigma-Aldrich #HPA027438	Rabbit	1:500	1:1000
Anti-GFP antibody [IgG1κ (clones 7.1 and 13.1)]	Roche #11814460001	Mouse	1:500	-
Anti-IMPDH2 antibody	Protein Tech # 12948-1-AP	Rabbit	1:1000	-
SECONDARY ANTIBODIES				
Goat anti-Rabbit, Alexa Fluor 488, IgG (H+L)	Invitrogen, Molecular Probes #A-11008	Rabbit	1:500	-
Goat anti-Mouse, Alexa Fluor 488, IgG (H+L)	Invitrogen, Molecular Probes #A-11029	Mouse	1:500	-
Goat anti-Rabbit Alexa Fluor 594, IgG (H+L)	Invitrogen, Molecular Probes #A-11037	Rabbit	1:500	-
Goat Anti-Mouse Alexa Fluor 594, IgG (H+L)	Invitrogen, Molecular Probes #A-11032	Mouse	1:500	-
Anti-Rabbit HRP	Sigma-Aldrich # A0545	Rabbit	-	1:20,000

Table 2.1. List of primary and secondary antibodies used in this thesis. Details of the primary and secondary antibodies used for immunofluorescence and Western blot experiments. The manufacturer and category number can be found for each antibody.

Filter set	Product ID	Manufacturer	Excitation (nm)	Emission (nm)
38 HE eGFP shift free	489038-9901-000	Carl Zeiss	BP 470/40	BP 525/50
43 HE Cy 3 shift free	489043-9901-000	Carl Zeiss	BP 550/25	BP 605/70
49 DAPI shift free	488049-9901-000	Carl Zeiss	G 365	BP 445/50

Table 2.2. Excitation and emission values are given as peak and spread. For example, in filter set 38 HE eGFP shift free, the excitation bandpass is centred at 470 nm with a 40 nm transmission permitted either side.

2.4. Site Directed Mutagenesis

pEGFP was a gift from the Schrader group (University of Exeter, UK). Full-length pEGFP-C3-EXOC8 was from Addgene (#53762). Primers containing the E265G patient mutation (5'GAGAGCCGTATTTTCCAGGCCGGCAATGCTAAAATCAAACGAGAG and 5'- CACTCTCGTTTGATTTTAGCATTGCCGGCCTGGAAAATACGGCTC) were designed to contain a NgoMIV restriction site. Polymerase chain reaction (PCR) amplification of pEGFP-C3-EXOC8 plasmid with above primers was performed using the Quickchange II Site-Directed Mutagenesis Kit (Agilent Technologies). The PCR product was transformed into XL10-Gold E.coli. Selected clones were checked by NgoMIV digest. The presence of the patient mutation and absence of other mutations were confirmed by sequencing (Eurofins Belgium; Figure 2.1).

2.5. GFP Trap

Two independent experiments R1 and R2, were conducted for each plasmid: pEGFP and pEGFP-C3-EXOC8. Cells were harvested, and collected pellets were washed in 10 ml of cold PBS, before being resuspended in 1.2 ml of ice-cold lysis buffer (130 mM Nacl, 20 mM Tris pH 8, 1 % NP-40) and rotated at 4°C for 30 minutes. Samples were centrifuged (16,000 xg, 15 min, 4°C) and the

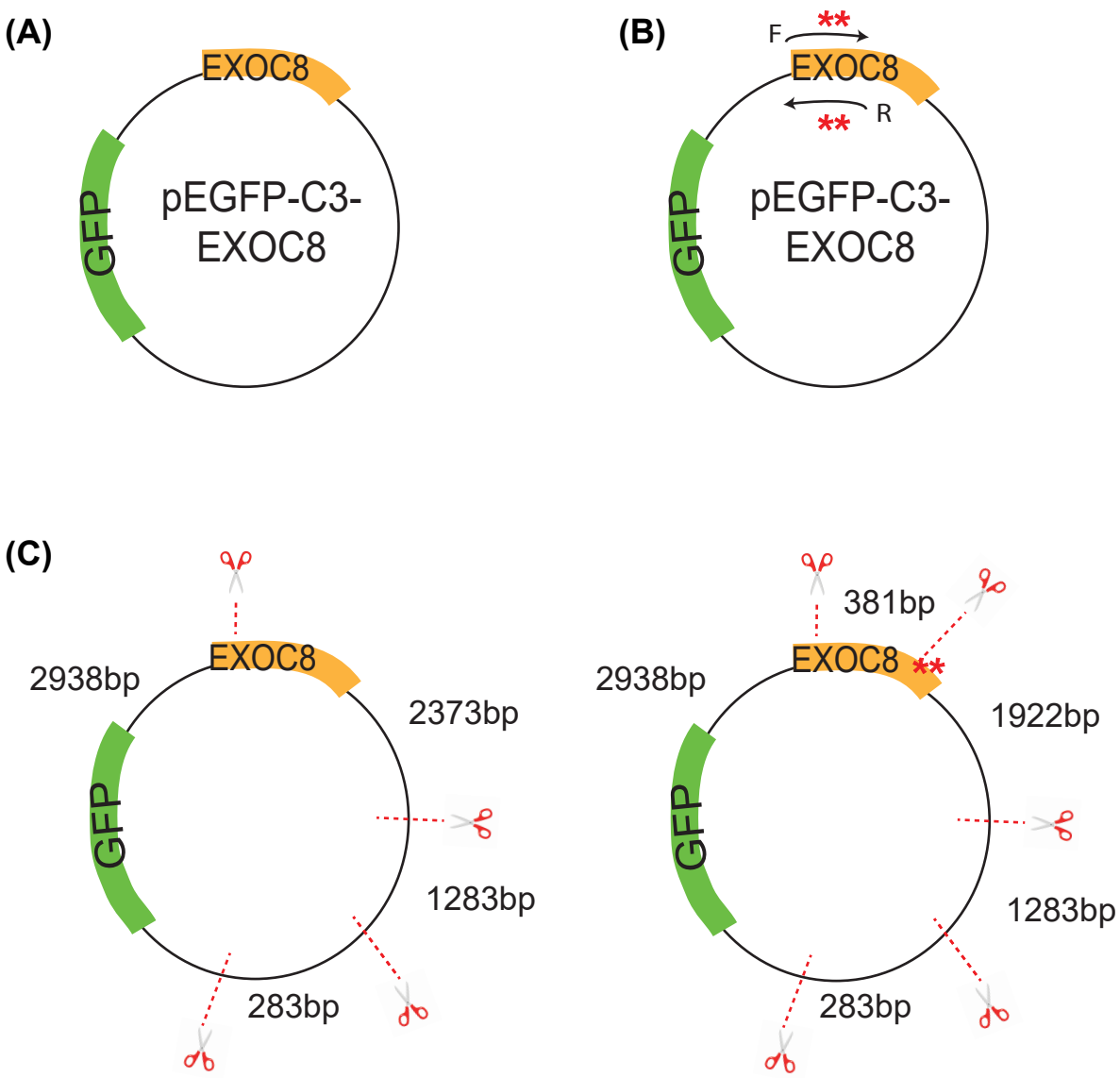

Figure 2.1. Site directed mutagenesis was used to introduce the E265G patient mutation into an existing EGFP-EXOC8 plasmid. **(A)** pEGFP-C3-EXOC8 was amplified by PCR, using matching primers containing the patient mutation **(B)**; see text for details).**(C)** Simplified pEGFP-C3-EXOC8 and pEGFP-C3-EXOC8-E265G plasmid maps, showing the positions of the NgoMIV restriction sites (scissors). Note the presence of an extra site in the E265G plasmid. .

supernatant retained as whole cell extract (WCE). 50 µl WCE was subsequently retained to confirm useable of GFP-tagged protein constructs by western blotting. 30 µl of washed GFP-Trap®_A beads (Chromotek GmBH) in lysis buffer were added to the remaining supernatant and incubated rolling overnight at 4°C. Beads were then centrifuged (700 xg, 1 min, 4°C) washed twice in 400 µl of lysis buffer, and resuspended in 50 µl of lysis buffer. 10 % of this final volume (5 µl) was retained for western blotting. The remaining 90 % (45 µl) was stored at -80°C before being sent for mass spectrometry at the Bristol proteomics facility (Figure 2.2).

2.5.1. Western Blotting

GFP-Trap samples were run on 10% SDS-polyacrylamide gels (Appendix Table 1). Gels were transferred overnight at 30 V to methanol-activated PVDF membranes. Membranes were blocked in PBS 5 % non-fat milk before incubating with 1:1000 anti-GFP antibody (Roche 11814460001) for one hour. Membranes were washed three times with PBS 0.05% Tween before incubation with 1:40,000 anti-mouse secondary antibody (Sigma, A9044) for one hour. Primary and secondary antibodies were both diluted in PBS 2.5% non-fat milk. Amersham ECL Western Blotting Detection Reagent (GE Healthcare, RPN2106) was used to develop membranes and chemiluminescent signal was detected using a Syngene G:BOX Chemi XRQ gel doc system.

2.5.2. Filtering of GFP-Trap data

The raw data from the GFP-Trap was filtered as follows. Proteins identified in the negative control GFP-Traps were combined to produce a list of ‘Negatives’ (n=1399) to which hits from the EXOC8 GFP-Traps were compared. Any protein either not detected in the ‘Negatives’, or having a score at least 2.5x higher in the GFP-exocyst pull-down, was considered a ‘true positive’ (n=974 for R1 and n=912 for R2). Lists were indexed against the MGI database and redundant (duplicate) entries were removed. Proteins that were true positives in both replicates were designated ‘double positive’ interactors (n=456, Figure 2.3, Appendix Table 2).

2.6. Immunoprecipitation

Cells were harvested, and collected pellets were washed in 10 ml of cold PBS, before being resuspended in 1 ml of ice-cold IP lysis buffer (20 mM Tris pH 7.2,

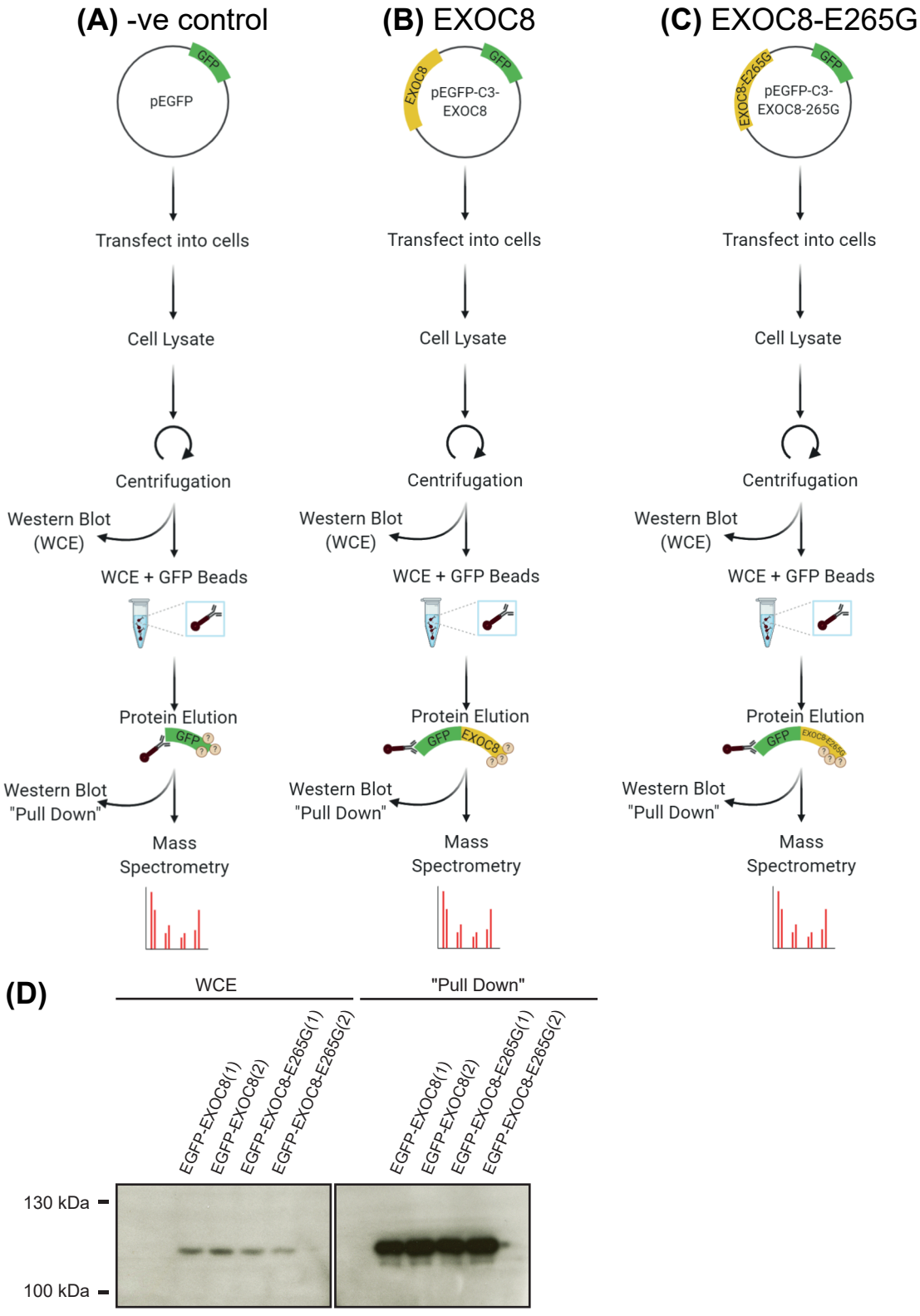

Figure 2.2. Illustration of GFP Trap methodology. Three GFP traps were performed, using **(A)** pEGFP as a negative control, **(B)** pEGFP-C3-EXOC8 or **(C)** pEGFP-C3-EX-OC8-E265G. **(D)** The presence of the GFP-EXOC8 and GFP-EXOC8-E265G before (WCE) and after (Pull Down) incubation with the beads was verified by western blot using an anti-GFP antibody. Two duplicates (1 and 2) are shown. See text for details. WCE, Whole Cell Extract.

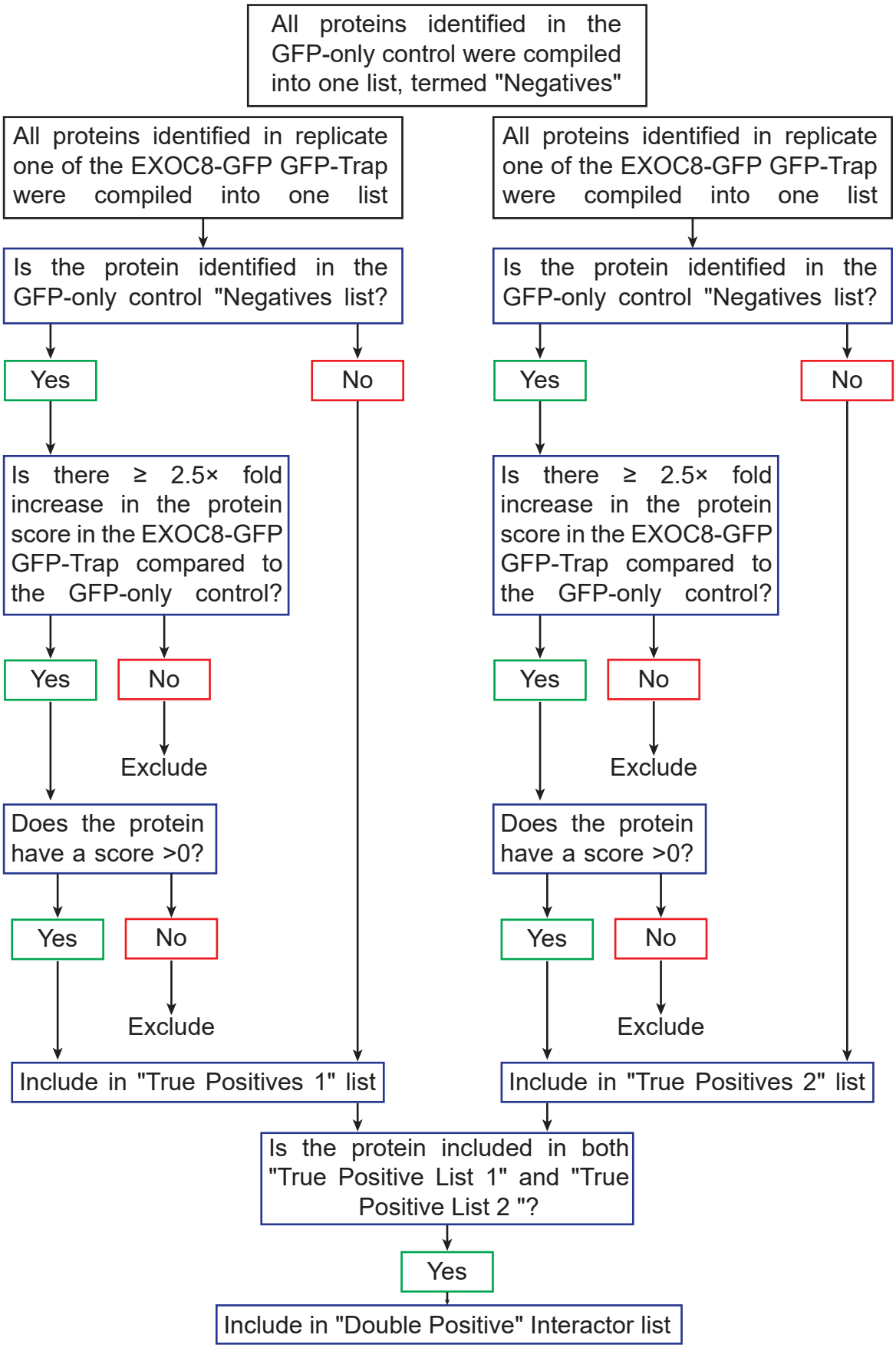

Figure 2.3. Flow chart showing method for GFP-Trap data analysis. The raw data from the GFP-Trap was analysed to generate a high-confidence "double positive" list of EXOC8 interactors. See text for further details.

150 mM NaCl, 1 mM $CaCl_2$, 1 mM $MgCl_2$, 0.1 mM PMSF, 0.01 % Triton-X-100, containing protease inhibitors). After incubating for 20 min on ice, samples were centrifuged (16,000 xg, 10 min, 4°C) and the supernatant retained as whole cell extract (WCE). The WCE was pre-cleared for 1 hour with Pierce™ Protein A/G Magnetic Beads (Thermo Fisher, Catalogue Number protein : 88802) on a rotator at 4°C. WCE's were then incubated with 2 µg antibody (Table 2.3) and Pierce™ Protein A/G Magnetic Beads overnight at 4°C. Beads were washed three times with IP wash buffer containing 0.2 % Tween 20. Immunoprecipitated proteins were eluted from the beads using 4 x Laemilli buffer and subjected to SDS-PAGE and western blotting using standard protocols.

Antibody	**Supplier, catalogue number**	**Species**
PRIMARY ANTIBODIES		
Anti-CTPS1 antibody	Protein Tech # 15914-1-AP	Rabbit
Anti-IMPDH2 antibody	Protein Tech # 12948-1-AP	Rabbit
Anti-PRF2 (L8C4) antibody -	Gift from Keith Gull, University of Oxford	Mouse
Anti-MYC antibody	Protein Tech # 10828-1-AP	Rabbit

Table 2.3. Primary antibodies used in immunoprecipitation experiments. Primary antibodies used for immunoprecipitation. The manufacturer and category number can be found for each antibody.

2.7. Statistical analysis

All quantitative data were tested for normality using the Shapiro-Wilk test, and parametric and non-parametric tests were conducted as appropriate using Graphpad Prism 7.03.

3. Results

3.1. The exocyst protein EXOC8 localises to rod and ring structures in the cytoplasm that resemble beads on a string

As a first step in analysing the role of EXOC8 in mammalian cells, EXOC8 localisation was examined in IMCD3 cells by immunofluorescence using an anti-EXOC8 antibody. As expected from previous studies (Bodemann et al., 2011; Hazelett and Yeaman, 2012), EXOC8 had a widespread cellular distribution, with punctate labelling present throughout the cytoplasm (Figure 3.1A), but an additional unexpected localisation to prominent rod and ring structures in the cytoplasm (Figure 3.1A bottom left, *) was also observed that has not been previously described for the exocyst. To test if this localisation of EXOC8 at rods and rings in the cytoplasm was due to the non-specific binding of the anti-EXOC8 antibody, IMCD3 cells were transfected with a plasmid expressing human EGFP-EXOC8. Similarly, to the anti-EXOC8 antibody, GFP-tagged EXOC8 also localised to rods and ring structures in the cytoplasm (figure 3.1A bottom right, *), suggesting a specific, novel localisation for EXOC8 at cytoplasmic rods and rings.

To examine the morphology of these structures at higher resolution than that allowed by standard wide-field imaging, IMCD3 cells immunostained for EXOC8 were imaged using a confocal microscope equipped with Airyscan (Figure 3.1B-D). Surprisingly, the signal from both EXOC8 rods and rings was not continuous, but instead these structures appeared as a series of linked round or oval shapes that resembled “beads on a string” (Figure 3.1C and D, arrowheads indicate individual bead-like structures). This type of discontinuous fluorescent signal is not typical for the membrane-bound organelles or parts of the cytoskeleton where the exocyst is known to function, indicating a probable association with a different cellular compartment.

3.2. EXOC8-containing rods and rings are present in a subset of mammalian cell lines

An increasing number of non-membrane bound organelles have been identified in recent years (Carcamo et al., 2014; He et al., 2012; Keppeke et al., 2015; Noble et al., 2016; Schiavon et al., 2018). Among these are various types of rod and

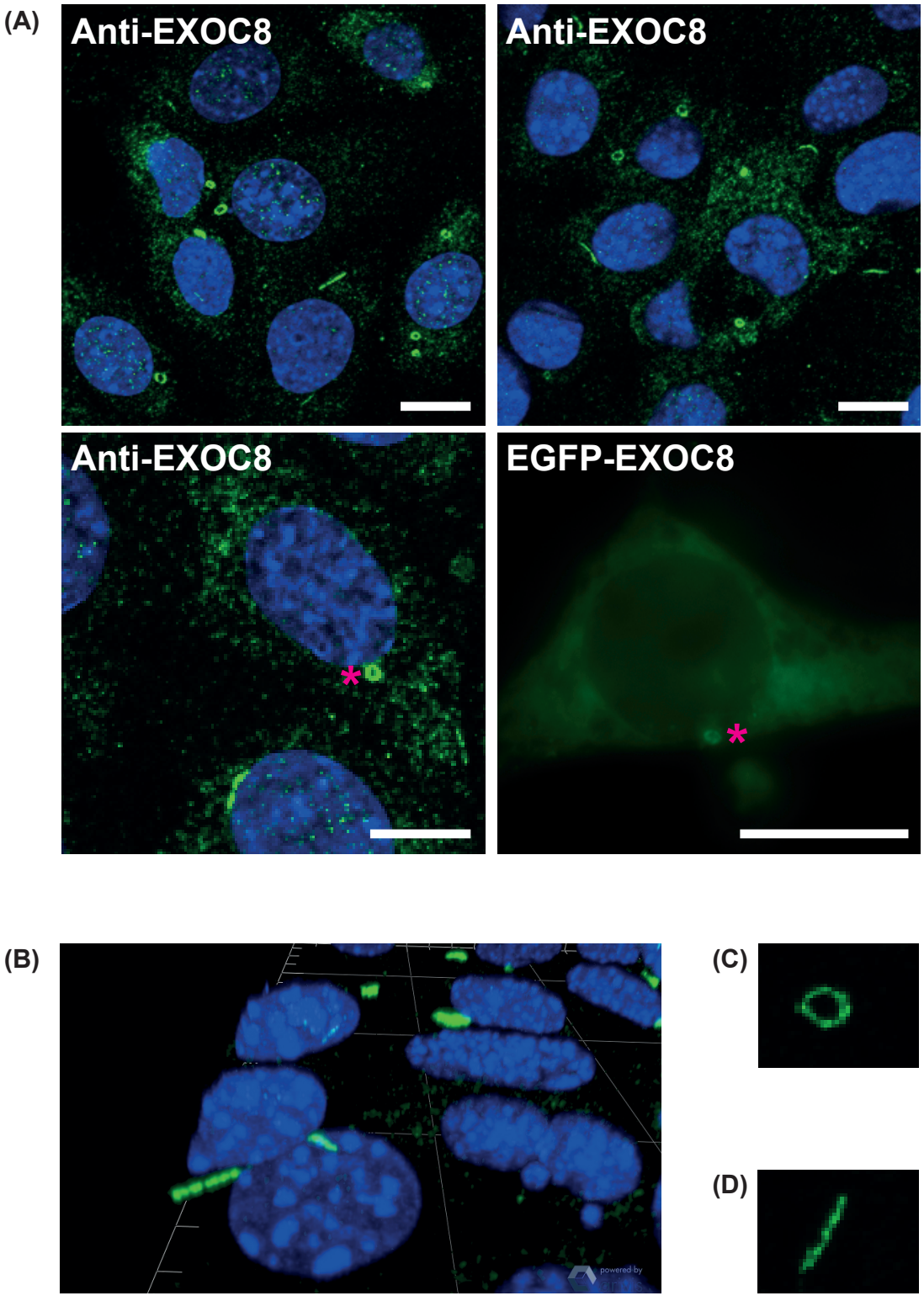

Figure 3.1. The exocyst protein EXOC8 localises to rods and ring structures in the cytoplasm that resemble beads on a string. (A) IMCD3 cells were either immunostained for EXOC8 (anti-EXOC8, green) and DNA (DAPI, blue) or transfected with pEGFP-C3-EXOC8. In both conditions EXOC8 localises to rods and rings structures in the cytoplasm (pink asterisks) **(B)** Confocal image of EXOC8 rods and rings **(C)** EXOC8 ring **(D)** EXOC8 rod. Bar = 5 μm

ring-shaped structures that include cytoplasmic rods and rings, cytoophidia, loukoumasomes and ACECs. These are not ubiquitously observed in cells, but instead are cell line specific. Therefore, the presence of EXOC8 rods and rings was assessed in a selection of different mammalian cell lines derived from different tissues and organisms (Figure 3.2; n>2000 cells per cell line). IMCD3 cells are an established mouse kidney cell line in which many cells are ciliated. To test if EXOC8 rods and rings are present in other cell types from different species, human cell lines HeLa (cervical adenocarcinoma) and HepG2 (hepatocarcinoma) were used alongside the monkey kidney cell line COS-7 and the mouse fibroblast cell line 3T3. Besides IMCD3 cells, EXOC8 rods and rings were only present in the highly transformed cancer cell line HeLa, hence they are not a kidney-specific phenomenon. Furthermore, 3T3 cells, which similarly to IMCD3 cells are of mouse origin, do not contain EXOC8 rods and rings and therefore EXOC8 rods and rings are not species-specific structures. Based on these data, rod and ring occurrence is not linked to cell differentiation, as IMCD3 are relatively differentiated cells in comparison with HeLa and 3T3. Finally, rods and rings are not an artefact of cell line transformation using SV40 virus, as IMCD3 and COS-7 were both immortalised using this method while HeLa is a human cancer line. Given that IMCD3 cells contain EXOC8 cytoplasmic rods and rings, ciliate and are straightforward to culture and to transfect, these cells were used for the rest of the experiments in this thesis.

3.3. Morphological characterisation of EXOC8 rods and rings

In order to establish if EXOC8 rods and rings correspond to previously described rod and ring structures, the morphology and position of EXOC8 rods and rings identified using anti-EXOC8 were characterised and related to published parameters for other rod/ring structures (Carcamo et al., 2011; Carcamo et al., 2014; Schiavon et al., 2018). In 92 % of cells (n=300), only one EXOC8 rod or ring were present, whereas in 2 % of cells three EXOC8 rods and/or rings were present (Figure 3.3A), indicating that under conventional culture conditions these structures occur singly in each cell. The average diameter and perimeter of an EXOC8 ring were 1.3 µm +/- 0.4 µm and 2.4 +/- 0.6 µm, respectively, while rod length was 2.5 µm +/-0.9 µm (Figure 3.3B). This similarity in rod length and ring perimeter might indicate that rods and rings represent different morphologies of

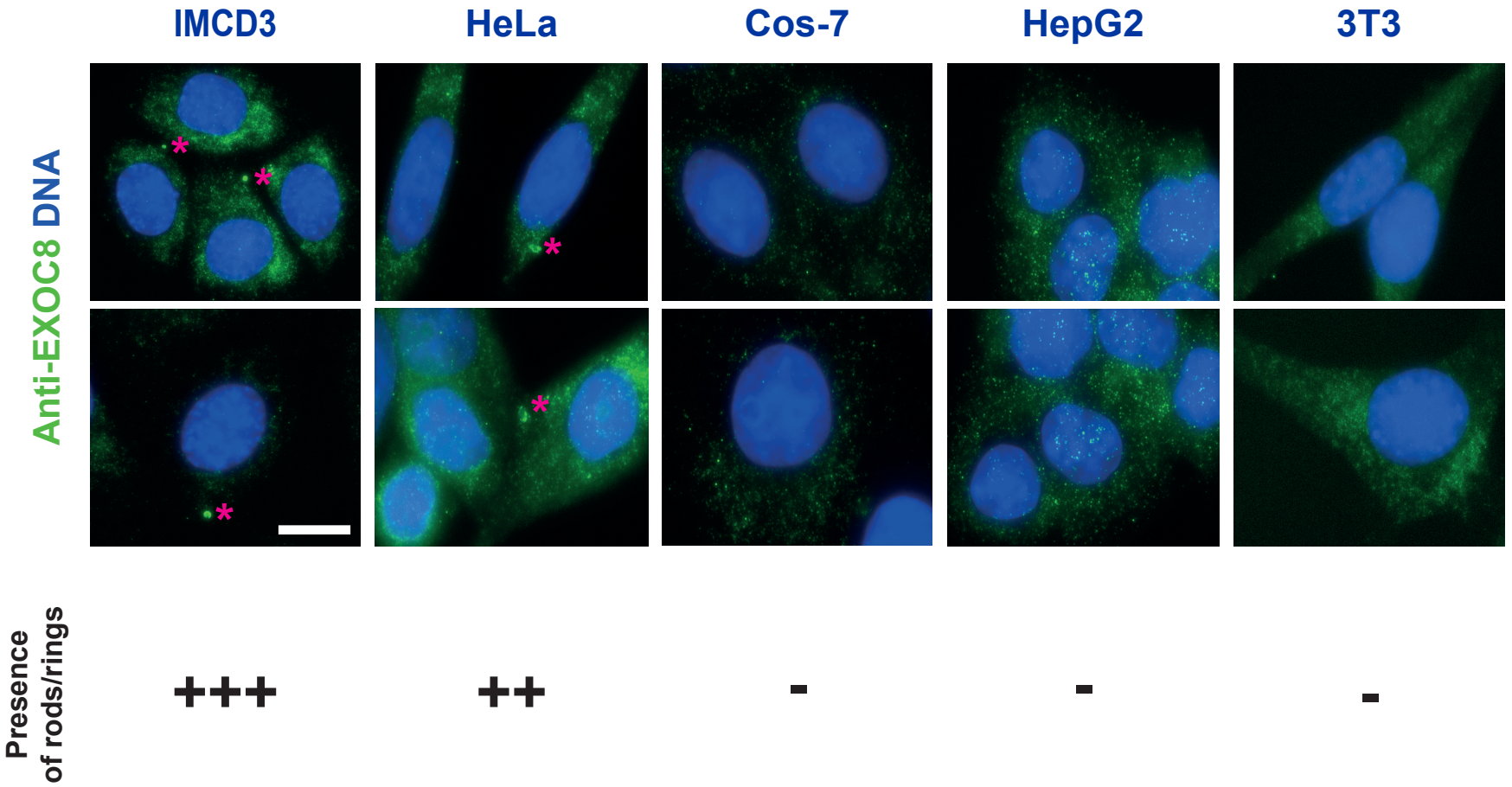

Figure 3.2. EXOC8 containing rods and rings are present in a subset of mammalian cell lines. Various cell lines were immunostained for EXOC8 (anti-EXOC8, green) and DNA (DAPI, blue). In both IMCD3 cells and HeLa cells, EXOC8 localises to rods and rings in the cytoplasm (pink asterisks). Cell lines are listed along the top. A plus sign (+) indicates the presence of EXOC8 rods and rings, with additional plus signs (+++) indicating a higher frequency of rods and rings and a minus sign (-) indicating that no EXOC8 rods or rings were present. Bar = 5 μm

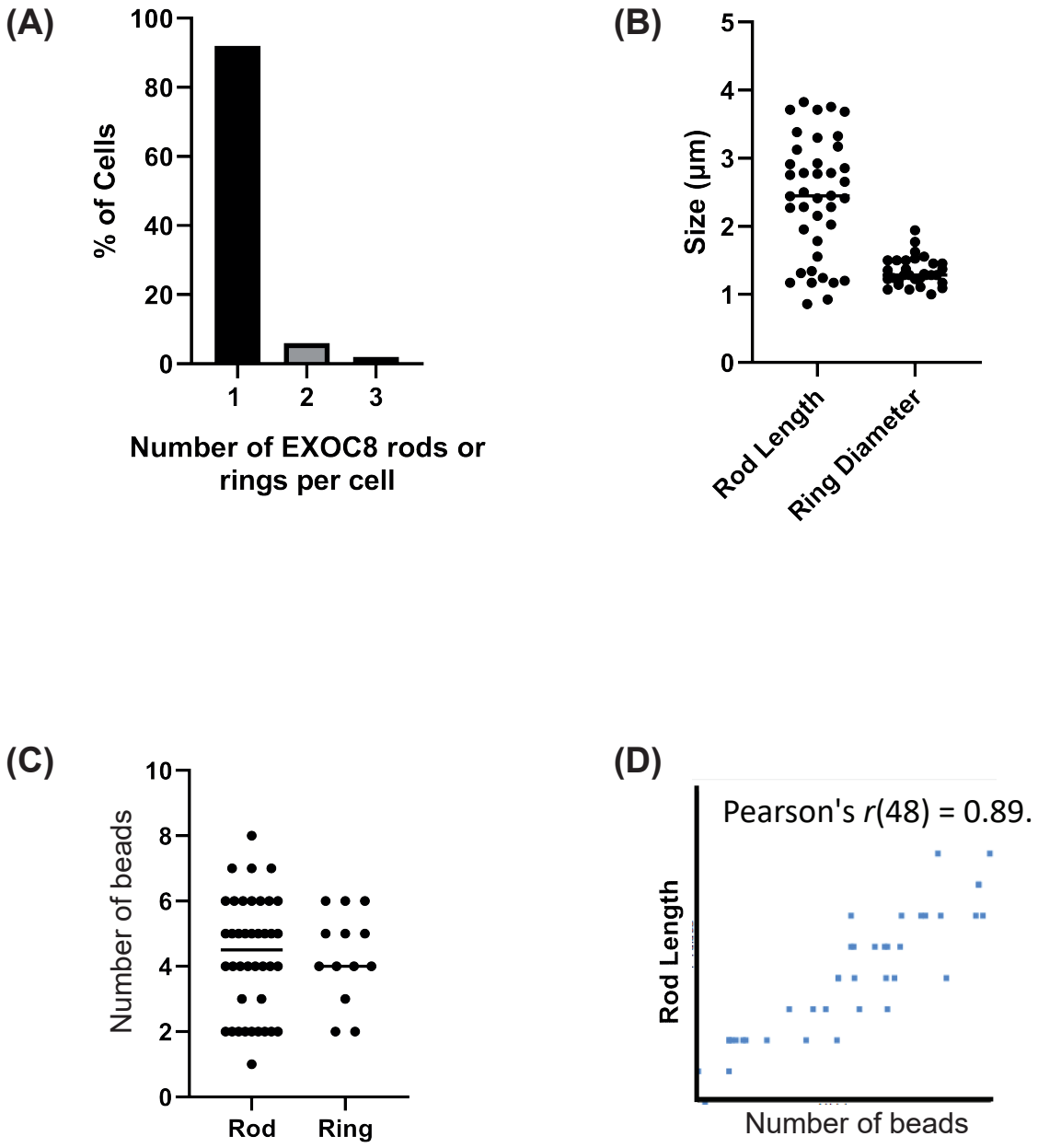

Figure 3.3. Morphological characterisation of EXOC8 rods and rings. IMCD3 cells were either immunostained for EXOC8 (anti-EXOC8, green) and DNA (DAPI, blue). **(A)** Number of EXOC8 rods or rings per cell **(B)** Length of EXOC8 rods and diameter of EXOC8 rings **(C)** Quantification of bead number **(D)** Pearson's correlation coefficient for rod length and number of beads. n=70 cells.

the same structure and raises the possibility that rods and rings are interconvertible, although live cell imaging will be needed to test this idea.

As previously mentioned, the signal from both EXOC8 rods and rings was not continuous but instead appeared as a series of linked round or oval shapes that resembled “beads on a string”. Quantification of bead number showed that both EXOC8 rods and EXOC8 rings contained on average four “beads” (Figure 3.3C), with a strong correlation between rod length and bead number (Figure 3.3D, Pearson's r(48) = 0.89), suggesting that EXOC8 rods might be composed of individual EXOC8-containing units that bind together to form a linear structure.

Given that the exocyst tethers secretory vesicles to the plasma membrane (Ahmed et al., 2018), it could be expected that EXOC8 rods and rings are localised near or at the plasma membrane. In line with this idea, all EXOC8-containing rods and rings were found within the cytoplasm, and there were no instances where a rod or ring was observed inside the nucleus. 47 % of EXOC8 rods and rings localised at the cell periphery within 2 µm of the plasma membrane, 40 % were localised between the nucleus and the cell periphery and 13 % above or adjacent to the nucleus in the middle of the cell (Figure 3.4).

3.4. EXOC8 rods are distinct structures from primary cilia

There is increasing evidence for a role for the exocyst in the formation of primary cilia (Lipschutz, 2019; Zuo et al., 2009), sensory organelles projecting from the cell surface which receive and transmit diverse signalling cues (Anvarian et al., 2019; Satir et al., 2010; Wheway et al., 2018). Since both IMCD3 cells and HeLa cells ciliate (Kowal and Falk, 2015), and EXOC8-containing rods resemble primary cilia, EXOC8 localisation was examined in confluent IMCD3 cells, which ciliate spontaneously upon contact inhibition of growth. Cells were co-stained with anti-EXOC8 together with anti-acetylated-α-tubulin to label the ciliary axoneme. In no case did EXOC8 rods and rings (Figure 3.5, green, asterisks) co-localise with the primary cilium (Figure 3.5, red, arrow), demonstrating that EXOC8 rods are distinct structures from primary cilia. Moreover, the size of EXOC8 rings is too large to correspond to the centrosome (~200 nm for a single centriole), and rings were never observed at the base of cilia where the centrosome is located under these culture conditions and where the apical enriched ceramide compartment is also found (He et al., 2012).

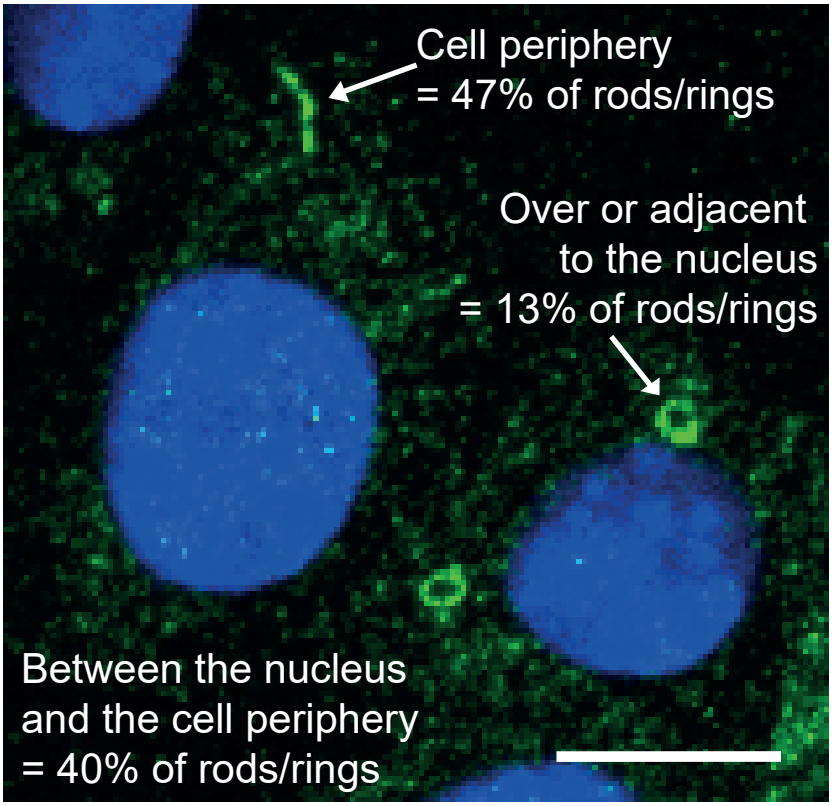

Figure 3.4. EXOC8 rods and rings are found predominately towards the cell periphery. IMCD3 cells were either immunostained for EXOC8 (anti-EXOC8, green) and DNA (DAPI, blue). Position of EXOC8 rods or rings, n=70 cells.Bar = 5 μm

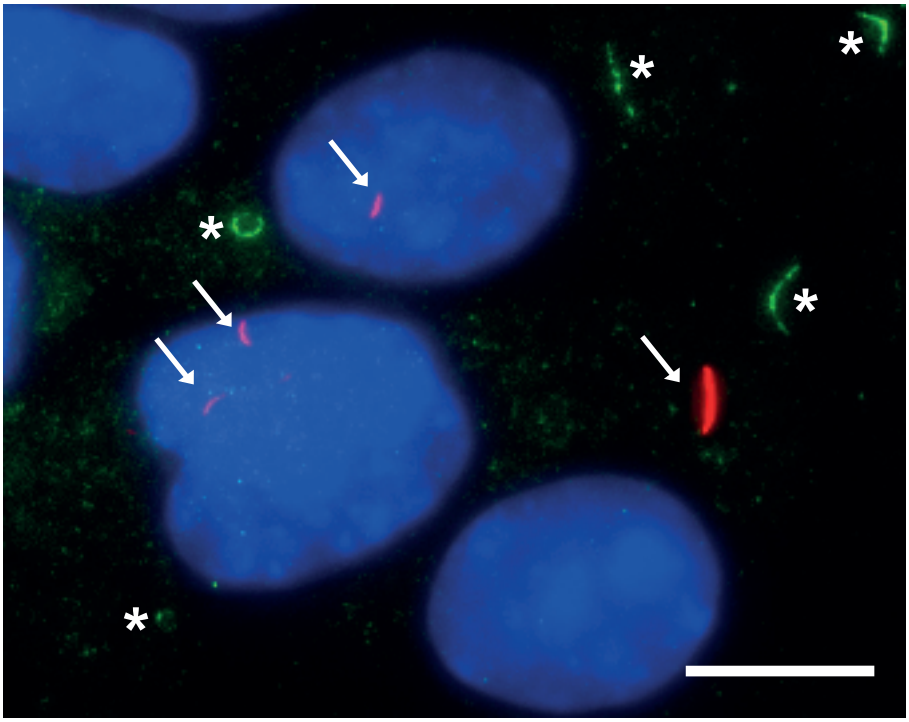

Figure 3.5. EXOC8 rods are distinct structures from primary cilia. IMCD3 cells were immunostained for EXOC8 (anti-EXOC8, green), cilia (anti-acetylatedα-tubulin, red) and DNA (DAPI, blue). EXOC8 rods and rings (white astericks) do not overlap with primary cilia (white arrow). Bar = 5 μm.

Having established that EXOC8 RR do not correspond to any known localisation of the exocyst, a literature search was carried out to obtain parameters of other published rod and ring structures for comparison (Table 3.1). Apical enriched ceramide compartments can be excluded based upon localisation and morphology, while the bead-like organisation has not been reported for cytoophidia or loukoumasomes. In contrast, EXOC8-containing rods and rings and IMPDH-containing cytoplasmic rods and rings are similar although not identical. Both have one to three rods and rings per cell of similar size and have a “bead on a string appearance”. Similarly, both EXOC8 rods and rings are present in the cytoplasm and are both present in IMCD3 cells.

3.5. EXOC8 interacts with rod-forming metabolic enzymes

To obtain a better insight into the cellular role of EXOC8, duplicate GFP-Trap experiments were performed to identify proteins that are novel candidate interaction partners for EXOC8. After filtering to remove false positives (proteins bound non-specifically to the GFP-beads), a list of putative interacting proteins was produced for replicate 1 and replicate 2 (Figure 3.6A and Appendix Table 2 and 3). Replicate 1 contained 974 proteins, and replicate 2 contained 912 proteins, with 456 proteins shared between the two that represent the highest confidence candidate binding partners. This shared set of proteins included the entire exocyst complex, which gives confidence that the GFP-Trap approach was successful.

To investigate the cellular roles and pathways in which the 456 putative EXOC8 partners are involved, functional annotation was used to cluster genes according to gene ontology. Proteins were clustered by “Biological Process” (“GOTERM_BP_DIRECT”) using DAVID 6.8. The most significantly enriched GOTERM was “poly(A) RNA binding” followed by “cadherin binding involved in cell-cell adhesion” and then “nucleotide binding” (Figure 3.6B) indicating that there was an over-representation of proteins in these clusters compared to the GFP-only control. The cluster “nucleotide binding” was selected for further studies as the role of the exocyst complex in relation to nucleotide binding is poorly understood in contrast to cell-cell adhesion.

	EXOC8 containing rods and rings	Cytoplasmic rods and rings	Cytoophidia	Loukoumasomes	Apical enriched ceramide compartment
Number of rods and rings per cell	1-3	1-3	1-5*	1-2	1
Ring Diameter	1.3 μm	~2-5 μm	~2 – 8 μm*	Toroidal structure ~ 6 μm	~1- 2 μm
Rod Length	2.5 μm	~3–10 μm	~1 – 10 μm*	N/A	N/A
Bead like appearance?	Yes	Yes	No	No	No
Position in cell	Cytoplasm at cell periphery	Cytoplasm	Cytoplasm and nucleus	Perinuclear and in cell periphery	At base of primary cilia
Same cell line specificity?	Present in IMCD3 cells and HeLa cells	Yes; present in IMCD3 cells No; present in MEF, NRK, MDCK and 3T3 cells	Yes; present in HeLa cells No; present in HEK-293 cells and HepG2 cells	No; present in a subset of adrenergic neurons within rat sympathetic ganglia	No; only present in MCDK cells

Table 3.1. EXOC8 rod and ring parameters do not overlap exactly with known types of rods and rings. Characteristics of EXOC8 containing rods and rings were compared to published parameters of cytoplasmic rods and rings in vertebrate cell lines (Calise et al., 2014; Calise et al., 2016; Carcamo et al., 2011; Juda et al., 2014; Keppeke et al., 2019; Schiavon et al., 2018), cytoophidia (Chang et al., 2018; Li et al., 2018; Liu, 2011; Liu, 2016) loukoumasomes (Noble et al., 2016; Ramer et al., 2010) and the Apical Enriched Ceramide Compartment (ACEC; He et al., 2012) N/A; Not Applicable. *All data in table directly extracted from papers, with the exception of number of rods and rings per cell for cytoophidia which was analysed from published images.

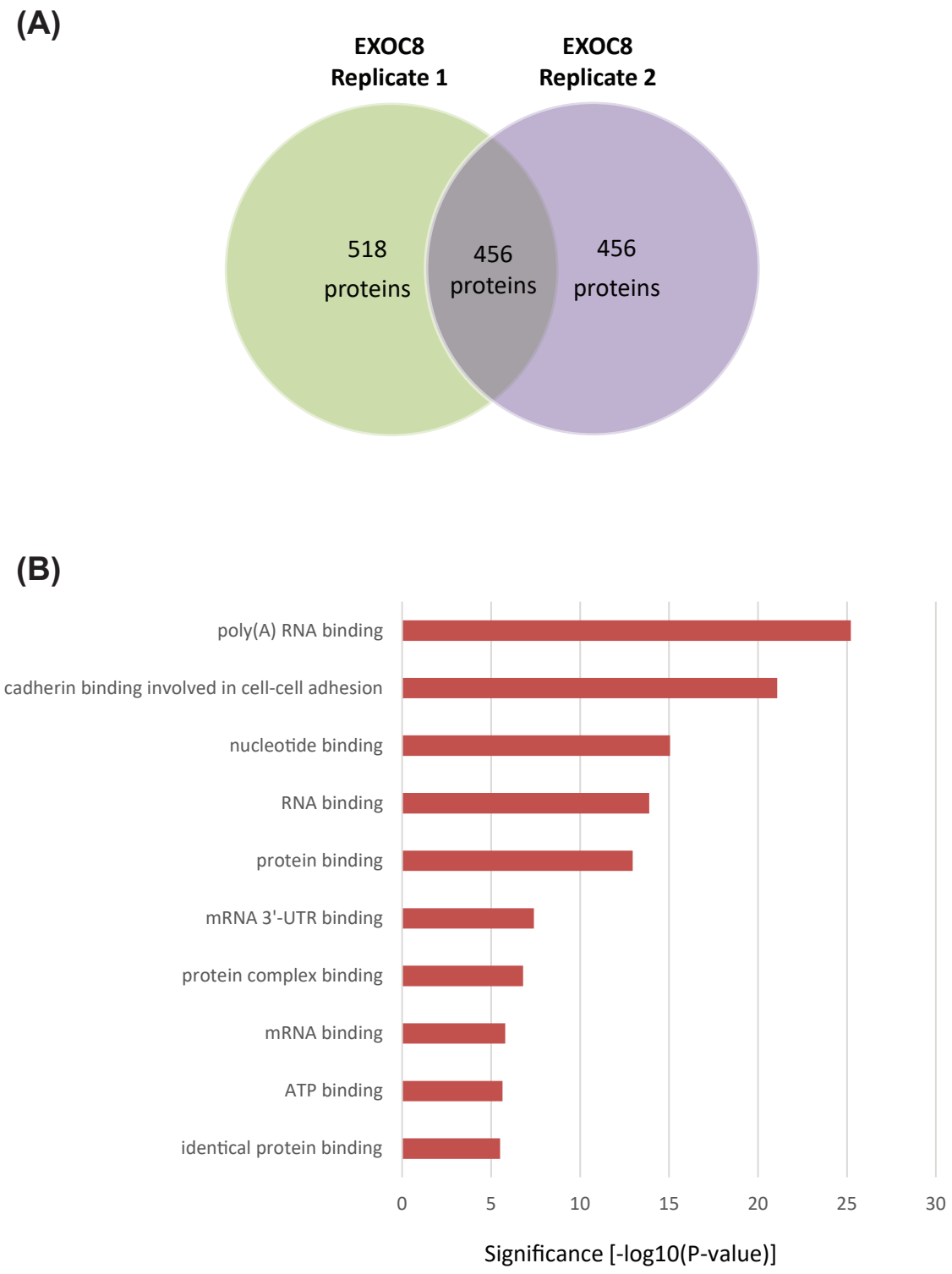

Figure 3.6. GFP-Trap was performed to discover novel EXOC8 interacting partners (A) Total single positive interactors in EXOC8 replicate 1 and EXOC8 replicate 2 and , and number of double positive interactors that came down in both **(B)** "Molecular Function" clustering revealed novel putative protein interactions of EXOC8

Given that EXOC8 rods and rings did not overlap exactly with known types of rod and ring structures, the GFP-Trap data were analysed to obtain a better insight into what the structures could be.

EXOC8 interacting partners were compared against a list of metabolic enzymes known to form filamentous structures including rods and rings in a cell (Park and Horton, 2019) (Figure 3.7B). Of the 27 metabolic enzymes that are known to form filaments, EXOC8 interacted with 48 % (13 enzymes). Such metabolic enzymes were then clustered into their associated biological process pathway. This revealed that EXOC8 interacted with 100 % of filament forming-metabolic enzymes involved in fatty acid biosynthesis (one enzyme), 75 % of filament forming-metabolic enzymes involved in glycolysis (three enzymes) and 75 % of filament forming-metabolic enzymes involved in nucleotide synthesis. Since functional annotation revealed that “nucleotide binding” was a highly enriched cluster, filament forming-metabolic enzymes involved in nucleotide synthesis was examined in more detail. Intriguingly, the four nucleotide synthesis metabolic enzymes that are known to form filament structures are all established components of cytoplasmic rods and rings and/or cytoophidia (Figure 3.7A).

The major components of cytoplasmic rods and rings are the enzymes inosine monophosphate dehydrogenase type 1 (IMPDH1) and inosine monophosphate dehydrogenase type 2 (IMPDH2), which share 84 % sequence homology (Calise et al., 2015). Analysis of the GFP-Trap data showed that although IMPDH1 was not associated with EXOC8 in either replicate 1 or 2, IMPDH2 was identified in both replicates of the GFP-Trap (Figure 3.7A). Similarly, major components of cytoophidia, CTPS1 and CTPS2 also interacted with EXOC8. CTPS2 associated with EXOC8 in one replicate of the GFP-Trap, whereas CTPS1 putatively interacts with both replicates of the GFP-Trap (Figure 3.8A). These data indicate that EXOC8 could either be a component of, or interact with IMPDH2 and/or CTPS1 containing cytoplasmic rods and rings/cytoophidia.

To confirm the interaction between EXOC8 and IMPDH2 and CTPS1, co-immunoprecipitation was performed using either IMPDH2 or CTPS1 antibody. In both cases, a single EXOC8 band of approximately ~ 90 kDa was detected using anti-EXOC8, while no signal was observed in any of the control lanes (Figure 3.8B). This raises the possibly that EXOC8 rods and rings and IMPDH2/CTPS1 containing rods and rings are analogous structures.

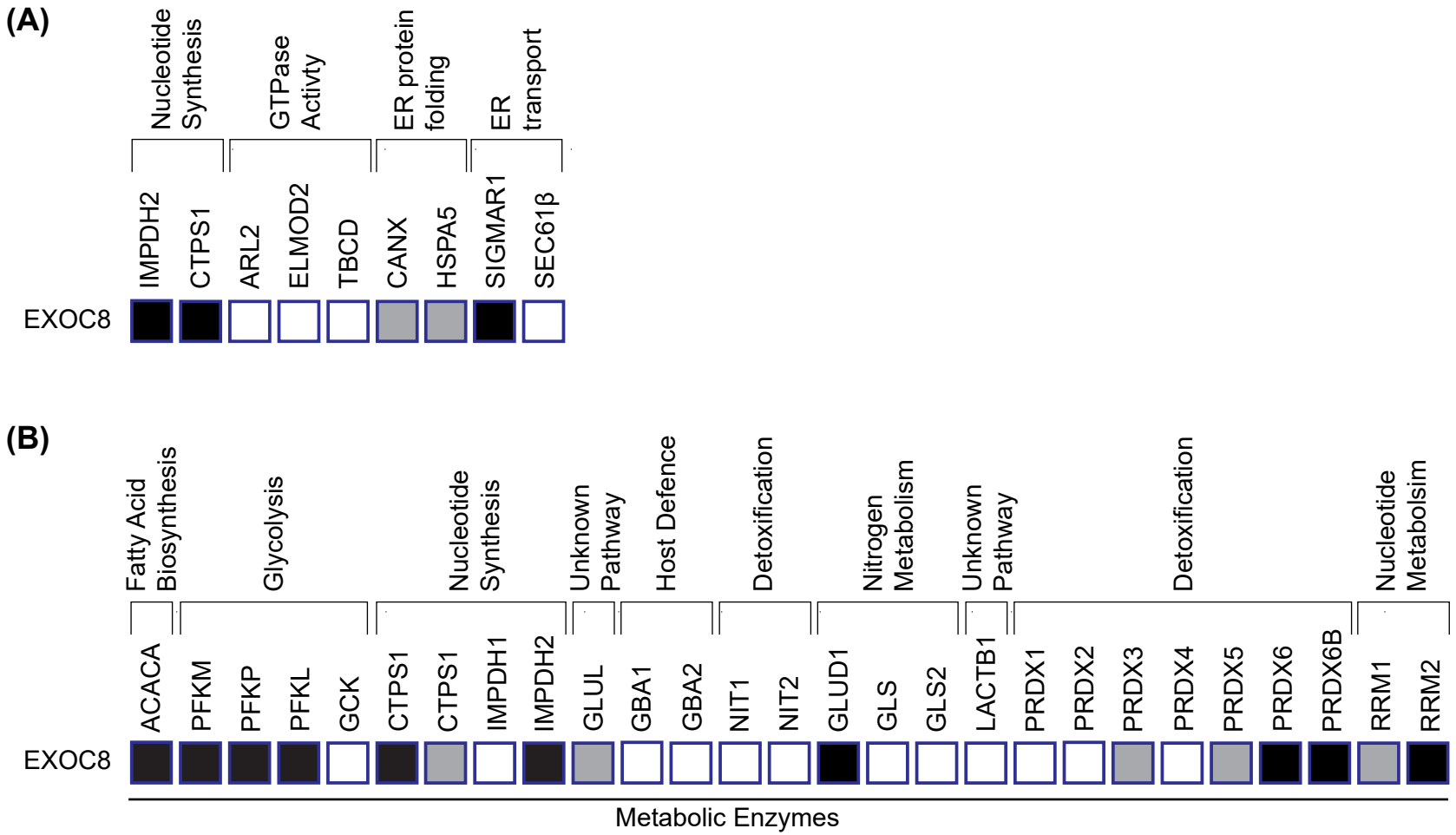

Figure 3.7. GFP-Trap identifies rod and ring-forming metabolic enzymes as putative exocyst interactors. (A) EXOC8 interacts with known components of cytoplasmic rods and rings **(B)** EXOC8 interacts with rod and ring-forming metabolic enzymes. Black box: high confidence interactor identified in duplicate GFP-Traps, grey box: single positive interactor identified in one GFP-Trap, white box: no interaction detected.

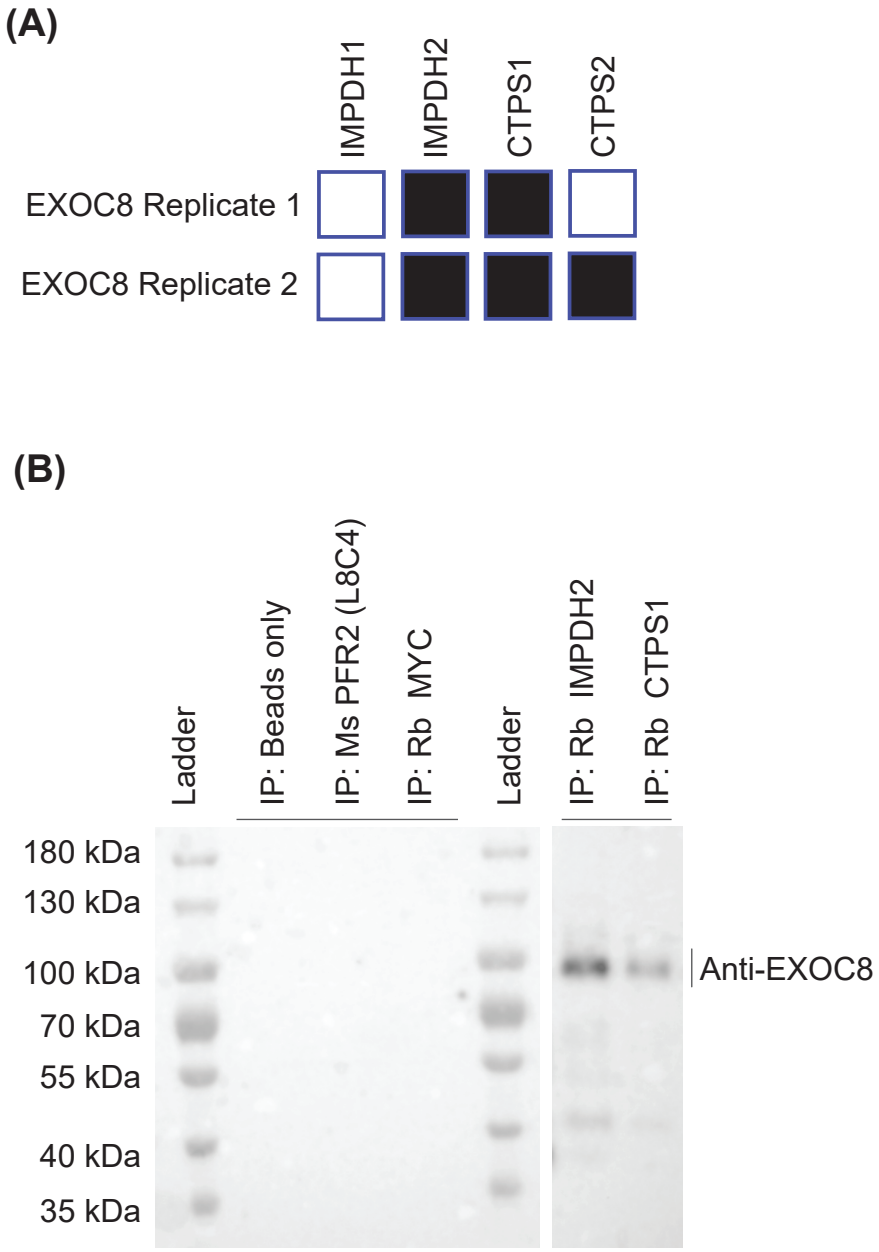

Figure 3.8. EXOC8 interacts with IMPDH2 and CTPS1. (A) GFP-Trap revealed that EXOC8 putatively interacts with IMPDH2 and CTPS1. Black box; interaction identified in GFP-Trap **(B)** EXOC8 immunoprecipitates with magnetic beads coupled to IMPDH2 or CTPS1. IMCD3 cell extracts were subjected to co-immunoprecipitation with an anti-IMPDH2 antibody or anti-CTPS1 antibody, followed by western blotting with an antibody against EXOC8.

3.6. EXOC8 rods and rings can be induced by compounds that induce cytoplasmic rods and rings

Both cytoplasmic rods and rings and cytoophidia can be induced by drug treatment (predominantly through the inhibition of IMPDH2 or CTPS1) or by altering growth conditions. To test if EXOC8 rods and rings and IMPDH2/CTPS1 containing rods and rings are analogous structures, IMCD3 cells were incubated with 1nM of Ribavirin for varying times between 15 minutes and 2 hours, and immunostained for EXOC8 or IMPDH2. Ribavirin is an anti-viral medication used to treat viral infections such as HCV and respiratory syncytial virus. It is a competitive IMPDH2 inhibitor, that has been shown to rapidly increase both the number and the size of cytoplasmic rods and rings *in vitro* and *in vivo* (Carcamo et al., 2011; Keppeke et al., 2015; Schiavon et al., 2018).

In IMCD3 cells treated with 1 nM of Ribavirin, the quantity of IMPDH2 containing cytoplasmic rods and rings increased dramatically at all time points (Figure 3.9, right panels), with effects were most noticeable in cells treated for a minimum of 45 minutes, where 100 % of cells contained IMPDH2-positive rod/ring structures. At all time points, the size of the cytoplasmic rods and rings remained constant. In contrast, no EXOC8-positive rods or rings could be detected in Ribivarin-treated cells at any time point between 15 minutes and 2 hours (Figure 3.9, left panels), suggesting either that IMPDH2 containing rods and rings and EXOC8 rods and rings are different structures, or that the kinetics of incorporation for the two proteins are very different. Similar results were found when IMCD3 cells were treated with 1 nM of DON, for varying times between 15 minutes and 2 hours and immunostained for EXOC8 or CTPS1 (data not shown). DON failed to induce the formation of EXOC8 rods and rings at any time point between 15 minutes and 2 hours. However, contrary to published literature which reports that DON induces the formation of cytoophidia (Keppeke et al., 2015; Liu, 2016), here DON also failed to induce the formation of CTPS1 containing cytoophidia in this time.

In contrast, EXOC8 RR could be induced over longer time periods by both compounds (Figure 3.10A). IMCD3 cells were treated with 1 nM of Ribavirin or DON for 24 hours and stained for EXOC8 and either IMPDH2 or CTPS1. Interestingly, Ribavirin and DON robustly increased the number of EXOC8 rods and rings in IMCD3 cells treated for 24 hours, with all ribavirin-treated cells

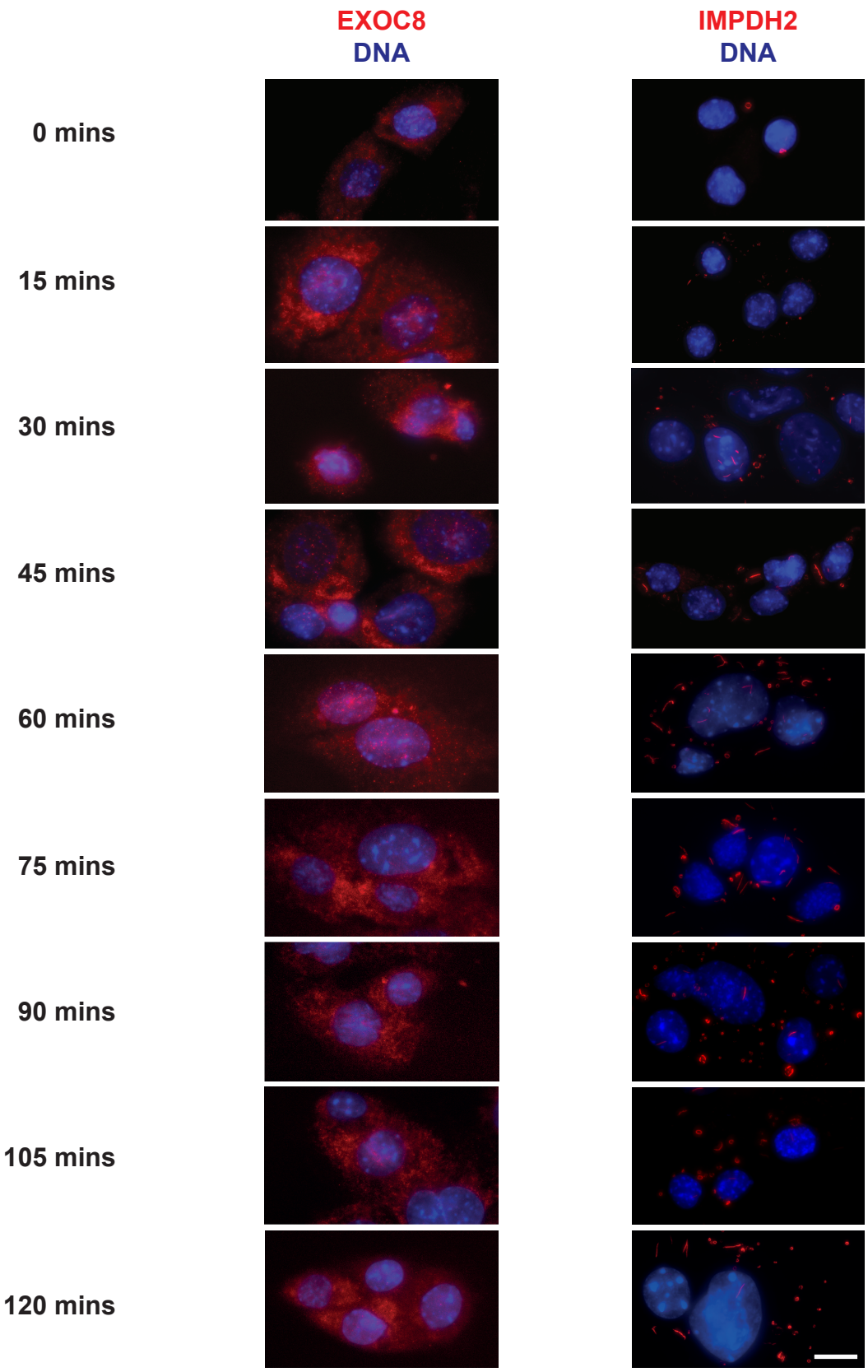

Figure 3.9. EXOC8 rods and rings cannot be induced over short periods by compounds that induce cytoplasmic rods and rings. IMCD3 cells were treated with 1 nM of Ribavirin, and fixed at the times shown and either immunostained for EXOC8 (anti-EXOC8, red) or IMPDH2 (anti-IMPDH2, red) and DNA (DAPI, blue). Bar = 5 μm.

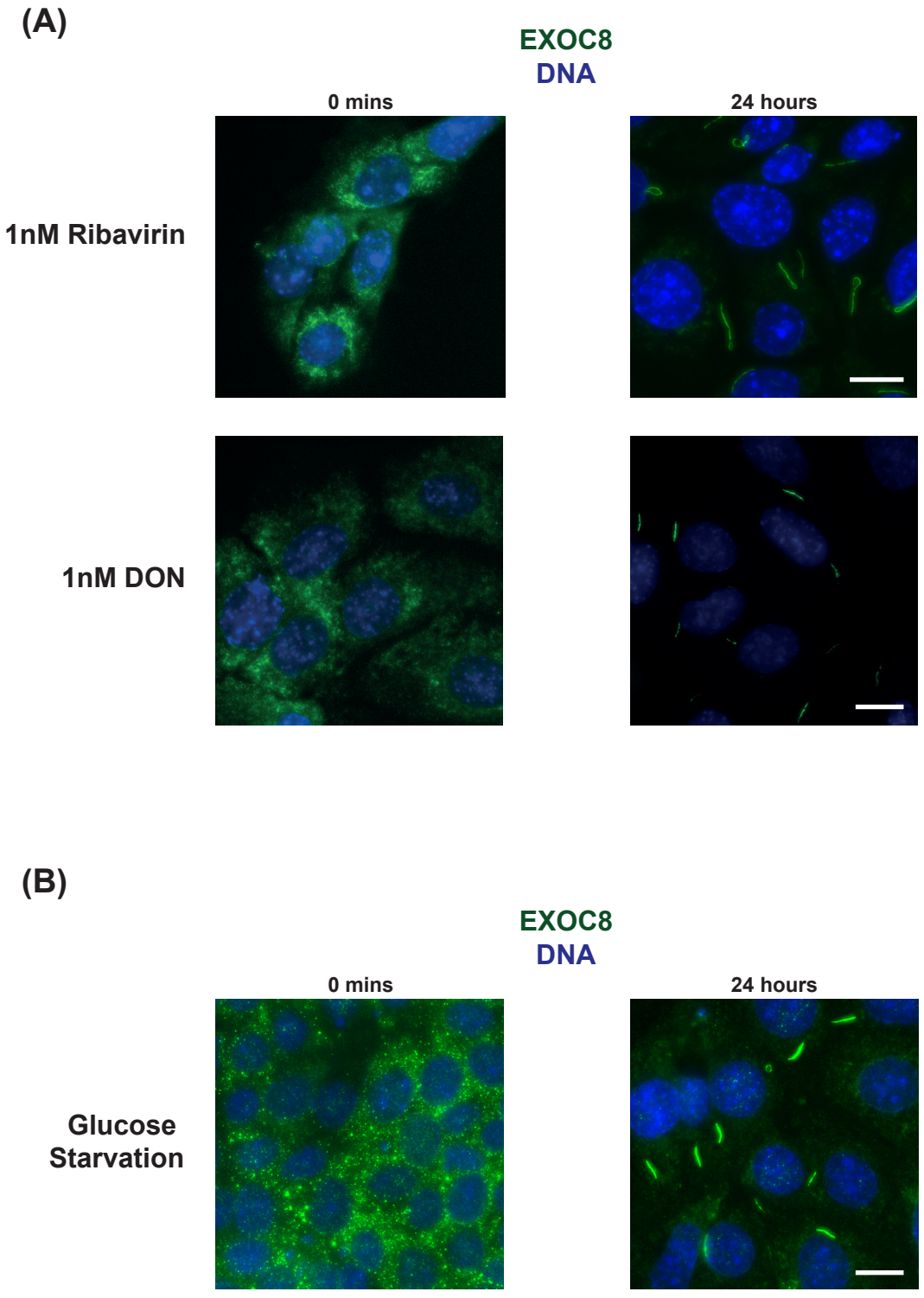

Figure 3.10. EXOC8 rods and rings can be induced over long time periods by compounds that induce cytoplasmic rods and rings. IMCD3 cells were either glucose starved or treated with 1 nM of Ribavirin or 1 nM of DON (6-diazo-5-oxo-l-norleucine) for 24 hours and immunostained for EXOC8 (anti-EXOC8, red) and DNA (DAPI, blue). Bar = 5 μm.

containing at least one EXOC8 rod or ring. Similarly, ribavirin and DON-treated cells contained an abundance of IMPDH2 and CTPS1 containing rods and rings, suggesting that the effect of the drugs are specific.

Glucose starvation has also been shown to increase the proportion of cells containing IMPDH2 containing cytoplasmic rods and rings (Schiavon et al., 2018). IMCD3 cells glucose starved for a maximum of 48 hours exhibit a moderate increase in the proportion of IMPDH2 containing rods and rings compared to the control 75 % cells contained IMPDH2 rods and rings compared to 58 % cells in the control (Schiavon et al., 2018). To test if glucose starvation also increased the proportion of EXOC8 rods and rings, IMCD3 cells were grown in DMEM lacking D-Glucose for 24 hours (see Materials and Methods). Comparable increases in EXOC8 rods and rings were observed following glucose starvation (Figure 3.10B), with at least one structure present in 85 % of cells.

Taken together, the induction of EXOC8 rods and rings by Ribavirin, DON and glucose starvation, suggest that EXOC8 rods and rings and IMPDH2 are probably analogous structures. Both form under conditions of IMPDH2 or CTPS1 inhibition, and in response to cellular metabolic changes. However, the induction time of EXOC8 rods and rings is longer than that of IMPDH2 rods and rings and CTPS1 containing cytoophidia, suggesting that EXOC8 rods and rings take longer to “form”.

3.7. EXOC8 is required for the correct morphology of Ribavirin induced IMPDH2 containing cytoplasmic rods and rings

Given the exocyst’s role in vesicle trafficking, it was hypothesised that the exocyst could traffic IMPDH2 monomers in the cell to enable the formation of IMPDH2 containing cytoplasmic rods and rings. To test this idea, *exoc8* was depleted by siRNA (success of knockdown was examined by immunofluorescence; Figure 3.11), and IMPDH2 cytoplasmic rods and rings quantified in the absence of ribavirin-mediated induction. IMPDH2 containing cytoplasmic rods and rings were still present, and there was no statistical difference between the numbers of either IMPDH2 rods or rings in depleted of EXOC8 compared to the control (Figure 3.12, paired t-test, 2 independent experiments). Thus, EXOC8 is not required for the formation of IMPDH2 containing cytoplasmic rods and rings under normal metabolic conditions.

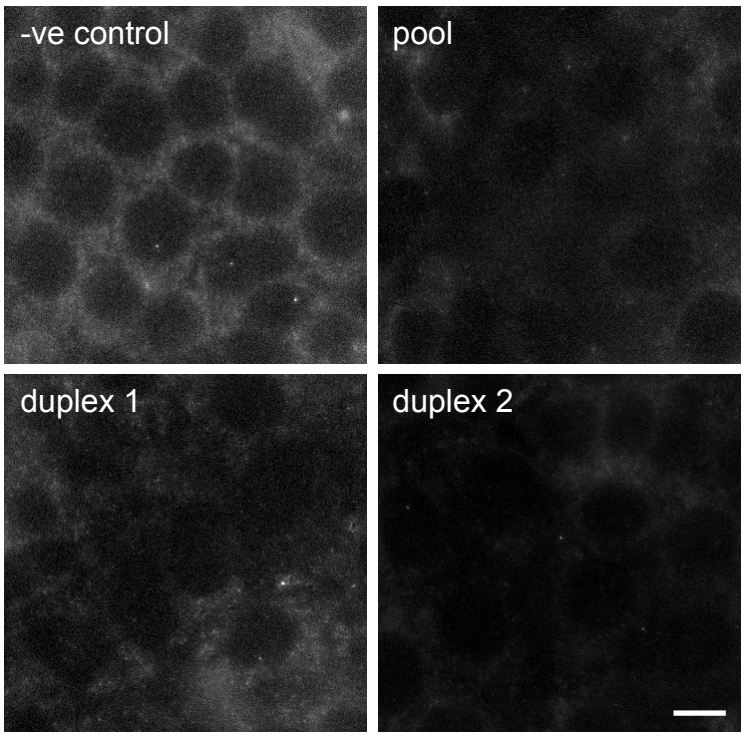

Figure 3.11. *exoc8* siRNA reduces cellular levels of EXOC8 effectively. IMCD3 cells were transfected with either non-targeting siRNA, *exoc8* siRNA single duplexes or an *exoc8* siRNA 3 duplex pool. Cells were incubated for 48 hours prior to fixation in methanol and immunostained using an anti-EXOC8 antibody. Bar = 5 µm.

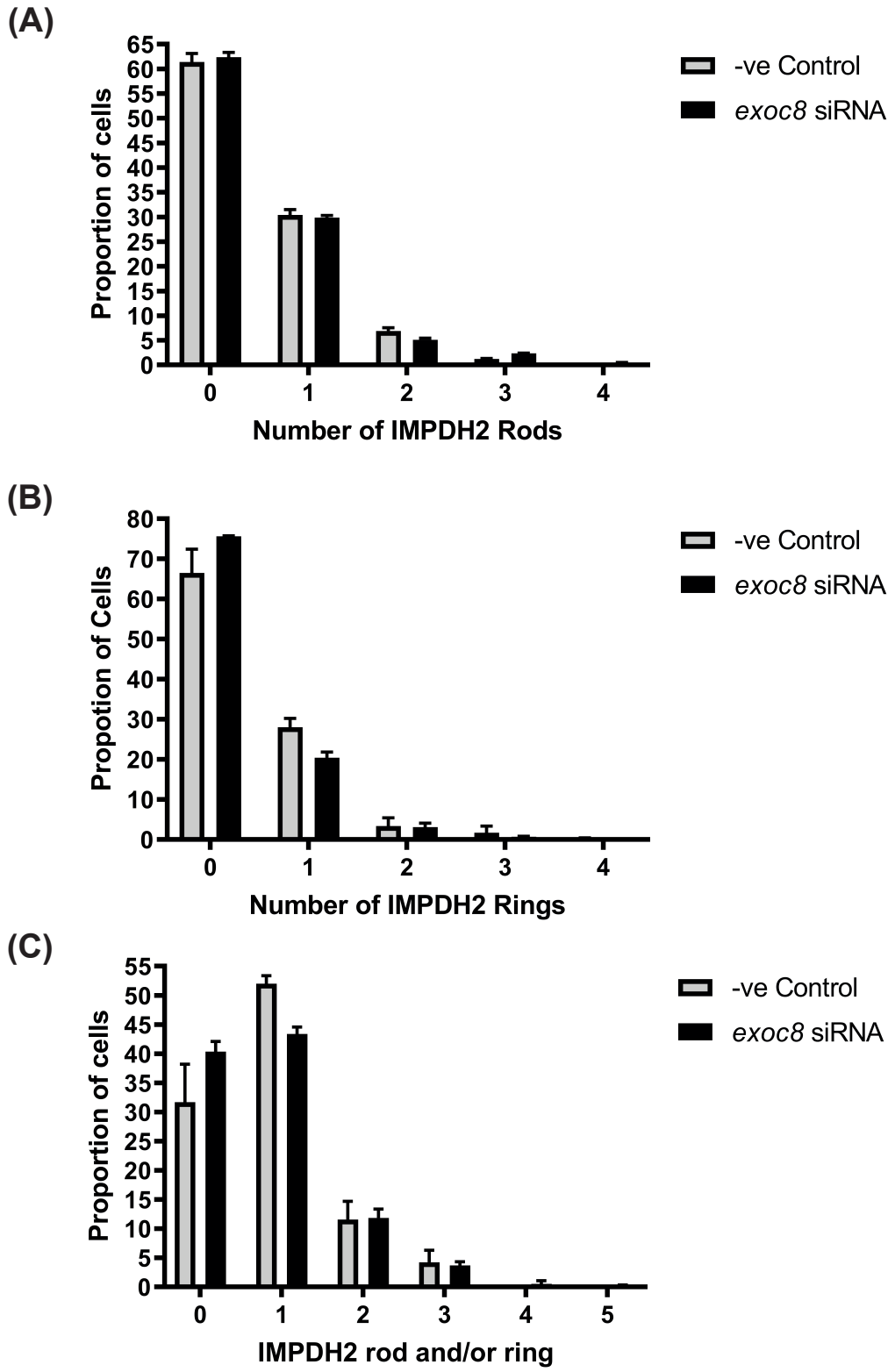

Figure 3.12. EXOC8 is not required for IMPDH2 containing-rod and ring formation. IMCD3 cells were transfected with non-targeting siRNA or *exoc8* siRNA and immunostained for IMPDH2 (anti-IMPDH2) and DNA (DAPI). EXOC8 is not required for **(A)** IMPDH2 rod formation or **(B)** IMPDH2 ring formation **(C)** IMPDH2 rod and/or ring formation

To test the effect of loss of EXOC8 on induction of rods and rings, *exoc8* was reduced in IMCD3 cells by siRNA and 1 nM of Ribavirin was added to cells for times ranging between 15 minutes and 2 hours (Figure 3.13A). In cells treated with 1 nM of Ribavirin for 15 minutes and depleted of EXOC8, short IMPDH2 rods were present. At longer time periods of induction, rods and rings were present and *exoc8* silencing did not affect the proportion of rods or rings in the population (n=at least 500 nuclei per condition, P>0.05, Kruskal-Wallis test). However, IMPDH2 rods were 2.7x longer than those in control cells (average lengths 8 µm and 3 µm, respectively). Moreover, the IMPDH2 signal in cells following 30 minutes of ribavirin treatment was less distinct, with fewer well-defined rods. Instead, in 55% of cells +/- 14, IMPDH2 appeared highly reticular (e.g. Figure 3.13B and C), and this alteration to IMPDH2 morphology was never observed in control cells. Thus, EXOC8 influences the morphology of induced IMPDH2 rods and rings, potentially through the trafficking of other proteins.

Having established a role for EXOC8 in the organisation of IMPDH2 rods and rings, the next experiment sought to address whether IMPDH2 is required for the formation of EXOC8 rods and rings. IMCD3 cells were transfected with IMPDH2 siRNA (success of knockdown was examined by immunofluorescence; Figure 3.14) and immunostained for EXOC8. In cells transfected with -ve control siRNA, EXOC8 rods and rings were present. After IMPDH2 ablation the proportion of cells containing EXOC8 rods or rings decreased (Figure 3.15). Whereas 27 % of cells contained EXOC8 rods in the negative control, only 8 % of cells contained EXOC8 rods in cells depleted of IMPDH2. Similar results were found for the proportion of cells that contained EXOC8 rings. Whereas 23 % of negative control cells contained EXOC8 rings, only 9 % of cells depleted of IMPDH2 contained IMPDH2 rings. Taken together, these results suggest that IMPDH2 is required for the formation of EXOC8 rods and rings, and that EXOC8 rods and rings are part of the same structure as IMPDH2 rods and rings. To test if EXOC8 rods and rings are indeed part of the same structure as IMPDH2 rods and rings, IMCD3 cells were to be immunostained for EXOC8 and IMPDH2/CTPS1. Unfortunately, Covid-19 restrictions prevented this planned investigation and future studies should endeavour to elucidate if EXOC8 rods and rings and IMPDH2/CTPS1 rods and rings co-localise and are therefore part of the same structure.

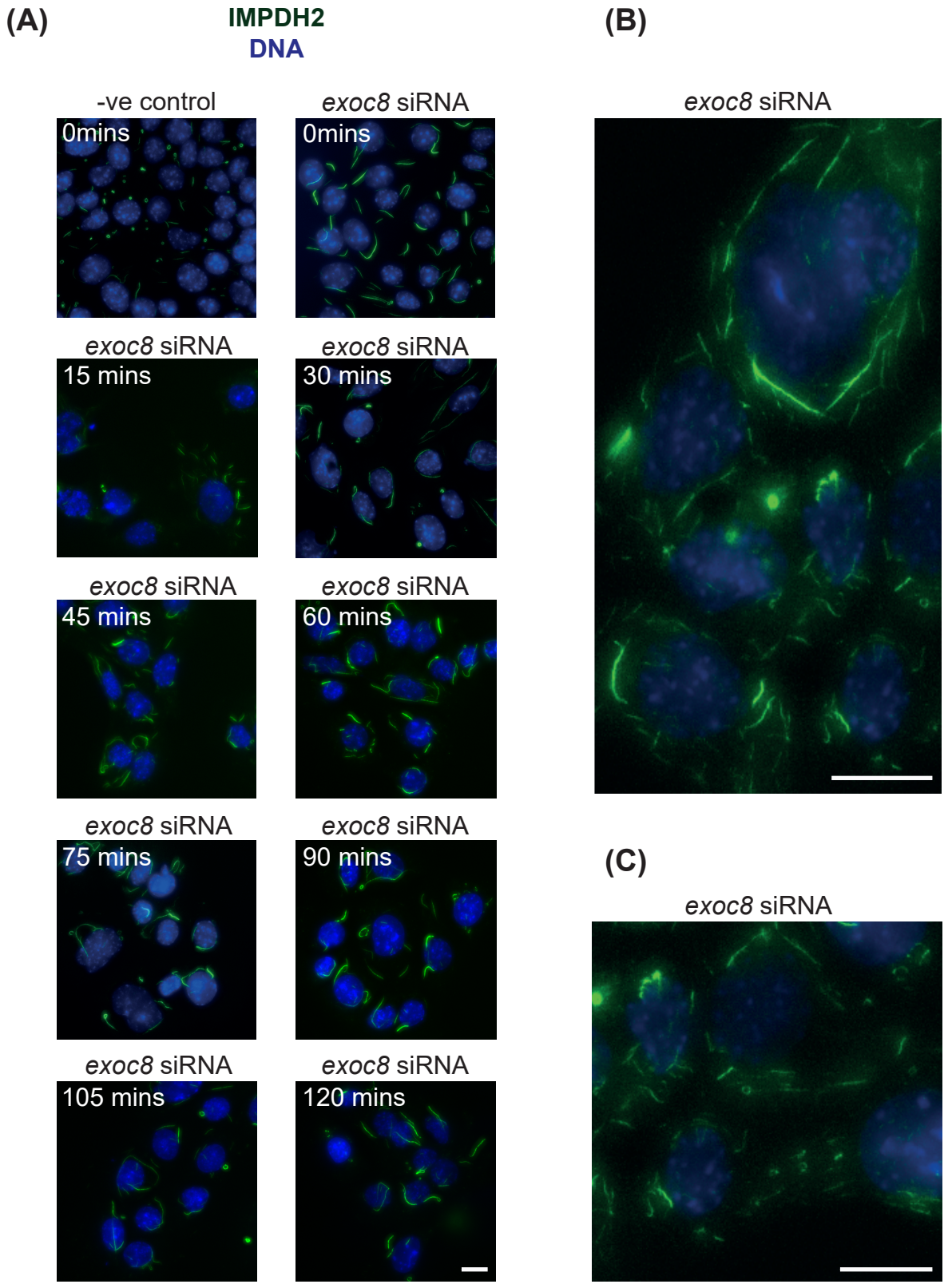

Figure 3.13. EXOC8 is required for the correct morphology of Ribavirin induced IMPDH2 rods and rings. (A) IMCD3 cells were transfected with non-targeting siRNA or *exoc8* siRNA and were treated with 1 nM of Ribavirin, and fixed at the times shown and immunostained for IMPDH2 (anti-IMPDH2, green) and DNA (DAPI, blue) **(B and C)** IMPDH2 appears highly reticular after *exoc8* knockdown. Bar = 5 μm.

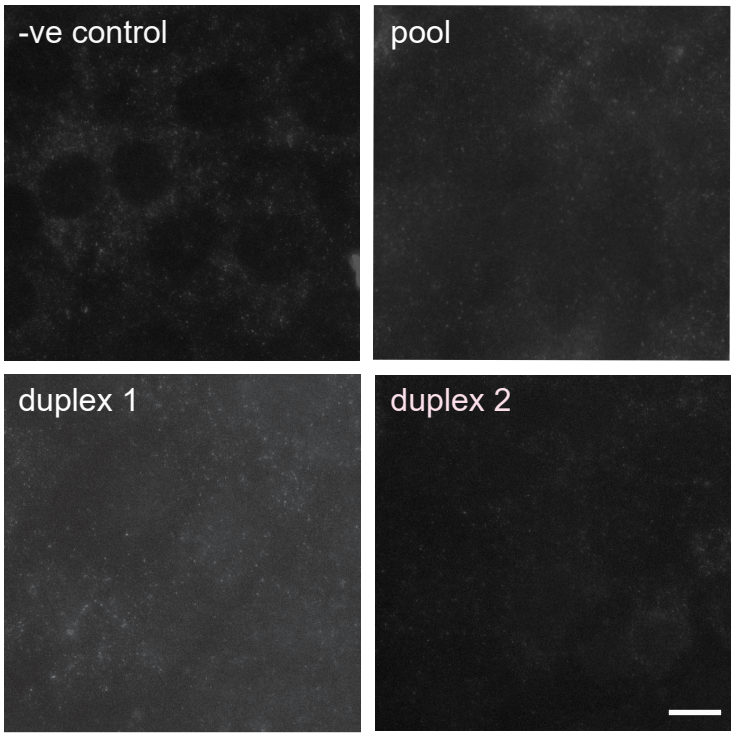

Figure 3.14. *impdh2* siRNA reduces cellular levels of IMPDH2 effectively. IMCD3 cells were transfected with either non-targeting siRNA, *impdh2* siRNA single duplexes or an *impdh2* siRNA 2 duplex pool. Cells were incubated for 48 hours prior to fixation in 4 % paraformaldehyde and immunostained using an anti-IMPDH2 antibody. Bar = 5 μm.

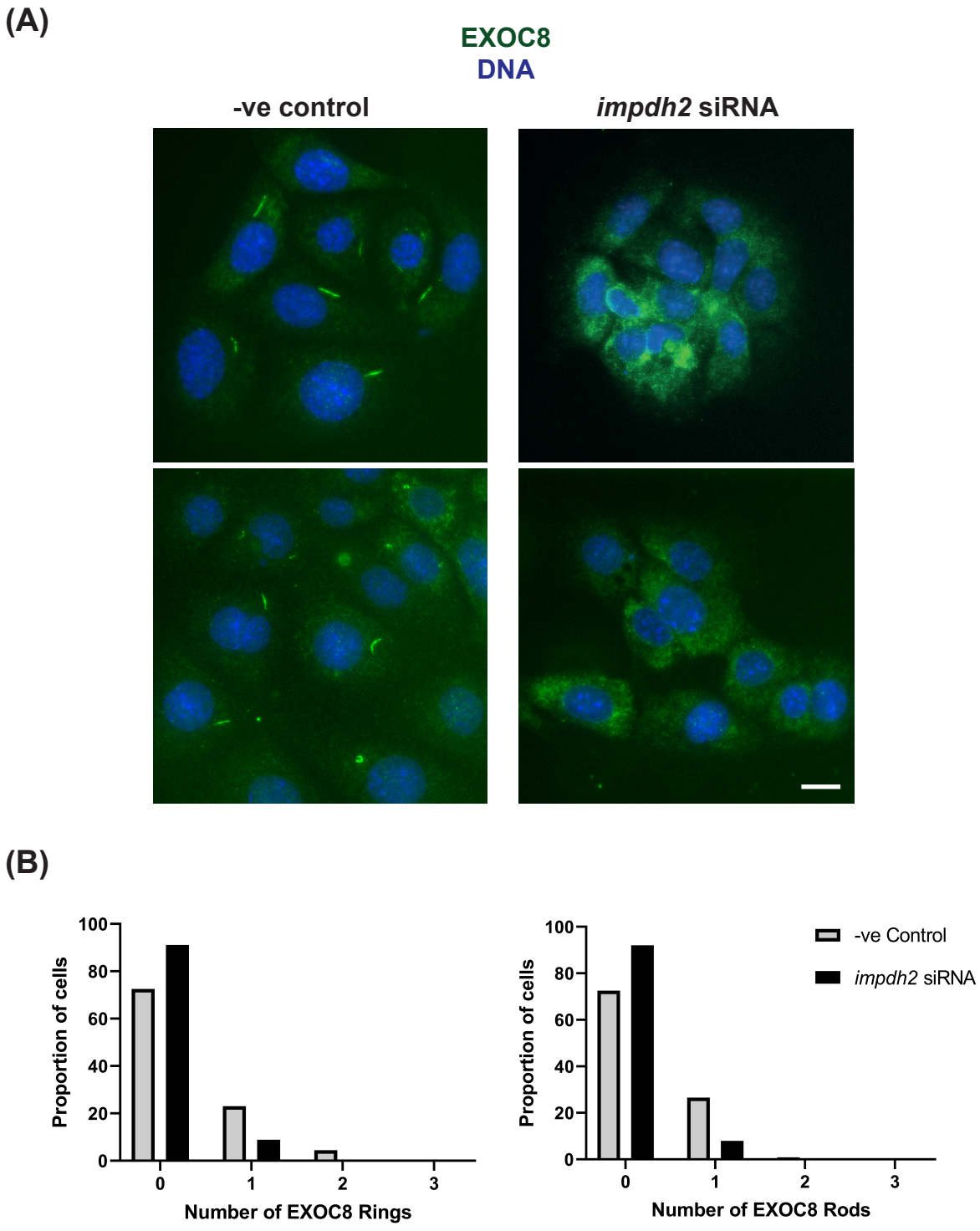

Figure 3.15. IMPDH2 is required for the formation of EXOC8 rods and rings. (A) IMCD3 cells were transfected with non-targeting siRNA (-ve control) or *impdh2* siRNA and immunostained for EXOC8 (anti-EXOC8, green) and DNA (DAPI, blue). Note the reduction of EXOC8 rods and rings in cells depleted of IMPDH2. Bar = 5 μm. **(B)** Graph showing the proportion of EXOC8 rods and rings in each condition (n= 115 cells, one independent experiment)

3.8. The EXOC8-IMPDH2 interaction is lost in an exocyst mutation linked to human disease

Recently, a previously undescribed mutation in the exocyst component *EXOC8* was found in a male with clinical features consistent with Joubert Syndrome (JBTS). JBTS is predominantly an autosomal recessive ciliopathy characterised by symptoms including hypotonia, ataxia, polydactyly and polycystic kidneys(Brancati et al., 2010; Dixon-Salazar et al., 2012; Nag et al., 2013) . Site directed mutagenesis was used to introduce the E265G patient mutation into the EGFP-EXOC8 plasmid used throughout this study. To test if the EXOC8 E265G mutation affected the localisation also to rods and rings, IMCD3 cells were transfected with GFP-tagged wild-type and mutant EXOC8 plasmids. Unlike EGFP-EXOC8, the EGFP-EXOC8-E265 plasmid did not localise to cytoplasmic rods and rings (Figure 3.16A). To assess if the interaction with IMPDH2 or CTPS1 was perturbed by the E265G mutation, duplicate GFP-Traps were performed to identify candidate binding partners for EXOC8-E265G. Replicate 1 contained 988 proteins, and replicate 2 contained 1049 proteins, which yielded a list of 606 high confidence ‘double positive’ interacting proteins. The exocyst complex remained associated with the mutant form of EXOC8, but interestingly neither IMPDH1 nor IMPDH2 was detected (Figure 3.16B, red box border indicates loss of interaction in the E265G mutant compared to the control). Thus, the EXOC8 JBTS-associated mutation affects the interaction between EXOC8 and IMPDH2, providing a possible explanation for the lack of rod/ring localisation and an intriguing hint that cytoplasmic rod and ring organisation and/or function might be impaired in human genetic disease.

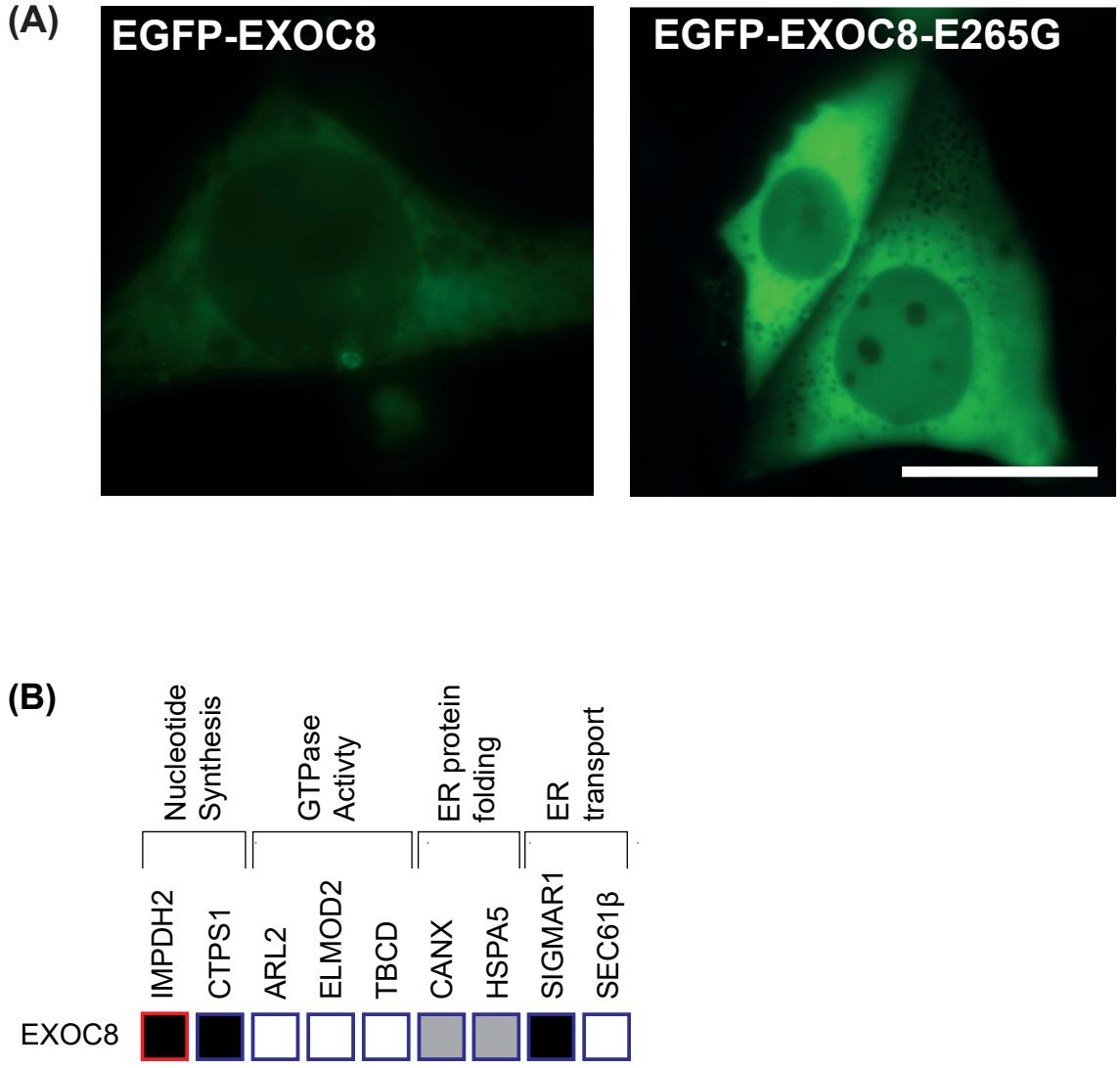

Figure 3.16. The EXOC8-IMPDH2 interaction is lost in an exocyst mutation linked to human disease. (A) The EGFP-EXOC8-E265G plasmid does not localise to cytoplasmic rods and rings **(B)** Interaction between EXOC8 and IMPDH2 is lost in the EXOC8-E265G patient mutation. Black box: high confidence interactor identified in duplicate GFP-Traps, grey box: single positive interactor identified in one GFP-Trap, white box: no interaction detected, red outline: interactor lost in patient mutation. Bar = 5 μm

4. Discussion

4.1. EXOC8 is associated with rod and ring structures in the cytoplasm

Although the exocyst complex is best studied in tethering secretory vesicles to the plasma membrane, it has other cellular roles. Since EXOC8 is the least characterised member of the exocyst complex and its function is obscure, information found as a result of this study can aid our understanding of the widespread and diverse roles of this important cellular membrane trafficking complex.

This thesis explored the novel localisation of EXOC8 to rod and ring structures in the cytoplasm. EXOC8-containing rod and ring structures resemble beads on a string, but confocal microscopy revealed additional “figure of eight” and “pin-hole” structures in the cytoplasm whose relationship (if any) to rods and rings is unclear from fixed cell studies. It is possible to speculate that EXOC8 exists initially as individual bead monomers in the cytoplasm that form into filamentous rods, then “figure of eight”/ “pin-hole” structures, before ultimately forming a ring. The high correlation between rod length and bead number, and between rod length and ring perimeter, is consistent with this idea. Unfortunately, Covid-19 restrictions prevented the planned investigation into the dynamics of EXOC8 rod and ring assembly and turnover, and it remains for future studies to elucidate. Are there set stages of formation and if so, what are the kinetics for each stage? What is the half-life of an EXOC8 rod and a ring? Answering these questions and discovering the mechanism of EXOC8 rod and ring assembly, is pivotal if we are to understand the significance of rod and ring structures for cell function.

One big outstanding question is whether other exocyst members also localise to rods and ring structures. Preliminary examinations have indicated that, under normal metabolic conditions, neither EXOC1 nor EXOC4 localise into any shape that resembles a rod or a ring. It is possible that under metabolic conditions that induce EXOC8 rod and ring formation, such as treating cells with Ribavirin or DON for 24 hours, or starving cells of glucose, EXOC1 or EXOC4 can form into rod and ring structures. However, given that it is now apparent that the exocyst complex does not always function as an octameric entity (Ahmed et al., 2018;

Moskalenko et al., 2003), and that individual (Inamdar et al., 2016) subunits have different subcellular locations, and therefore non-conventional roles, it is plausible that it is only EXOC8 that forms rod and ring structures in a role independent to the rest of the exocyst.

4.2. EXOC8: a regulator of cytoplasmic rod and ring organisation?

Based on morphology, incidence and induction conditions, it seems most likely that EXOC8 rods and rings are equivalent structures to IMPDH2 cytoplasmic rods and rings. Indeed, reduction of IMPDH2 in IMCD3 cells prevented the formation of EXOC8 rod and ring, demonstrating that IMPDH2 is required for their formation. However, induction of EXOC8 rods and rings takes substantially longer than induction of IMPDH2 and CTPS1 rod and ring counterparts, suggesting that IMPDH2 and/or CTPS1 rods and rings are a prerequisite for EXOC8 rod and ring formation.

Although the various types of rod and ring structures are sometimes described as non-membrane bound organelles (Calise et al., 2016; Carcamo et al., 2011; Thomas et al., 2012), several ER resident membrane proteins do localise to IMPDH2 cytoplasmic rods and rings (Schiavon et al., 2018), suggesting that the distinction between membrane-bound and non-membrane bound organelles is not clear cut. Perhaps some types of rods and rings, including those formed from IMPDH, should be thought of as having the potential to be membrane-associated. If this is the case, it makes sense that one of the major cellular membrane trafficking complexes should be able to interact with cytoplasmic rods and rings when cellular conditions require.

Co-localisation of ER proteins with IMPDH2 rods and rings is regulated temporally, and components are recruited in an ordered and sequential manner. IMPDH2 polymerisation into higher order rod and ring filaments is a prerequisite for localisation of the small GTPase ARL2, which in turn occurs prior to recruitment of calnexin, a transmembrane resident ER protein, and GRP78, an ER chaperone (Schiavon et al., 2018).

Given that approximately a third of mammalian proteins pass through the ER and Golgi on route to their final destination (Wang et al., 2020), it seems likely that factor(s) required to regulate cytoplasmic rods and rings are among them. This therefore begs the question of what recruits and transports protein cargo to

mature IMPDH2 rods and rings? Could the missing link be EXOC8 and the exocyst complex? After all, the exocyst is best studied in its known in vesicle trafficking, and this thesis has identified both calnexin and GRP78 as putative EXOC8-interaction partners in addition to the immunoprecipitation-verified structural rod/ring enzymes. Although EXOC8 is not required to form IMPDH2-containing rods and rings, it is required for the correct organisation of Ribavirin-induced IMPDH2 rods and rings. Moreover, EXOC8 localisation to rods and rings following Ribavirin treatment occurs over the longest time period of any protein studied to date, implying a post-assembly role.

Given that EXOC8 is a member of the exocyst complex, this leads to a model whereby EXOC8, probably alongside other exocyst subunits, traffics proteins required for IMPDH2 rod and ring maturation and/or turnover. Although many of the events are unclear, the following represents one possibility: (1) IMPDH assembles rapidly into higher order filaments in response to changing purine levels (2) a hierarchy of ER resident proteins associates with the newly formed rod/ring structures (3) rod/ring remodelling and turnover are regulated by association or disassociation with unknown “Protein X” to maintain rod and ring numbers appropriately. Based on the data in this thesis, EXOC8 represents a good candidate for trafficking vesicles containing “Protein X” to and from rods and rings. In the absence of EXOC8 (Figure 4.1 bottom), IMPDH2 rods and rings are still able to form constitutively and can still be induced. However, the highly ordered rod morphology is disrupted in induced cells, with both long rods and wispy reticular structures appearing over time, implying that EXOC8 Is required for maintenance of rod and ring morphology. The functional consequences of this alteration to IMPDH2 distribution are unknown, but one obvious hypothesis would be that purine synthesis is disrupted, with profound consequences for metabolism.

So, what proteins could EXOC8 traffic, and what could be the identity of “Protein(s) X”? A large high throughput screen performed by the Human Protein Atlas (HPA) identified 19 other proteins besides IMPDH1 and IMPDH2 which localise to rod and ring structures in the cytoplasm and/or nucleus (Thul et al., 2017). Analysis of the GFP-Trap data shows that, of these 19 proteins, EXOC8 interacts with two proteins: Scribbled planar cell polarity protein, and BTB domain containing 1 protein.

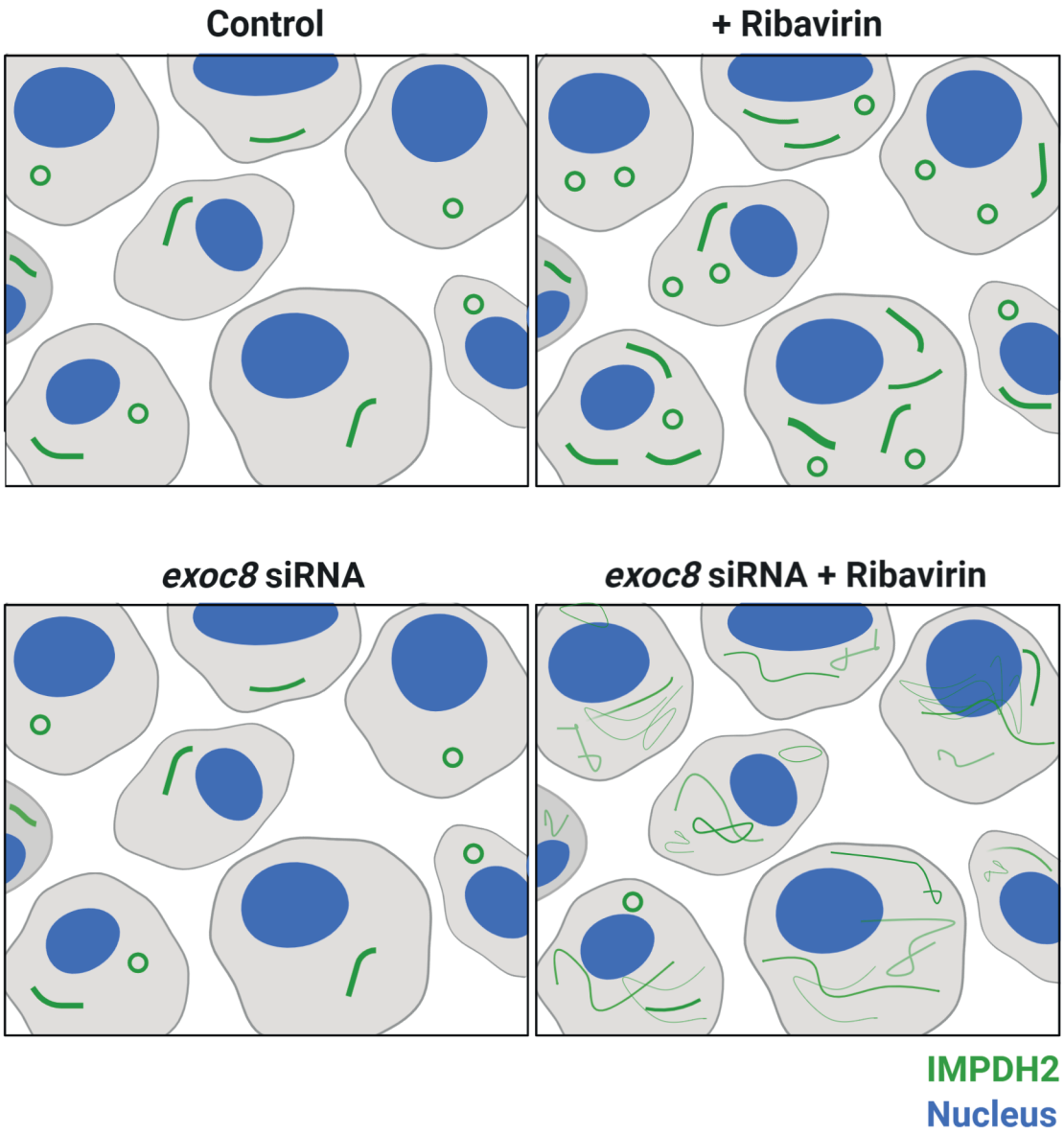

Figure 4.1. EXOC8 could traffic vesicles containing "Protein X" to and from rods and rings. In the absence of EXOC8 (bottom), IMPDH2 rods and rings are still able to form constitutively and can still be induced. However, the highly ordered rod morphology is disrupted in induced cells, with both long rods and wispy reticular structures appearing over time, implying that EXOC8 is required for maintenance of rod and ring morphology. EXOC8 could traffic vesicles containing proteins required for rod and ring maintenance. Figure created with BioRender.com

SCRIB is a scaffold protein involved in cell polarisation, cell adhesion, cell shape and tumour suppression (Humbert et al., 2003; Nola et al., 2008; Petit et al., 2005). It is possible that both cytoplasmic rods and rings and cytoophidia require a “tether” or a “scaffold” to form the characteristic rod and ring morphology. It is feasible that SCRIB fulfils this function, and that EXOC8 traffics SCRIB to locations where IMPDH rods and rings are required.

BTBD1 is a substrate-specific adapter of an E3 ubiquitin-ligase complex that mediates the ubiquitination of proteins (Furukawa et al., 2003). Asides the classical role of ubiquitination in proteasomal degradation, ubiquitination also modulates and induces protein conformational changes (Dittmar and Winklhofer, 2020). For example, it has already been established that ubiquitination of CTPS1 in *Drosophila* promotes CTPS1 rod and ring filament assembly (Pai et al., 2016; Wang et al., 2015). As a result, studies have tried to elucidate the role of ubiquitin post-translational modifications on IMPDH2 filament assembly.

One study found that Ankyrin repeat domain-containing protein 9 (ANKRD9), regulated IMPDH2 abundance and filament assembly (Hayward et al., 2019). ANKRD9 is a substrate-receptor subunit of the CUL5-based ubiquitin ligase E3 complex, that interacts with IMPDH1 and IMPDH2, to facilitate IMPDH ubiquitination and degradation (Lee et al., 2018). Under normal metabolic conditions, ANKRD9 localised to vesicle like structures (Hayward et al., 2019). However, upon nutrient deprivation or Ribavirin treatment ANKRD9 formed rod structures that co-localised with IMPDH2 rods. Interestingly, in nutrient deprived cells overexpressing ANKRD9, the length of IMPDH2 rods increased 2.5-fold, suggesting that ANKRD9 stabilised IMPDH2 filaments. Furthermore, ANKRD9 silencing prevented IMPDH2 rod formation in nutrient deprived cells, suggesting that ANKRD9 stabilised IMPDH2 in cells where the GTP pool was depleted. It is therefore possible that ANKRD9, along with E3 ubiquitin ligase, ubiquitinates and stabilises IMPDH2 to promote rod and ring filament assembly. Similarly, to ANKRD9, BTBD1 is a substrate specific interactor of E3 ubiquitin-ligase complex. Although the precise role of ubiquitination on IMPDH filament assembly is unknown, given the similarities between ANKRD9 and BTBD1, it does not seem unlikely that EXOC8 could traffic BTBD1 to IMPDH2 rods and rings, to ubiquitinate and stabilise them, in order to promote filament formation. Future

experiments should therefore address the role of ubiquitination in IMPDH filament assembly and turnover.

Finally, as described in the introduction, the small GTPase RalA interacts with EXOC8 and is required for a multitude of EXOC8 functions. The GFP-Trap identified this known EXOC8-RalA interaction, and it is possible that the association facilitates the formation of EXOC8 rods and rings. The interaction between EXOC8 and RalA occurs via the β5 loop of the EXOC8 PH domain, and interestingly, crystallography studies indicate the E265G Joubert syndrome mutation is within the β6 loop, only one β sheet from where RalA binds (Jin et al., 2005). While it sounds plausible that the E265G mutation could change the conformation of the PH domain such that RalA can no longer bind, and therefore explain why the EGFP-EXOC8-E265G plasmid failed to localise to rod or ring structures, the EXOC8-RalA interaction was maintained when residue 265 was mutated.

It is possible that the interaction between the mutated form of EXOC8 and RalA is the result of indirect binding to other members of the exocyst complex or to a different protein. Given how much RalA is known to contribute to exocyst function, it is worth investigating the effects of RalA mutants on EXOC8 rod and ring formation. For example, do EXOC8 rods and rings still form in cells expressing constitutively active RalA72L D49E or RalA72L A48W, which are unable to interact with different subunits of the exocyst (Ommer et al., 2019)? Do these mutants have an effect on IMPDH2 rod morphology? The results from these experiments would help to determine firstly if RalA is required for the formation of EXOC8 rods and rings and secondly, if other exocyst subunits are also involved.

4.3. EXOC8 rods and rings: a role in sequestering the exocyst?

Indeed, it is possible that EXOC8 rods and rings and IMPDH2 and/or CTPS1 rods and rings are not analogous structures and exist as separate entities. If this is the case, then what could be the role of EXOC8 rods and rings? As aforementioned, EXOC8 rods and rings can be induced over long time periods by Ribavirin, DON and glucose starvation. Given that Ribavirin and DON deplete intracellular pools of GTP and CTP, it is possible that localisation of EXOC8 to rods and rings plays a role in sequestering the exocyst complex away from its normal function in trafficking, as a way of regulating trafficking in response to changing nucleotide

levels (Carcamo et al., 2011). For example, in response to decreased intracellular GTP and/or CTP levels, the exocyst may form into rod and ring structures in the cytoplasm, which prevent the exocyst tethering post-Golgi secretory vesicles to the plasma membrane. As a result, secretory vesicles which may contain proteins required for the synthesis of GTP/CTP are not exocytosed and such proteins can be released from vesicles to restore intracellular GTP/CTP levels. It is therefore possible that EXOC8 forms into rods and ring structures to sequester the exocyst in order to modulate nucleotide levels.

4.4. Cytoplasmic rods and rings in human disease

Rods and rings are present in people who have HCV or are receiving treatment with Ribavirin and α-interferon (Covini et al., 2012; Keppeke et al., 2019). However, it has since been established that cytoplasmic rods and rings are present in patients who do not have HCV and who have not received ribavirin or α-interferon treatment (Zhang et al., 2020). In a large retrospective study that examined the presence of cytoplasmic rods and rings in patients' sera, 16 % of patients displayed rod and ring structures in a wide range of diseases unrelated to HCV (Climent et al., 2016). Moreover, rod and ring structures have been observed in multiple cancers including human hepatocellular carcinoma, acral lentiginous melanoma and clear cell renal cell carcinoma (Chang et al., 2017; Keppeke et al., 2020; Ruan et al., 2020). At present the link between rods and rings and disease seems clear, but the functional relevance remains unknown. Their presence is in part correlated with auto-immune diseases (Climent et al., 2016), but our understanding is at a very early stage and will take time to uncover.

The work in this thesis relates more to inherited disease. Given that EXOC8 is a candidate ciliopathy protein, this thesis explored the effect of a ciliopathy patient mutation of EXOC8 rod and ring formation. Whereas cells expressing a human EGFP-EXOC8 were able to form into rods and rings, cells expressing human EGFP-EXOC8-E265G were not. Furthermore, the mutated form of EXOC8 lost interaction with IMPDH2.

If EXOC8 rods and rings are lost in a patient with ciliopathy, is it possible that EXOC8 rods and rings contribute to normal ciliary formation and function? Unpublished data from the Dawe lab have identified that EXOC8 and amino acid 265 is important for ciliogenesis. It is therefore possible that EXOC8, binds to

IMPDH2 rods and rings and transports IMPDH2 associated proteins and enzymes to PM to regulate cilium formation. Alternatively, it is possible that EXOC8 rods and rings form as a consequence of cilium signalling and act as “sinks” for metabolic enzymes. For example, it is known that cilia contribute to the regulation of energy metabolism (Deng et al., 2018; Song et al., 2018). As cytoplasmic rods and rings are thought to be required for maintaining intracellular guanine nucleotide levels, and IMPDH2 and EXOC8 rods and rings share many similarities, it is possible that primary cilia regulate the formation of EXOC8 rods and rings to maintain and regulate cellular growth and metabolism. In this scenario, in cells expressing EGFP-EXOC8-E265G, aberrant ciliogenesis would no longer contribute to the maintenance of cellular metabolism and as a result EXOC8 rods and rings could no longer be formed. However, all this is speculative and such hypotheses would need to be tested experimentally.

The EXOC8 E265G mutation was first identified in a patient with symptoms consistent with a diagnosis of Joubert syndrome (Dixon-Salazar et al., 2012). JBTS is a clinically heterogeneous neurodevelopmental disorder that can exhibit additional non-CNS involvement including retinal dystrophy, polydactyly, hepatic fibrosis, and cystic renal disease (Brancati et al., 2010; Dixon-Salazar et al., 2012; Nag et al., 2013). The retinal dystrophy manifests as retinitis pigmentosa or Leber congenital amaurosis (LCA), with the visual impairment ranging from postnatal blindness to a mild progressive loss of vision over a period of decades. Intriguingly, these same retinal disorders are associated with mutations in IMPDH1 (Bowne et al., 2002; Bowne et al., 2006) and account for approximately 2 % of autosomal dominant cases of retinitis pigmentosa in North America as well as isolated (spontaneously manifesting) cases of LCA (Wada et al., 2005).

Considering the similarity in clinical presentations when EXOC8 and IMPDH1 are mutated, why was no interaction between EXOC8 and IMPDH1 observed? The answer could be due to IMPDH isoform expression. While both IMPDH1 and 2 are ubiquitously expressed, IMPDH2 is the predominant isoform in most tissues, including the kidney cells used in this thesis, and is upregulated in proliferating cells (Thomas et al., 2012). In contrast, IMPDH1 is expressed at high levels in the retina from late development onwards (Gunter et al., 2008). Therefore, it would be worth repeating the immunoprecipitation experiments in cell lines such as hTERT-RPE1 retinal epithelial cells – although the presence of IMPDH rods

and rings in this cell type would need verification as it has not been tested in this cell line to date. hTERT-RPE1 cells are ciliated, and might enable experiments to be designed which investigate links between clinically relevant IMPDH1 mutations, the exocyst, rod/ring organisation, and ciliogenesis and ciliary trafficking. Sequence comparisons reveal that key amino acids linked to retinitis pigmentosa are conserved between IMPDH1 and IMPDH2, and several of these - including the arginine at position 224 and the asparagine at position 226 - lie within the region identified as required for rod/ring formation (Thomas et al., 2012). It is tempting to speculate that mutations that prevent IMPDH from assembling into rods and rings, e.g. R224P (Thomas et al., 2012), might also affect interaction with EXOC8, and thus provide a mechanistic explanation for the pathophysiology of rod/ring-linked retinal degeneration. However, this has yet to be examined.

An alternative explanation for the pathology is via the regulation of the major phototransduction pigment protein rhodopsin (McGrew and Hedstrom, 2012). The IMPDH1 D226N mutant has reduced binding to nucleic acids and reduced ribosome association, leading to the idea that rhodopsin biosynthesis could be perturbed. The observation that EXOC8 has unexplored putative interactions with proteins involved in poly(A) RNA binding fits in with this idea. However, rhodopsin visual transduction requires intraflagellar transport–mediated transport between rod inner and outer segments via the connecting cilium (Chadha et al., 2019; Wolfrum and Schmitt, 2000), and loss of EXOC8 function perturbs cilium formation (see above). Whether IMPDH1/2 are also required for ciliogenesis also requires testing, and any observed link would have to be studied in detail to determine if it is direct or not, given that IMPDH1 mediates production of most of the guanine in photoreceptors (Aherne et al., 2004) and thus has wide-ranging effects on retinal metabolism. However, many of the disease-linked IMPDH1 mutations do not affect enzyme activity (Aherne et al., 2004), and therefore other cellular roles for this protein are not implausible.

5. Conclusion

Despite the exocyst being discovered some 20 years ago, an abundance of evidence suggests that besides the canonical role of the exocyst in exocytosis, the exocyst complex contributes to non-exocytic functions.

This thesis has shown a novel localisation for the exocyst complex member EXOC8 at rod and ring structures. Characterisation of EXOC8 rods and rings shows that EXOC8 rods and rings assemble “beads on a string” and are cell line specific. This is the first time that an exocyst subunit – and indeed any membrane trafficking complex - has been linked to cytoplasmic rods and rings, and supports the increasing evidence for exocyst function in roles distinct from exocytosis.

EXOC8 rods and rings are morphologically most similar to IMPDH-containing cytoplasmic rods and rings, and the EXOC8-IMPDH2 interaction is lost in EXOC8 containing a pathogenic mutation that is a candidate for the neurodevelopmental ciliopathy Joubert syndrome. While there are intriguing links between IMPDH, the exocyst, and retinal dystrophy, there are many different potential explanations for the cellular basis of the disease. Much further work is therefore required to understand the connections between membrane trafficking, cytoplasmic rods and rings, and phototransduction.

6. Appendices

Appendix Table 1. Recipe for 10 % Polyacrylamide Running Gel.

Ingredient	Manufacturer	Concentration
Tris-HCl pH=8.8	Sigma-Aldrich	375 mM
SDS	Sigma-Aldrich	0.1 %
Protogel Running Gel	National Diagnostics	8.3 %
APS	Sigma-Aldrich	0.1 %
TEMED	Sigma-Aldrich	0.1 %

Appendix Table 2. Double Positive Interactors in the EXOC8-GFP Trap

MGI	Mouse GN	WT (1) Score	EXOC8 (1) Score	WT (2) Score	EXOC8 (2) Score	AVG Score
MGI:2142527	Exoc8	67.9	1298.18	40.37	1224.4607	1261.32
MGI:1277961	Plec	#N/A	1046.59	#N/A	479.50133	763.05
MGI:95566	Fn1	#N/A	516.493	26.57	121.53678	319.01
MGI:88461	Col6a3	97.8	499.814	19.63	116.73067	308.27
MGI:103147	Dync1h1	40.68	389.258	11.35	181.25472	285.26
MGI:1341878	Ehd1	#N/A	98.145	#N/A	304.21143	201.18
MGI:1095409	Tuba1c	#N/A	166.051	#N/A	211.86978	188.96
MGI:1316648	Ahnak	59.15	353.93	#N/A	23.514944	188.72
MGI:88467	Col1a1	19.13	295.29	10.4	54.518481	174.90
MGI:95557	Flnc	46.6	195.435	#N/A	91.587316	143.51
MGI:97838	Eprs	67.89	200.639	21.8	77.077711	138.86
MGI:1342292	Hspa4	34.34	144.296	#N/A	127.47805	135.89
MGI:1916969	Cad	#N/A	170.084	#N/A	90.699183	130.39
MGI:97547	Pfkl	#N/A	129.094	#N/A	119.81612	124.46
MGI:88468	Col1a2	#N/A	171.684	#N/A	10.301073	90.99
MGI:98158	Rps4x	#N/A	104.564	#N/A	76.952827	90.76
MGI:1921372	Tmem43	#N/A	74.0896	#N/A	103.65842	88.87
MGI:96794	Lmna	37.84	95.6344	6.682	81.062391	88.35
MGI:1349438	Mprip	#N/A	156.16	#N/A	7.2004943	81.68
MGI:88459	Col6a1	33.71	131.326	#N/A	26.627125	78.98
MGI:1923864	Immt	#N/A	73.816	#N/A	84.045799	78.93
MGI:2446089	Flnb	28.31	103.687	#N/A	51.834834	77.76
MGI:1890773	Actn4	#N/A	59.9055	#N/A	95.173232	77.54
MGI:1932395	Rrbp1	26.48	103.509	#N/A	48.146497	75.83
MGI:88246	Anxa2	#N/A	68.0543	19.78	82.863861	75.46
MGI:106919	Vdac1	15.26	95.272	#N/A	50.143484	72.71
MGI:1917599	Copb1	18.09	54.6468	10.4	81.847072	68.25
MGI:1922896	Rai14	#N/A	123.067	1.842	12.546045	67.81
MGI:A1E2B8		#N/A	41.4031	#N/A	91.70318	66.55
MGI:98085	Rpn2	9.138	98.652	5.398	34.441524	66.55
MGI:1096584	Psmd2	23.14	59.3554	#N/A	71.356143	65.36
MGI:104689	Cct4	#N/A	47.8507	#N/A	81.313396	64.58
MGI:1341628	Atrn	#N/A	77.8892	#N/A	48.918966	63.40
MGI:106915	Vdac2	13.53	60.8326	7.408	65.242677	63.04
MGI:2384784	Eif4g1	#N/A	93.1122	#N/A	31.633092	62.37
MGI:99256	Hdlbp	#N/A	90.9821	#N/A	25.497518	58.24

MGI:1917473	Nars	9.124	38.0154	#N/A	73.778976	55.90
MGI:1917497	Psmd1	#N/A	45.7223	#N/A	65.664938	55.69
MGI:1926080	Slc25a12	#N/A	38.5939	9.078	69.456181	54.03
MGI:97548	Pfkm	13.17	60.6789	6.155	46.867893	53.77
MGI:99894	Hnrnpk	#N/A	47.08	#N/A	57.235359	52.16
MGI:88460	Col6a2	10.88	93.8376	#N/A	8.6861541	51.26
MGI:99432	Arf3	#N/A	57.5578	#N/A	44.201448	50.88
MGI:88110	Atp2a2	2.71	46.2272	2.49	53.473552	49.85
MGI:105053	Hsph1	#N/A	55.3647	#N/A	43.74805	49.56
MGI:95698	Gfpt1	0	54.5507	#N/A	43.530779	49.04
MGI:1919192	Myof	17.39	69.219	2.05	27.728173	48.47
MGI:107422	Hspa4l	#N/A	48.7646	#N/A	45.132051	46.95
MGI:1858234	Caprin1	#N/A	61.1023	4.347	30.798078	45.95
MGI:1298373	Rpl9	#N/A	41.6147	#N/A	48.957191	45.29
MGI:88561	Ctsb	#N/A	64.3322	5.246	26.200912	45.27
MGI:1278330	Smpd2	#N/A	36.6244	#N/A	52.075888	44.35
MGI:1925544	Rps27a	10.57	55.7147	6.184	31.297137	43.51
MGI:95485	Fasn	#N/A	64.3037	#N/A	21.565588	42.93
MGI:1919619	Ehd4	#N/A	15.8739	#N/A	69.882758	42.88
MGI:1858304	Ctps1	8.694	32.0896	#N/A	52.520574	42.31
MGI:97503	Pcna	#N/A	47.4239	#N/A	34.853942	41.14
MGI:1261820	Cand1	13.76	50.3979	1.76	30.977033	40.69
MGI:101920	Ap2a2	1.736	54.5214	1.916	25.614036	40.07
MGI:88105	Atp1a1	#N/A	51.2332	#N/A	27.062691	39.15
MGI:101921	Ap2a1	5.731	54.184	4.031	23.92679	39.06
MGI:1914347	Rps10	15.7	53.6553	#N/A	24.23208	38.94
MGI:1915113	Slc25a11	#N/A	38.7334	#N/A	37.927297	38.33
MGI:90675	Vars	#N/A	47.5456	#N/A	25.061447	36.30
MGI:1919666	Lrpprc	12.85	56.6451	2.046	15.369848	36.01
MGI:1914670	Far1	5.348	27.9149	#N/A	43.618239	35.77
MGI:1929899	Sqor	6.951	24.5427	#N/A	45.199598	34.87
MGI:107184	Cct7	#N/A	23.8804	#N/A	44.102869	33.99
MGI:2137679	Sfxn3	#N/A	39.6571	#N/A	27.869524	33.76
MGI:2145645	Exoc5	#N/A	27.2353	#N/A	37.874747	32.56
MGI:1914198	Acad8	#N/A	44.3928	#N/A	20.135978	32.26
MGI:1333871	Hsd17b10	#N/A	37.4982	#N/A	26.740766	32.12
MGI:1858195	Hnrnpu	#N/A	38.8677	#N/A	24.754115	31.81
MGI:105047	Psmc5	#N/A	22.2001	#N/A	41.272802	31.74
MGI:2145219	Iars	8.345	48.0726	0	14.689691	31.38
MGI:106341	Atp5o	#N/A	35.6412	#N/A	26.327089	30.98
MGI:1891731	Stub1	#N/A	35.3326	#N/A	26.341045	30.84
MGI:2447670	Mgrn1	#N/A	27.714	#N/A	33.378683	30.55
MGI:1926465	Hnrnpm	#N/A	29.6788	3.993	30.069656	29.87
MGI:1929260	Mtch2	5.565	29.5634	4.671	30.017719	29.79
MGI:107995	Upf1	#N/A	46.0245	#N/A	13.272257	29.65
MGI:107752	Myo1b	#N/A	52.7356	#N/A	6.1447246	29.44
MGI:1351465	G3bp1	11.12	37.3405	#N/A	21.451214	29.40
MGI:1919020	Ap2b1	#N/A	33.6854	#N/A	24.395896	29.04
MGI:106922	Vdac3	3.235	35.7571	1.658	21.768476	28.76
MGI:1918054	Pgrmc2	#N/A	37.9854	#N/A	18.595226	28.29
MGI:1298398	Mcm7	5.86	23.9781	#N/A	32.504517	28.24
MGI:106013	Slc16a1	1.825	31.6861	#N/A	23.986503	27.84
MGI:1918944	Ipo9	#N/A	32.7976	#N/A	22.505414	27.65
MGI:1859270	Exoc7	#N/A	18.0445	#N/A	37.024722	27.53

MGI:2152414	Ipo7	5.764	32.7526	3.097	22.066928	27.41
MGI:1321161	Ppp2cb	#N/A	24.6372	#N/A	30.024908	27.33
MGI:1858696	Copg1	6.699	25.6288	#N/A	28.368091	27.00
MGI:1913906	Eef1d	#N/A	44.6289	#N/A	9.3598642	26.99
MGI:1096376	Exoc4	#N/A	32.3828	#N/A	21.288305	26.84
MGI:106248	Eif5a	2.969	25.0522	3.095	28.144228	26.60
MGI:1330294	Hnrnpab	9.062	24.7496	#N/A	27.896481	26.32
MGI:1931882	Dnaja2	#N/A	9.01507	#N/A	43.498918	26.26
MGI:108202	Pcbp2	#N/A	25.9974	#N/A	26.113848	26.06
MGI:1202384	Ddb1	#N/A	34.9462	#N/A	16.523086	25.73
MGI:3642408	Gm10250	#N/A	41.4074	#N/A	9.7062064	25.56
MGI:1929520	Eef1b	#N/A	47.9447	#N/A	2.6377673	25.29
MGI:1353497	Slc25a10	1.971	26.1932	7.753	23.852221	25.02
MGI:1917171	Hnrnpa3	#N/A	28.1604	#N/A	21.493852	24.83
MGI:107494	Myl12b	12.78	36.5922	#N/A	12.120178	24.36
MGI:894407	Tmem165	#N/A	23.9907	#N/A	24.124299	24.06
MGI:88264	Capn2	#N/A	19.4194	#N/A	28.672976	24.05
MGI:102854	Rpl5	#N/A	26.9785	8.055	20.862461	23.92
MGI:104819	Hnrnpa2b1	7.322	33.7557	1.763	13.530137	23.64
MGI:1349450	Vat1	2.467	16.1557	#N/A	31.052815	23.60
MGI:107728	Myo1d	#N/A	40.6871	#N/A	6.3953989	23.54
MGI:98386	Sptan1	0	40.2033	#N/A	6.3210077	23.26
MGI:2137677	Sfxn1	#N/A	29.5119	#N/A	16.960471	23.24
MGI:1270129	Dnaja1	3.256	12.2621	2.338	34.067204	23.16
MGI:1913775	Timm50	5.398	18.1155	6.101	28.104044	23.11
MGI:2448388	Hist1h2bj	#N/A	30.0769	#N/A	16.122881	23.10
MGI:104872	Ppp1cc	#N/A	23.0522	#N/A	23.064794	23.06
MGI:1100851	Elavl1	#N/A	36.5546	2.401	9.42377	22.99
MGI:98927	Vcl	10.76	40.8673	#N/A	5.0307013	22.95
MGI:2148924	Clic1	8.922	26.4838	7.348	18.985199	22.73
MGI:1891833	Pfkp	#N/A	25.1655	#N/A	20.205544	22.69
MGI:1913325	Chchd3	#N/A	29.8634	#N/A	15.380024	22.62
MGI:1891254	Bag2	1.88	28.8453	#N/A	15.850304	22.35
MGI:95784	Gnb2	#N/A	15.8518	#N/A	27.061278	21.46
MGI:104652	Capzb	3.952	24.8995	#N/A	17.928811	21.41
MGI:1338801	Cyfip1	#N/A	24.137	#N/A	18.335344	21.24
MGI:98388	Sptbn1	#N/A	39.9863	#N/A	1.6165149	20.80
MGI:1915337	Dcakd	#N/A	29.0247	#N/A	12.437044	20.73
MGI:1330239	Dpm1	#N/A	32.3835	#N/A	9.0721354	20.73
MGI:94871	Eci1	4.101	23.5915	2.408	17.519378	20.56
MGI:2144831	Ahnak2	#N/A	38.5792	#N/A	2.37725	20.48
MGI:2138281	Lbr	6.419	18.4289	5.929	22.162615	20.30
MGI:95301	Eif3a	6.251	26.916	#N/A	13.244958	20.08
MGI:2183441	Psat1	6.594	20.2302	#N/A	17.658608	18.94
MGI:103038	Stat3	#N/A	7.74916	#N/A	30.082252	18.92
MGI:1096368	Ap1b1	#N/A	19.5118	#N/A	18.201564	18.86
MGI:1927593	Ptges	#N/A	17.7327	#N/A	19.960703	18.85
MGI:106314	Tars	10.64	28.1355	#N/A	9.5221226	18.83
MGI:98283	Srsf1	1.965	28.0411	1.875	9.2782062	18.66
MGI:97178	Map4	1.918	30.2727	#N/A	6.8264444	18.55
MGI:1890359	Igf2bp3	2.579	18.4687	4.034	18.349877	18.41
MGI:96435	Igf2r	#N/A	19.6149	#N/A	17.103264	18.36
MGI:1353561	Vapa	2.867	28.0063	2.885	8.6514692	18.33
MGI:1338759	Sec22b	#N/A	25.2576	2.786	11.253839	18.26

MGI:1891702	Cope	4.613	22.0756	4.963	14.18227	18.13
MGI:1345283	Slc25a1	#N/A	19.7879	2.006	16.142875	17.97
MGI:1194508	Ddost	3.525	13.4193	#N/A	22.302325	17.86
MGI:1349419	Aifm1	#N/A	9.15486	#N/A	26.207578	17.68
MGI:1917160	Slc25a24	#N/A	14.5011	#N/A	20.403903	17.45
MGI:2444248	Gcn1	#N/A	21.2161	#N/A	13.398074	17.31
MGI:105922	Rpl13	#N/A	18.4022	#N/A	16.171063	17.29
MGI:1915831	Tmed10	#N/A	24.7223	#N/A	9.3843426	17.05
MGI:2158650	Idh3b	#N/A	11.1248	#N/A	22.287887	16.71
MGI:1858417	Sec61a1	2.032	17.463	4.429	15.736238	16.60
MGI:108177	Dhx9	#N/A	26.0021	#N/A	7.0564618	16.53
MGI:1298379	Matr3	#N/A	22.521	#N/A	10.467633	16.49
MGI:1354721	Slc25a13	#N/A	10.4174	#N/A	22.35041	16.38
MGI:1913808	Lars	9.162	25.9703	#N/A	6.4036436	16.19
MGI:1888676	Rps27	#N/A	20.4439	#N/A	11.840907	16.14
MGI:96955	Slc3a2	#N/A	9.94439	#N/A	22.194919	16.07
MGI:1351657	Abcf2	2.142	19.4923	#N/A	12.52973	16.01
MGI:1351628	Rps26	5.176	15.3307	5.944	16.34805	15.84
MGI:3704362	Gm10273	#N/A	16.4393	#N/A	15.215839	15.83
MGI:102790	Rab18	2.331	15.4726	1.801	15.863038	15.67
MGI:102581	Rdh11	#N/A	22.7987	2.865	8.1998172	15.50
MGI:106478	Eif3b	5.636	18.1912	2.536	12.733265	15.46
MGI:108515	Cbx3	#N/A	19.4259	#N/A	11.356188	15.39
MGI:1923164	Exoc6b	#N/A	11.3274	#N/A	19.38558	15.36
MGI:1859293	Atxn10	#N/A	5.77709	4.36	23.764672	14.77
MGI:2387629	Tardbp	#N/A	12.9999	#N/A	16.325356	14.66
MGI:2140220	Ecm29	#N/A	19.8074	#N/A	9.4657115	14.64
MGI:97531	Pdgfrb	#N/A	14.3696	#N/A	14.690887	14.53
MGI:105124	Stt3a	3.502	15.2745	3.96	13.694038	14.48
MGI:1924015	Mlec	#N/A	20.1207	#N/A	8.5343068	14.33
MGI:95299	Eif2s1	#N/A	16.6192	#N/A	11.632906	14.13
MGI:2444680	Aldh1l2	2.519	8.25392	#N/A	19.821107	14.04
MGI:99436	Arl1	#N/A	18.8658	#N/A	9.025423	13.95
MGI:2448326	Hist1h3e	6.466	19.1253	#N/A	8.664896	13.90
MGI:104653	Atp2b1	#N/A	22.0774	#N/A	5.4583158	13.77
MGI:106920	Tmpo	5.238	19.1009	#N/A	8.4280757	13.76
MGI:1277956	Pycr2	#N/A	23.6256	#N/A	3.5799823	13.60
MGI:1916840	Gpx8	#N/A	17.3748	#N/A	9.6890128	13.53
MGI:1915295	RTRAF	#N/A	24.4459	#N/A	2.6153953	13.53
MGI:1917822	Ipo5	#N/A	16.0894	#N/A	10.965664	13.53
MGI:96817	Lox	#N/A	12.7921	#N/A	14.221673	13.51
MGI:2684937	Lclat1	#N/A	14.054	#N/A	12.94807	13.50
MGI:1927244	Ralb	#N/A	15.9495	#N/A	9.828458	12.89
MGI:2443162	Uggt1	#N/A	21.1745	#N/A	4.4554235	12.81
MGI:1915173	Eloc	#N/A	16.9311	#N/A	8.1971667	12.56
MGI:1861457	Dynll1	#N/A	15.9784	#N/A	8.3983181	12.19
MGI:1921455	Acsl3	#N/A	12.1762	#N/A	11.979003	12.08
MGI:1858259	Tomm40	#N/A	5.78927	#N/A	18.212094	12.00
MGI:101816	Msh2	#N/A	10.487	#N/A	13.424963	11.96
MGI:109153	Ktn1	#N/A	22.1641	#N/A	1.7185017	11.94
MGI:1860603	Rpl36	5.977	15.5016	2.517	8.333076	11.92
MGI:2446163	FAM120A	2.421	12.7791	0	10.76	11.77
MGI:1915070	Tmed4	#N/A	14.1981	#N/A	9.2246301	11.71
MGI:1353586	Lmo7	#N/A	14.7378	#N/A	8.5809226	11.66

MGI:1347014	Psmb3	#N/A	11.283	3.666	11.913577	11.60
MGI:1346093	Psmc4	#N/A	2.07647	#N/A	21.055907	11.57
MGI:1914708	Ergic1	#N/A	10.3838	#N/A	12.292182	11.34
MGI:1194513	Psmb5	#N/A	11.2835	#N/A	11.35285	11.32
MGI:2144013	Xpo1	2.771	12.6286	3.186	9.4681245	11.05
MGI:1914135	Acadsb	#N/A	7.01614	#N/A	14.819194	10.92
MGI:2183260	Luc7l2	2.275	13.413	#N/A	8.2820823	10.85
MGI:88351	Cdk1	#N/A	14.595	#N/A	6.9180653	10.76
MGI:104888	Fdps	#N/A	12.5751	#N/A	8.8946302	10.73
MGI:108064	Siah1a	2.006	15.3541	#N/A	6.1053771	10.73
MGI:1355326	Preb	#N/A	7.12776	#N/A	14.015574	10.57
MGI:98445	Surf4	#N/A	13.8542	#N/A	7.0008405	10.43
MGI:1923959	Arpc2	1.689	5.68721	4.247	15.069352	10.38
MGI:1913677	Cyb5b	#N/A	13.024	#N/A	7.6860231	10.36
MGI:1913697	Mgst3	#N/A	10.959	#N/A	9.7214205	10.34
MGI:1306824	Suclg2	1.714	7.65021	1.755	12.794726	10.22
MGI:1914930	Sdhb	#N/A	11.049	#N/A	9.3223826	10.19
MGI:1342299	Ruvbl2	#N/A	4.9634	#N/A	15.18881	10.08
MGI:1859652	Mtx2	#N/A	15.9696	#N/A	4.179471	10.07
MGI:1336880	Eftud2	#N/A	15.6777	#N/A	4.2069731	9.94
MGI:106028	Rhoc	#N/A	17.1202	#N/A	2.5166469	9.82
MGI:2387591	Arcn1	#N/A	8.93444	#N/A	10.579001	9.76
MGI:105093	Cnn2	#N/A	6.98567	#N/A	12.458425	9.72
MGI:95755	Slc2a1	#N/A	9.8521	#N/A	9.5865059	9.72
MGI:96907	Marcks	#N/A	12.0294	#N/A	7.2635324	9.65
MGI:105305	Slc1a5	#N/A	5.31043	#N/A	13.824027	9.57
MGI:1336214	Khsrp	2.413	13.5529	#N/A	5.5803909	9.57
MGI:2450248	Tomm22	1.704	9.92972	#N/A	9.1708724	9.55
MGI:95654	Gart	#N/A	10.6477	#N/A	8.3822081	9.51
MGI:1915851	Qars	#N/A	11.6055	#N/A	7.2501569	9.43
MGI:1915128	Tmem33	#N/A	11.4194	#N/A	7.3368193	9.38
MGI:104885	Psma2	#N/A	9.97206	#N/A	8.6691051	9.32
MGI:1927243	Rala	#N/A	9.89518	#N/A	8.6793245	9.29
MGI:95772	Gnai2	#N/A	7.68425	#N/A	10.701971	9.19
MGI:1352493	Bag3	#N/A	10.5781	#N/A	7.7356825	9.16
MGI:1098684	Eif2a	#N/A	5.07876	#N/A	13.070635	9.07
MGI:1855692	Nono	#N/A	8.14107	#N/A	9.9484169	9.04
MGI:1932339	Sf3b1	#N/A	15.7534	#N/A	2.2599525	9.01
MGI:3644226	Gm8994	#N/A	6.11652	#N/A	11.871705	8.99
MGI:105066	Rab10	#N/A	7.38795	#N/A	10.588925	8.99
MGI:98886	U2af2	#N/A	11.9548	#N/A	5.94398	8.95
MGI:1928744	Vapb	#N/A	12.4381	#N/A	5.4508414	8.94
MGI:105491	Cdipt	#N/A	12.5391	#N/A	5.1424234	8.84
MGI:1915903	Samm50	#N/A	7.42855	#N/A	10.123283	8.78
MGI:1890358	Igf2bp2	#N/A	9.87862	#N/A	7.561723	8.72
MGI:2387215	Erlin2	#N/A	2.23476	#N/A	14.955512	8.60
MGI:1923827	Faf2	#N/A	2.41777	#N/A	14.554371	8.49
MGI:1341044	Alyref	#N/A	11.3275	#N/A	5.5484524	8.44
MGI:1194505	C1qbp	#N/A	13.5858	#N/A	3.1901209	8.39
MGI:1913416	S100a14	#N/A	7.99624	#N/A	8.6591513	8.33
MGI:1924134	Cyfip2	#N/A	9.74019	#N/A	6.9133291	8.33
MGI:1927155	Clptm1	#N/A	14.2508	#N/A	2.3379252	8.29
MGI:97776	Prps2	#N/A	5.47526	#N/A	10.95568	8.22
MGI:88516	Cryab	#N/A	10.8205	#N/A	5.4962074	8.16

MGI:98763	Tk1	#N/A	12.1324	#N/A	4.0355202	8.08
MGI:106379	Rtcb	#N/A	1.83186	#N/A	13.993015	7.91
MGI:97887	Rdx	#N/A	2.93561	#N/A	12.868795	7.90
MGI:1915615	Rab14	#N/A	7.00451	#N/A	8.7903825	7.90
MGI:2179381	Prpf8	#N/A	12.1542	#N/A	3.6188254	7.89
MGI:1339468	S100a10	1.863	11.4668	#N/A	4.2973394	7.88
MGI:1339951	Cse1l	#N/A	4.82297	#N/A	10.907911	7.87
MGI:1913498	Alg5	#N/A	3.76961	#N/A	11.813508	7.79
MGI:1298405	Ap2m1	1.655	10.3299	#N/A	5.2082683	7.77
MGI:1277958	Pcm1	#N/A	9.4134	#N/A	5.9876804	7.70
MGI:1347045	Psmb2	2.736	11.5175	#N/A	3.7838233	7.65
MGI:1929264	Sae1	#N/A	6.22469	#N/A	8.6412516	7.43
MGI:2135962	Gorasp2	#N/A	5.5925	#N/A	9.2569697	7.42
MGI:95609	Gaa	#N/A	7.31982	#N/A	7.5003684	7.41
MGI:1343176	Timm17b	#N/A	12.4634	#N/A	2.3106527	7.39
MGI:1890149	Tpm3	#N/A	10.7016	#N/A	3.9469454	7.32
MGI:2442040	G3bp2	#N/A	6.11488	#N/A	8.5206769	7.32
MGI:1353633	Fus	0	7.46049	#N/A	7.1207733	7.29
MGI:1914172	Rras2	#N/A	5.29102	3.698	9.2595043	7.28
MGI:1914461	Armc10	#N/A	12.6612	#N/A	1.7836658	7.22
MGI:1347006	Psma6	#N/A	8.20934	2.083	6.1959248	7.20
MGI:105100	Ctnnd1	#N/A	4.48885	#N/A	9.8610759	7.17
MGI:2445121	Slfn9	#N/A	9.64807	#N/A	4.5977335	7.12
MGI:1913348	Chchd6	#N/A	8.44517	#N/A	5.7527893	7.10
MGI:2384802	Eif2b1	#N/A	9.07043	#N/A	5.0303801	7.05
MGI:107750	Dync1i2	2.385	7.16893	#N/A	6.9032576	7.04
MGI:2449202	Tpm4	#N/A	11.258	#N/A	2.7224858	6.99
MGI:98287	Srsf5	#N/A	9.12915	#N/A	4.7659709	6.95
MGI:104810	Plaa	0	10.7542	#N/A	3.1377802	6.95
MGI:97532	Pdha1	#N/A	4.33078	#N/A	9.5543275	6.94
MGI:1858305	Pgrmc1	#N/A	12.0158	#N/A	1.8404496	6.93
MGI:95775	Gnao1	#N/A	8.06093	#N/A	5.6676502	6.86
MGI:1890165	Larp1	#N/A	11.0784	#N/A	2.6041877	6.84
MGI:99425	Rab11b	#N/A	9.70925	#N/A	3.8257736	6.77
MGI:1914248	Psmd5	#N/A	3.88178	#N/A	9.6043293	6.74
MGI:2149821	Hsd17b11	#N/A	5.89409	#N/A	7.4881968	6.69
MGI:2441984	Lrrc41	#N/A	2.71271	#N/A	10.621809	6.67
MGI:1931787	Scyl1	#N/A	10.2261	#N/A	3.046478	6.64
MGI:2154274	Ehd2	#N/A	7.48933	#N/A	5.7285054	6.61
MGI:1917403	2210016F16Rik	#N/A	5.73508	#N/A	7.4194502	6.58
MGI:1891112	Gmds	#N/A	4.44351	#N/A	8.5743408	6.51
MGI:2441772	Eif5b	#N/A	10.6556	#N/A	2.2662342	6.46
MGI:104976	Ddx6	#N/A	6.3095	0	6.5450057	6.43
MGI:1929282	Ptges3	#N/A	8.37266	#N/A	4.3281235	6.35
MGI:2151483	Derl2	#N/A	7.47732	#N/A	5.2169363	6.35
MGI:104667	Hmmr	#N/A	7.96816	#N/A	4.6811719	6.32
MGI:96915	Maoa	#N/A	5.3397	#N/A	7.161045	6.25
MGI:1098257	Psmb4	2.297	7.8472	#N/A	4.4336045	6.14
MGI:88357	Cdk4	#N/A	8.54986	#N/A	3.7030048	6.13
MGI:1349216	Abcd3	#N/A	5.72879	#N/A	6.46682	6.10
MGI:106098	Etfb	#N/A	8.83648	#N/A	2.9602847	5.90
MGI:109367	Impdh2	#N/A	3.0565	2.924	8.6968205	5.88
MGI:105082	Ssr1	#N/A	5.44233	#N/A	6.2053087	5.82
MGI:104816	Hnrnpl	#N/A	8.56376	#N/A	3.0817733	5.82

MGI:105099	Pcolce	#N/A	9.5625	#N/A	2.0314243	5.80
MGI:1915069	Derl1	1.949	6.68178	#N/A	4.796186	5.74
MGI:1858232	Nudt5	#N/A	8.23777	#N/A	3.2332671	5.74
MGI:1913335	Eif3f	#N/A	4.6967	#N/A	6.7608705	5.73
MGI:104995	Gclm	#N/A	7.34556	#N/A	3.9812015	5.66
MGI:1913607	Ostc	#N/A	5.75313	#N/A	5.222631	5.49
MGI:2145316	Txndc5	#N/A	2.27459	#N/A	8.4908955	5.38
MGI:894681	Usp9x	#N/A	8.18439	#N/A	2.5017323	5.34
MGI:99926	ATP8	#N/A	8.1351	#N/A	2.5292182	5.33
MGI:97831	Ppa1	#N/A	7.19263	#N/A	3.4567995	5.32
MGI:1345633	Mars	1.847	8.30947	#N/A	2.2228148	5.27
MGI:1926232	Srsf7	#N/A	6.94093	#N/A	3.5801299	5.26
MGI:2442174	Mic13	#N/A	5.43076	#N/A	4.8690462	5.15
MGI:95753	Glud1	#N/A	2.09727	#N/A	7.9640806	5.03
MGI:1926178	Pigt	#N/A	1.75544	#N/A	8.2321978	4.99
MGI:98884	U2af1	#N/A	7.46268	#N/A	2.4586289	4.96
MGI:1306799	D17H6S56E-5	#N/A	5.09771	#N/A	4.7907935	4.94
MGI:97744	Por	#N/A	2.53956	#N/A	7.3385912	4.94
MGI:104967	Glg1	#N/A	7.50793	#N/A	2.3218224	4.91
MGI:108278	Ube2m	#N/A	5.19161	#N/A	4.6029246	4.90
MGI:2180203	Tmlhe	#N/A	2.03748	1.991	7.7404306	4.89
MGI:1928488	Akap8	#N/A	4.51162	#N/A	5.1698101	4.84
MGI:1915517	Slc25a22	#N/A	7.6253	#N/A	1.9990079	4.81
MGI:1914285	Dnajb4	#N/A	3.63692	#N/A	5.9596665	4.80
MGI:1261415	Sgpl1	#N/A	5.14751	#N/A	4.2397711	4.69
MGI:1351597	Atp5l	#N/A	5.03208	#N/A	4.3361779	4.68
MGI:104563	Napa	#N/A	3.08351	#N/A	6.2172717	4.65
MGI:1914375	Tspan31	#N/A	6.04477	#N/A	3.1616833	4.60
MGI:1099786	Dhx15	#N/A	4.73503	#N/A	4.4062684	4.57
MGI:1344381	Dnajb6	#N/A	2.95083	#N/A	6.1596739	4.56
MGI:1913293	Atp5d	#N/A	7.10873	#N/A	1.9928714	4.55
MGI:1332236	Cds2	#N/A	6.49194	#N/A	2.5699508	4.53
MGI:2444401	Snrnp200	2.019	5.35677	#N/A	3.6818626	4.52
MGI:2384309	Polr2h	#N/A	3.3481	#N/A	5.6446927	4.50
MGI:1916818	Vkorc1l1	#N/A	2.70545	#N/A	6.2543406	4.48
MGI:2384568	Kank2	#N/A	5.40564	#N/A	3.4704413	4.44
MGI:1925905	Eif3j	#N/A	4.47862	#N/A	4.2922212	4.39
MGI:104860	Fxr1	#N/A	6.4657	#N/A	2.2987487	4.38
MGI:88158	Bgn	#N/A	1.9264	#N/A	6.7801011	4.35
MGI:1914731	Alg2	#N/A	3.72559	#N/A	4.9276209	4.33
MGI:Q8C5J1		#N/A	1.94991	#N/A	6.6595116	4.30
MGI:106211	Cdc42	2.306	6.70776	#N/A	1.8287909	4.27
MGI:1915367	Apool	#N/A	6.79668	#N/A	1.7154199	4.26
MGI:1915401	Wls	#N/A	4.25358	#N/A	4.1685557	4.21
MGI:2687325	Pigs	#N/A	2.26227	#N/A	5.9766464	4.12
MGI:1341265	Camk2d	#N/A	1.99665	#N/A	6.2422357	4.12
MGI:3026965	Mcu	#N/A	4.84644	#N/A	3.2943749	4.07
MGI:1914132	Bzw1	#N/A	3.71676	#N/A	4.203567	3.96
MGI:1914430	Yipf5	#N/A	2.82554	#N/A	5.0653751	3.95
MGI:1913866	Snx9	#N/A	5.22215	#N/A	2.394573	3.81
MGI:106916	Msra	#N/A	5.34751	#N/A	2.2531397	3.80
MGI:103123	Serpinb6a	#N/A	4.85226	#N/A	2.7068808	3.78
MGI:108451	Acaca	#N/A	3.59297	#N/A	3.8567849	3.72
MGI:1930187	Maged1	#N/A	3.64123	#N/A	3.7184596	3.68

MGI:1922004	Dhcr24	#N/A	2.41773	#N/A	4.893553	3.66
MGI:1913687	Fis1	#N/A	4.57284	#N/A	2.6957095	3.63
MGI:1914648	Srpra	#N/A	2.41707	#N/A	4.8190198	3.62
MGI:1338762	Fhl2	#N/A	3.35376	#N/A	3.8487035	3.60
MGI:1261855	Cisd1	#N/A	3.09898	#N/A	4.0559392	3.58
MGI:88548	Csnk2b	#N/A	2.39118	#N/A	4.6633182	3.53
MGI:1919792	Pgam5	#N/A	4.76877	#N/A	2.1310084	3.45
MGI:108117	Emd	#N/A	3.896	#N/A	2.862941	3.38
MGI:1860763	Eif3i	#N/A	4.57673	#N/A	2.1637282	3.37
MGI:1915080	Rer1	#N/A	3.43516	#N/A	3.2131081	3.32
MGI:4439893	Ighv5-2	#N/A	2.0713	#N/A	4.406818	3.24
MGI:894320	Prdx6	#N/A	4.71331	#N/A	1.7020644	3.21
MGI:1929872	Mogs	#N/A	3.37407	#N/A	3.0234463	3.20
MGI:3818630	Sco2	#N/A	2.12664	#N/A	4.056051	3.09
MGI:2138584	Gigyf2	#N/A	3.27938	#N/A	2.8740416	3.08
MGI:1914273	Use1	#N/A	3.20375	#N/A	2.9076426	3.06
MGI:107795	Hnrnpc	#N/A	4.03409	#N/A	2.0614357	3.05
MGI:109283	Pdcd6	#N/A	3.09534	#N/A	2.9679303	3.03
MGI:106442	Vkorc1	#N/A	1.96228	#N/A	4.0807304	3.02
MGI:105926	Rab5a	#N/A	2.14568	#N/A	3.8323379	2.99
MGI:1859607	Praf2	#N/A	2.77731	#N/A	3.1302459	2.95
MGI:1926014	Fbxo22	#N/A	2.57514	#N/A	3.33143	2.95
MGI:1913838	Cmpk1	#N/A	2.50382	#N/A	3.3720431	2.94
MGI:1914247	Psmd12	#N/A	2.27694	#N/A	3.5421512	2.91
MGI:1918711	Ptk7	#N/A	2.01313	#N/A	3.7992551	2.91
MGI:104602	Prpf39	#N/A	2.06899	#N/A	3.731378	2.90
MGI:95543	Fkbp4	#N/A	2.60676	#N/A	3.0933208	2.85
MGI:1931013	Abhd1	#N/A	1.70221	#N/A	3.9909282	2.85
MGI:1914208	Tmx2	#N/A	3.65131	#N/A	1.8566977	2.75
MGI:1196314	Dhrs1	#N/A	2.96207	#N/A	2.5013463	2.73
MGI:2448481	Mgst2	#N/A	1.75416	#N/A	3.6912553	2.72
MGI:1915789	Tmem109	#N/A	3.04817	#N/A	2.3772647	2.71
MGI:1915814	Nufip2	#N/A	2.88478	#N/A	2.5322556	2.71
MGI:2149842	Sdf2l1	#N/A	3.2522	#N/A	2.1050532	2.68
MGI:109572	Tuft1	#N/A	3.60984	#N/A	1.7336158	2.67
MGI:1920374	Golim4	#N/A	2.82107	#N/A	2.4397354	2.63
MGI:2135756	Hspb8	#N/A	3.44696	#N/A	1.7942654	2.62
MGI:106908	Srpk1	#N/A	2.35397	#N/A	2.8589802	2.61
MGI:1855672	Tsnax	#N/A	2.49535	0	2.6363552	2.57
MGI:95832	Grn	#N/A	2.61048	#N/A	2.506794	2.56
MGI:103063	Stat1	#N/A	2.18432	#N/A	2.9128883	2.55
MGI:1913670	Polr2e	#N/A	3.03518	#N/A	2.0596304	2.55
MGI:1890357	Igf2bp1	#N/A	2.47723	#N/A	2.5800798	2.53
MGI:2384849	Tnpo2	#N/A	2.63734	#N/A	2.3899264	2.51
MGI:893586	Snu13	#N/A	2.3269	#N/A	2.6681662	2.50
MGI:1202066	Sec61g	#N/A	2.36278	#N/A	2.5756028	2.47
MGI:98427	Il1rl1	#N/A	2.42897	#N/A	2.4781029	2.45
MGI:1888908	Aldh18a1	#N/A	3.08986	#N/A	1.7766949	2.43
MGI:1915009	Plgrkt	#N/A	2.88707	#N/A	1.9111543	2.40
MGI:1889341	Hacd3	#N/A	2.29254	#N/A	2.3512194	2.32
MGI:88255	Anxa6	0	2.02361	#N/A	2.599627	2.31
MGI:1918611	Aifm2	#N/A	2.02298	#N/A	2.5963559	2.31
MGI:1915731	Mpzl1	#N/A	2.33598	#N/A	2.2823873	2.31
MGI:1097667	Ganab	#N/A	2.75823	#N/A	1.8332127	2.30

MGI:1355333	Nckap1	#N/A	1.80052	#N/A	2.7218857	2.26
MGI:2142581	Nsd3	#N/A	2.40295	#N/A	2.1170578	2.26
MGI:87881	Acp1	#N/A	2.33193	#N/A	2.141979	2.24
MGI:1915246	Srsf6	#N/A	1.95982	#N/A	2.4522932	2.21
MGI:1913863	Pigk	#N/A	1.92105	#N/A	2.4741066	2.20
MGI:109263	Tsn	#N/A	2.21681	#N/A	2.176661	2.20
MGI:98284	Srsf2	#N/A	2.19062	#N/A	2.1928589	2.19
MGI:2149021	Unc13c	#N/A	2.22032	#N/A	2.1077785	2.16
MGI:1341822	Eif4h	#N/A	2.08129	#N/A	2.2409604	2.16
MGI:1888921	P3h1	#N/A	1.9267	#N/A	2.360605	2.14
MGI:1860508	Abcb10	#N/A	2.10301	#N/A	2.1781538	2.14
MGI:1914693	Map1lc3b	#N/A	2.1367	#N/A	2.1347728	2.14
MGI:1860267	Set	#N/A	1.90874	#N/A	2.3553257	2.13
MGI:1913302	Sdhc	#N/A	2.04837	#N/A	2.2134275	2.13
MGI:108074	Sptlc2	#N/A	2.05831	#N/A	2.1723495	2.12
MGI:1351645	Prmt5	#N/A	1.86959	#N/A	2.3325813	2.10
MGI:1914497	37316	#N/A	2.07065	#N/A	2.1104999	2.09
MGI:102547	Fau	#N/A	2.35834	#N/A	1.77025	2.06
MGI:1918007	Hacd2	#N/A	2.2299	#N/A	1.8975658	2.06
MGI:106247	Prpf19	#N/A	1.90649	#N/A	2.1979742	2.05
MGI:98512	Ubtf	#N/A	2.16478	#N/A	1.9286851	2.05
MGI:1338041	Tfg	#N/A	1.91486	#N/A	2.1781416	2.05
MGI:3036255	Tmtc3	#N/A	1.87134	#N/A	2.1995404	2.04
MGI:109279	Nnt	#N/A	2.01972	#N/A	2.0485501	2.03
MGI:1202392	Gpaa1	#N/A	2.26935	#N/A	1.6407698	1.96
MGI:96745	Lamp1	#N/A	2.05057	#N/A	1.8325564	1.94
MGI:1855688	Vti1b	#N/A	1.96402	#N/A	1.9146755	1.94
MGI:2181182	Nup155	#N/A	1.76596	#N/A	2.0872622	1.93
MGI:106636	Atp5i	#N/A	1.88925	#N/A	1.9401492	1.91
MGI:1924059	Bri3bp	#N/A	2.04413	#N/A	1.7832477	1.91
MGI:3052714	Ano7	#N/A	1.84371	#N/A	1.9640635	1.90
MGI:1921766	A730049H05Rik	#N/A	1.62148	#N/A	2.1667061	1.89
MGI:1914738	Calcoco1	#N/A	1.79886	#N/A	1.9561554	1.88
MGI:2446173	Farp1	#N/A	2.02714	#N/A	1.6856879	1.86
MGI:97797	Ptgs1	#N/A	1.77968	#N/A	1.8795661	1.83
MGI:109620	Arvcf	#N/A	1.79236	#N/A	1.8106303	1.80
MGI:3641975	Gm10714	#N/A	1.91605	#N/A	1.6638538	1.79
MGI:1914262	Tm9sf3	#N/A	1.72415	#N/A	1.8247149	1.77
MGI:1201789	Rpl36a	#N/A	1.92472	0	1.6229012	1.77
MGI:2447063	Tenm4	#N/A	1.62286	#N/A	1.8884625	1.76
MGI:2442440	Efcab5	#N/A	1.81537	#N/A	1.6747447	1.75
MGI:3609260	Chrna10	#N/A	1.70942	#N/A	1.7080473	1.71

Appendix Table 3. Double Positive Interactors in the EXOC8-E265G-GFP Trap

MGI	Mouse GN	WT (1) Score	EXOC8 (1) Score	WT (2) Score	EXOC8 (2) Score	AVG Score
MGI:2142527	Exoc8	67.9	1541.95	40.37	1106.5088	1324.23
MGI:1277961	Plec	#N/A	411.933	#N/A	504.42157	458.18
MGI:105384	Hspa8	150.3	432.493	#N/A	387.47152	409.98
MGI:107812	Tubb5	149.5	426.11	83.76	344.65196	385.38
MGI:1915472	Tubb4b	132.4	403.847	79.15	313.1625	358.50
MGI:95566	Fn1	#N/A	460.298	#N/A	223.16441	341.73

MGI:88461	Col6a3	97.8	460.803	19.63	208.96369	334.88
MGI:1341878	Ehd1	#N/A	346.358	#N/A	310.84641	328.60
MGI:107861	Tubb2a	122.1	349.789	#N/A	292.50695	321.15
MGI:98869	Tuba1a	75.38	287.822	57	226.53891	257.18
MGI:1095409	Tuba1c	#N/A	276.052	#N/A	206.92908	241.49
MGI:103147	Dync1h1	40.68	208.352	11.35	224.28505	216.32
MGI:88115	Atp5a1	75.2	194.455	32.41	176.58329	185.52
MGI:88467	Col1a1	19.13	124.603	10.4	193.93	159.27
MGI:1316648	Ahnak	59.15	218.764	#N/A	92.574601	155.67
MGI:96794	Lmna	37.84	214.577	6.682	94.787663	154.68
MGI:1915201	Tubb6	56.33	167.732	29.31	120.7346	144.23
MGI:98535	Tcp1	34.91	165.725	12.25	120.98593	143.36
MGI:97547	Pfkl	#N/A	151.058	#N/A	135.43047	143.24
MGI:107801	Atp5b	64.85	171.275	10.43	113.2203	142.25
MGI:107186	Cct2	31.85	135.674	#N/A	125.29663	130.49
MGI:1342292	Hspa4	34.34	108.511	#N/A	125.85897	117.19
MGI:1921372	Tmem43	#N/A	132.678	#N/A	97.657843	115.17
MGI:1923864	Immt	#N/A	129.396	#N/A	93.707905	111.55
MGI:87909	Acta2	#N/A	113.841	#N/A	103.99521	108.92
MGI:88459	Col6a1	33.71	155.986	#N/A	61.124016	108.55
MGI:1916969	Cad	#N/A	109.347	#N/A	93.300659	101.32
MGI:104689	Cct4	32.41	117.369	#N/A	80.576113	98.97
MGI:107183	Cct8	#N/A	124.25	#N/A	68.045704	96.15
MGI:1919619	Ehd4	#N/A	104.571	#N/A	84.116809	94.34
MGI:106919	Vdac1	15.26	101.243	#N/A	81.364202	91.30
MGI:95698	Gfpt1	0	102.551	#N/A	75.733869	89.14
MGI:96414	Idh2	27.63	92.5399	21.63	85.583044	89.06
MGI:1926080	Slc25a12	#N/A	92.2878	9.078	76.197996	84.24
MGI:1917599	Copb1	18.09	92.6818	10.4	69.457111	81.07
MGI:98158	Rps4x	#N/A	77.1403	#N/A	79.426564	78.28
MGI:1917473	Nars	9.124	78.829	#N/A	76.971435	77.90
MGI:1096584	Psmd2	23.14	82.8195	#N/A	72.541903	77.68
MGI:1929899	Sqor	#N/A	82.0176	#N/A	64.33128	73.17
MGI:1306778	Map1b	5.373	141.56	#N/A	2.5591073	72.06
MGI:106915	Vdac2	13.53	75.5429	7.408	67.274239	71.41
MGI:88460	Col6a2	10.88	106.294	#N/A	36.251958	71.27
MGI:98084	Rpn1	15.06	83.0552	10.56	59.327597	71.19
MGI:2138741	Hnrnpf	27.42	77.6234	9.22	62.041416	69.83
MGI:1195456	Rnh1	19.61	77.5451	4.725	61.370802	69.46
MGI:97503	Pcna	#N/A	80.0836	#N/A	58.524853	69.30
MGI:97548	Pfkm	13.17	76.1196	6.155	59.407361	67.76
MGI:98858	Psmd3	13.33	73.8386	10.99	61.211531	67.53
MGI:1914410	Eef1g	33.91	98.8496	#N/A	33.081478	65.97
MGI:1859270	Exoc7	#N/A	85.6038	#N/A	45.728232	65.67
MGI:107185	Cct5	17.33	76.8825	6.468	54.130913	65.51
MGI:99894	Hnrnpk	#N/A	56.0204	17.25	70.813446	63.42
MGI:107943	Cct6a	24.27	65.2303	#N/A	61.336348	63.28
MGI:1914253	Uqcrc2	11.47	65.5205	3.152	59.899185	62.71
MGI:107184	Cct7	#N/A	79.244	#N/A	44.525129	61.88
MGI:99146	Ybx1	13.25	57.2778	14.92	65.075351	61.18
MGI:105110	Rps2	#N/A	57.1192	#N/A	62.5269	59.82
MGI:1278330	Smpd2	#N/A	72.8757	#N/A	44.169275	58.52
MGI:98085	Rpn2	9.138	72.9465	5.398	44.040873	58.49
MGI:105047	Psmc5	#N/A	69.945	#N/A	43.94884	56.95

MGI:1858304	Ctps1	8.694	59.2665	#N/A	54.605594	56.94
MGI:88264	Capn2	#N/A	67.1449	#N/A	45.507794	56.33
MGI:1917497	Psmd1	#N/A	53.0853	#N/A	57.770901	55.43
MGI:1923164	Exoc6b	#N/A	74.7647	#N/A	30.189186	52.48
MGI:98118	Rps16	10.59	45.5534	19.43	56.34822	50.95
MGI:1298398	Mcm7	5.86	39.4652	#N/A	61.619727	50.54
MGI:1915061	Poldip2	#N/A	54.5105	#N/A	44.962065	49.74
MGI:1915113	Slc25a11	#N/A	49.5391	#N/A	49.023776	49.28
MGI:101761	Hmga2	8.264	74.6284	5.793	23.334576	48.98
MGI:88561	Ctsb	#N/A	49.2553	5.246	47.894805	48.58
MGI:105053	Hsph1	#N/A	37.0505	#N/A	58.176874	47.61
MGI:88468	Col1a2	#N/A	31.9789	#N/A	62.72883	47.35
MGI:1298373	Rpl9	#N/A	45.9893	#N/A	48.397338	47.19
MGI:2145645	Exoc5	#N/A	56.2021	#N/A	35.701645	45.95
MGI:88105	Atp1a1	#N/A	47.6921	#N/A	41.810912	44.75
MGI:1891925	Hnrnph1	17.31	45.5946	#N/A	42.028085	43.81
MGI:107422	Hspa4l	#N/A	28.6771	#N/A	58.760171	43.72
MGI:1913906	Eef1d	#N/A	68.6289	#N/A	18.350984	43.49
MGI:88110	Atp2a2	2.71	53.4549	2.49	33.084448	43.27
MGI:1277989	Shmt2	#N/A	40.4536	5.339	46.040141	43.25
MGI:1914198	Acad8	#N/A	44.7985	#N/A	40.616573	42.71
MGI:95303	Eif4a1	#N/A	42.8019	#N/A	42.107745	42.45
MGI:1914670	Far1	5.348	45.8961	#N/A	36.967717	41.43
MGI:1321161	Ppp2cb	#N/A	29.2458	#N/A	53.474796	41.36
MGI:1855693	Nap1l1	8.727	47.3297	#N/A	33.058211	40.19
MGI:2138133	Lrrc59	8.972	43.8921	7.946	35.493527	39.69
MGI:1931882	Dnaja2	#N/A	54.5499	#N/A	24.608581	39.58
MGI:1349419	Aifm1	#N/A	41.3867	#N/A	37.081607	39.23
MGI:2447670	Mgrn1	#N/A	43.8537	#N/A	34.438843	39.15
MGI:1917160	Slc25a24	#N/A	43.9643	#N/A	32.934639	38.45
MGI:1922896	Rai14	#N/A	42.9273	1.842	33.210241	38.07
MGI:1101358	Npepps	#N/A	39.3858	#N/A	36.320213	37.85
MGI:1270129	Dnaja1	3.256	45.2048	2.338	29.475212	37.34
MGI:108202	Pcbp2	#N/A	30.8515	#N/A	43.76462	37.31
MGI:106920	Tmpo	#N/A	58.7696	#N/A	15.83773	37.30
MGI:1925544	Rps27a	10.57	39.6431	6.184	34.07082	36.86
MGI:1354721	Slc25a13	#N/A	33.8219	#N/A	39.711343	36.77
MGI:98146	Rps18	#N/A	31.6402	#N/A	40.357159	36.00
MGI:1913775	Timm50	5.398	34.45	6.101	35.712047	35.08
MGI:2137679	Sfxn3	#N/A	44.3321	#N/A	25.70296	35.02
MGI:1926465	Hnrnpm	#N/A	40.2534	3.993	29.572945	34.91
MGI:1891833	Pfkp	#N/A	46.0181	#N/A	23.413334	34.72
MGI:1891731	Stub1	#N/A	39.9464	#N/A	28.3584	34.15
MGI:99256	Hdlbp	#N/A	17.8474	#N/A	50.256396	34.05
MGI:1915903	Samm50	#N/A	43.4562	#N/A	24.195122	33.83
MGI:96413	Idh1	#N/A	33.1405	#N/A	34.111021	33.63
MGI:1341628	Atrn	#N/A	40.58	#N/A	26.480049	33.53
MGI:106341	Atp5o	#N/A	32.4849	#N/A	34.119237	33.30
MGI:1859293	Atxn10	11.11	28.9143	4.36	37.149436	33.03
MGI:1934754	Kars	9.72	36.6312	10.28	28.526999	32.58
MGI:2448388	Hist1h2bj	#N/A	42.8756	#N/A	20.799584	31.84
MGI:2158650	Idh3b	#N/A	34.4549	#N/A	28.074027	31.26
MGI:101920	Ap2a2	1.736	29.1543	1.916	33.023747	31.09
MGI:1333871	Hsd17b10	#N/A	23.4936	#N/A	38.552411	31.02

MGI:1349763	Dpysl2	7.57	22.6435	#N/A	39.223244	30.93
MGI:1929260	Mtch2	5.565	34.3486	4.671	26.256135	30.30
MGI:1349438	Mprip	#N/A	11.1317	#N/A	49.458675	30.30
MGI:1918944	Ipo9	#N/A	32.0845	#N/A	28.28891	30.19
MGI:1917171	Hnrnpa3	#N/A	41.1927	#N/A	18.66401	29.93
MGI:1346330	Banf1	8.605	47.4629	2.2	11.9319	29.70
MGI:1891690	Syncrip	12.52	32.1097	#N/A	26.99668	29.55
MGI:1194508	Ddost	3.525	27.2534	#N/A	31.051729	29.15
MGI:101921	Ap2a1	5.731	28.7462	4.031	29.498397	29.12
MGI:106092	Etfa	5.166	23.5611	6.011	33.501032	28.53
MGI:106379	Rtcb	#N/A	33.3279	#N/A	23.48302	28.41
MGI:1858234	Caprin1	4.281	12.9352	#N/A	43.487717	28.21
MGI:1346859	Mapk3	#N/A	25.4619	#N/A	30.921823	28.19
MGI:1346093	Psmc4	#N/A	37.5971	#N/A	17.75641	27.68
MGI:1858696	Copg1	6.699	37.9309	#N/A	17.232328	27.58
MGI:105386	Dbt	2.628	52.284	#N/A	2.2259338	27.25
MGI:2444680	Aldh1l2	#N/A	28.4276	#N/A	25.725793	27.08
MGI:1349450	Vat1	2.467	29.3513	#N/A	24.699089	27.03
MGI:109555	Psmc2	2.163	28.0496	#N/A	25.879099	26.96
MGI:1096376	Exoc4	#N/A	33.5239	#N/A	20.335736	26.93
MGI:1202384	Ddb1	#N/A	29.0874	#N/A	24.658391	26.87
MGI:106013	Slc16a1	1.825	33.5579	#N/A	19.911849	26.73
MGI:1928760	Ruvbl1	#N/A	20.7375	#N/A	32.670458	26.70
MGI:1858195	Hnrnpu	#N/A	29.4097	#N/A	23.923684	26.67
MGI:1915337	Dcakd	#N/A	28.8605	#N/A	23.840157	26.35
MGI:1913695	Cyc1	2.51	18.7653	10.39	33.424718	26.10
MGI:2137677	Sfxn1	#N/A	34.7331	#N/A	17.346862	26.04
MGI:106922	Vdac3	3.235	32.6492	1.658	19.408408	26.03
MGI:1351657	Abcf2	2.142	28.247	#N/A	23.507679	25.88
MGI:2385311	Dlat	0	45.4336	#N/A	6.3060424	25.87
MGI:894407	Tmem165	#N/A	30.8531	#N/A	20.601065	25.73
MGI:88261	Canx	3.098	27.3082	#N/A	23.873626	25.59
MGI:1353497	Slc25a10	1.971	23.1504	7.753	27.565012	25.36
MGI:1919363	Adck1	#N/A	28.7826	#N/A	21.912751	25.35
MGI:1329037	Strap	5.703	29.2719	2.458	21.34999	25.31
MGI:104819	Hnrnpa2b1	7.322	28.3232	1.763	21.525199	24.92
MGI:95299	Eif2s1	#N/A	23.4093	#N/A	26.082691	24.75
MGI:1913840	Farsa	2.307	25.5726	#N/A	23.89276	24.73
MGI:1858259	Tomm40	#N/A	35.8553	#N/A	13.116385	24.49
MGI:2138281	Lbr	6.419	23.856	5.929	24.126627	23.99
MGI:102854	Rpl5	#N/A	27.4118	#N/A	20.53766	23.97
MGI:107728	Myo1d	#N/A	33.971	#N/A	13.669978	23.82
MGI:1913866	Snx9	#N/A	16.0653	#N/A	31.437813	23.75
MGI:1914135	Acadsb	#N/A	22.3382	#N/A	24.909498	23.62
MGI:104872	Ppp1cc	#N/A	20.4385	#N/A	26.432029	23.44
MGI:1926209	Dek	7.053	30.4655	#N/A	15.089546	22.78
MGI:1890359	Igf2bp3	#N/A	20.289	#N/A	25.013097	22.65
MGI:3642408	Gm10250	#N/A	31.213	#N/A	13.818407	22.52
MGI:107384	Dnm1	#N/A	21.4915	#N/A	23.501929	22.50
MGI:1919020	Ap2b1	4.588	15.0827	#N/A	29.791395	22.44
MGI:1277968	Cavin1	#N/A	18.1085	#N/A	26.675857	22.39
MGI:1918764	Sfpq	6.921	26.7632	#N/A	17.999913	22.38
MGI:1306824	Suclg2	1.714	19.3327	#N/A	25.394877	22.36
MGI:2152414	Ipo7	5.764	30.6195	3.097	14.002436	22.31

MGI:1098754	Psmc3	#N/A	22.5252	#N/A	21.68958	22.11
MGI:96522	Rbpj	3.86	38.281	#N/A	5.8994013	22.09
MGI:97712	Prrx1	#N/A	38.3715	#N/A	5.5841539	21.98
MGI:105922	Rpl13	#N/A	20.4643	#N/A	23.050245	21.76
MGI:2144727	Ddx1	#N/A	23.1839	#N/A	20.193693	21.69
MGI:97298	37500	#N/A	15.471	#N/A	27.760978	21.62
MGI:1891254	Bag2	1.88	25.8747	#N/A	16.23162	21.05
MGI:106248	Eif5a	2.969	19.8972	3.095	22.145283	21.02
MGI:106054	Psmc1	#N/A	24.85	#N/A	17.000896	20.93
MGI:1921455	Acsl3	#N/A	22.5812	#N/A	18.947654	20.76
MGI:1330294	Hnrnpab	9.062	24.612	#N/A	16.710138	20.66
MGI:2154274	Ehd2	#N/A	22.2155	#N/A	19.045764	20.63
MGI:1349431	Eif2s3x	7.947	23.3139	#N/A	17.939813	20.63
MGI:96955	Slc3a2	#N/A	19.8089	#N/A	21.380189	20.59
MGI:107752	Myo1b	#N/A	19.4224	#N/A	21.214246	20.32
MGI:1330239	Dpm1	#N/A	24.4939	#N/A	16.134364	20.31
MGI:1351658	Abcf1	#N/A	18.0021	4.878	22.549891	20.28
MGI:1342299	Ruvbl2	7.585	20.9894	#N/A	19.508103	20.25
MGI:1335094	39326	#N/A	22.1027	#N/A	18.359867	20.23
MGI:95609	Gaa	#N/A	28.3099	#N/A	12.081407	20.20
MGI:3704362	Gm10273	#N/A	25.4009	#N/A	14.860092	20.13
MGI:1915513	Pdhb	8.264	26.4606	2.516	13.792645	20.13
MGI:1923827	Faf2	#N/A	26.3873	#N/A	13.743127	20.07
MGI:97463	P4ha1	#N/A	27.5877	2.833	12.012815	19.80
MGI:97532	Pdha1	#N/A	29.8579	#N/A	8.9067332	19.38
MGI:95654	Gart	#N/A	17.9544	#N/A	20.743233	19.35
MGI:104888	Fdps	#N/A	22.2698	#N/A	16.214224	19.24
MGI:102774	Aimp1	2.112	26.5508	#N/A	11.422819	18.99
MGI:94871	Eci1	4.101	16.0084	2.408	21.917256	18.96
MGI:105099	Pcolce	#N/A	15.9862	#N/A	21.899944	18.94
MGI:1915831	Tmed10	#N/A	16.2362	#N/A	21.17827	18.71
MGI:2387215	Erlin2	#N/A	17.8175	#N/A	19.385964	18.60
MGI:2441984	Lrrc41	#N/A	13.3229	#N/A	23.826927	18.57
MGI:1276121	Bckdk	#N/A	31.7991	#N/A	5.1884797	18.49
MGI:1891112	Gmds	#N/A	22.5292	#N/A	14.415422	18.47
MGI:101816	Msh2	#N/A	16.7994	#N/A	20.048296	18.42
MGI:101845	Mcm3	4.541	17.5634	#N/A	19.118751	18.34
MGI:2387613	Erlin1	#N/A	22.1011	#N/A	14.529273	18.32
MGI:1349765	Rcn2	#N/A	27.0013	#N/A	9.5314646	18.27
MGI:1095396	Col16a1	#N/A	17.3928	#N/A	18.900764	18.15
MGI:98423	Ssb	#N/A	15.266	6.614	20.842286	18.05
MGI:98003	Rpl18	#N/A	16.0488	#N/A	19.897782	17.97
MGI:1346868	Map2k3	#N/A	17.9559	#N/A	17.821781	17.89
MGI:1858417	Sec61a1	2.032	13.5508	4.429	22.093938	17.82
MGI:108064	Siah1a	2.006	23.0133	#N/A	12.619461	17.82
MGI:104653	Atp2b1	#N/A	19.5408	#N/A	15.961908	17.75
MGI:1352493	Bag3	#N/A	23.6138	#N/A	11.557901	17.59
MGI:1336214	Khsrp	2.413	15.4492	#N/A	19.455429	17.45
MGI:1100851	Elavl1	#N/A	15.7903	2.401	18.667444	17.23
MGI:96817	Lox	#N/A	19.4837	#N/A	14.930275	17.21
MGI:1927234	Suclg1	4.746	13.6734	#N/A	20.684891	17.18
MGI:1915088	Dnajb11	#N/A	16.7376	#N/A	17.593016	17.17
MGI:1890358	Igf2bp2	#N/A	15.1032	#N/A	19.039422	17.07
MGI:2385237	Aimp2	5.787	17.3241	#N/A	16.705635	17.01

MGI:2387629	Tardbp	#N/A	15.9888	#N/A	17.548088	16.77
MGI:1914248	Psmd5	#N/A	20.1813	#N/A	13.196716	16.69
MGI:1913325	Chchd3	#N/A	21.4109	#N/A	11.907918	16.66
MGI:1338779	Purb	#N/A	7.81679	#N/A	24.892211	16.35
MGI:102581	Rdh11	#N/A	10.8153	2.865	21.660179	16.24
MGI:1345283	Slc25a1	#N/A	16.2403	2.006	16.225034	16.23
MGI:104976	Ddx6	#N/A	14.034	0	18.18704	16.11
MGI:95772	Gnai2	#N/A	18.0668	#N/A	14.137684	16.10
MGI:101947	Hnrnpd	#N/A	20.1973	#N/A	11.529573	15.86
MGI:105979	G6pdx	#N/A	13.8501	#N/A	17.851932	15.85
MGI:105100	Ctnnd1	#N/A	16.8069	#N/A	13.874261	15.34
MGI:1918054	Pgrmc2	#N/A	15.327	#N/A	15.192637	15.26
MGI:105082	Ssr1	#N/A	13.6731	#N/A	16.414427	15.04
MGI:2443731	Mat2a	#N/A	17.0433	#N/A	12.836639	14.94
MGI:102579	Nmt1	4.991	12.8485	#N/A	16.981487	14.91
MGI:1194505	C1qbp	#N/A	16.8901	#N/A	12.92293	14.91
MGI:1891702	Cope	#N/A	11.2683	4.963	18.414578	14.84
MGI:95784	Gnb2	#N/A	15.3658	#N/A	14.044695	14.71
MGI:99436	Arl1	#N/A	14.7426	#N/A	14.382111	14.56
MGI:95896	H2-D1	#N/A	15.5123	#N/A	13.349162	14.43
MGI:96435	Igf2r	#N/A	9.46107	#N/A	19.146603	14.30
MGI:3041177	Taok3	#N/A	26.0218	#N/A	2.4064724	14.21
MGI:1914708	Ergic1	#N/A	16.5218	#N/A	11.835335	14.18
MGI:894286	P4ha2	#N/A	21.7985	#N/A	6.4497957	14.12
MGI:1927593	Ptges	#N/A	18.4331	#N/A	9.6011744	14.02
MGI:1914864	Atp6v1h	#N/A	13.6634	#N/A	14.174188	13.92
MGI:1353633	Fus	#N/A	21.1054	#N/A	6.7032955	13.90
MGI:103123	Serpinb6a	#N/A	14.5836	#N/A	13.169176	13.88
MGI:1349658	Cul1	#N/A	19.6542	1.947	8.0785959	13.87
MGI:1929264	Sae1	#N/A	10.3505	#N/A	17.374721	13.86
MGI:1915076	Snap47	#N/A	12.5313	#N/A	15.061186	13.80
MGI:1201670	Psmd4	#N/A	10.5355	#N/A	16.888931	13.71
MGI:96907	Marcks	#N/A	14.2655	#N/A	12.971603	13.62
MGI:95753	Glud1	#N/A	15.7341	#N/A	11.268903	13.50
MGI:1915173	Eloc	#N/A	15.8884	#N/A	10.963661	13.43
MGI:1098623	Acaa2	#N/A	14.279	#N/A	12.359669	13.32
MGI:1888676	Rps27	#N/A	13.2726	#N/A	12.773411	13.02
MGI:1339951	Cse1l	#N/A	8.9771	#N/A	17.012703	12.99
MGI:2444248	Gcn1	#N/A	13.606	#N/A	12.313574	12.96
MGI:1927243	Rala	#N/A	17.9992	#N/A	7.900194	12.95
MGI:2140220	AI314180	#N/A	10.0912	#N/A	15.722887	12.91
MGI:98445	Surf4	#N/A	13.6194	#N/A	12.05882	12.84
MGI:2183260	Luc7l2	2.275	17.4505	#N/A	8.199041	12.82
MGI:1920040	Ssbp1	#N/A	16.5171	#N/A	9.0271444	12.77
MGI:3026965	Mcu	#N/A	18.7443	#N/A	6.7976327	12.77
MGI:101834	Tubg1	#N/A	16.024	#N/A	9.0888827	12.56
MGI:105124	Stt3a	3.502	11.2271	3.96	13.695433	12.46
MGI:1353561	Vapa	2.867	14.6439	2.885	10.273661	12.46
MGI:1277122	Rcn3	#N/A	15.2608	#N/A	9.4853555	12.37
MGI:1100495	Atp5f1	2.335	12.7559	4.525	11.791155	12.27
MGI:105305	Slc1a5	#N/A	15.5323	#N/A	8.936893	12.23
MGI:1194513	Psmb5	#N/A	5.86499	#N/A	18.467509	12.17
MGI:1298227	Mcm6	#N/A	11.2133	#N/A	13.082955	12.15
MGI:2687325	Pigs	#N/A	11.4598	#N/A	12.599933	12.03

MGI:1298405	Ap2m1	1.655	14.004	#N/A	9.9969029	12.00
MGI:1928488	Akap8	#N/A	10.9562	#N/A	13.013179	11.98
MGI:88351	Cdk1	#N/A	12.2009	#N/A	11.61673	11.91
MGI:1261415	Sgpl1	#N/A	12.9249	#N/A	10.799278	11.86
MGI:2387591	Arcn1	#N/A	10.4954	#N/A	13.148034	11.82
MGI:1914285	Dnajb4	#N/A	6.40979	#N/A	16.792286	11.60
MGI:1298379	Matr3	#N/A	10.5081	#N/A	12.632414	11.57
MGI:107995	Upf1	#N/A	2.68506	#N/A	20.336433	11.51
MGI:98886	U2af2	#N/A	18.0365	#N/A	4.7869166	11.41
MGI:1349389	Gcat	#N/A	19.5377	#N/A	3.273726	11.41
MGI:1914930	Sdhb	#N/A	11.7954	#N/A	10.586937	11.19
MGI:1917611	Lman1	#N/A	12.371	#N/A	9.9453323	11.16
MGI:96915	Maoa	#N/A	10.0032	#N/A	12.134894	11.07
MGI:1349216	Abcd3	#N/A	15.9665	#N/A	5.8604341	10.91
MGI:104560	Nsf	1.711	7.34489	#N/A	14.481213	10.91
MGI:1915678	Steap3	#N/A	15.2037	#N/A	6.5432225	10.87
MGI:97531	Pdgfrb	#N/A	12.1711	#N/A	9.4143176	10.79
MGI:97178	Map4	1.918	15.0597	#N/A	6.4366597	10.75
MGI:1346035	Farsb	#N/A	9.50178	#N/A	11.636442	10.57
MGI:2144013	Xpo1	2.771	10.2625	3.186	10.559255	10.41
MGI:1338801	Cyfip1	#N/A	6.93854	#N/A	13.849425	10.39
MGI:1916840	Gpx8	#N/A	10.9136	#N/A	9.8094335	10.36
MGI:1915070	Tmed4	#N/A	15.2306	#N/A	5.4801247	10.36
MGI:102790	Rab18	2.331	6.90488	1.801	13.791256	10.35
MGI:1930197	Ncapg	2.536	18.9867	#N/A	1.6650871	10.33
MGI:1916412	Sec31a	#N/A	6.47779	#N/A	14.061294	10.27
MGI:1916327	Psmd11	#N/A	11.0416	#N/A	9.4503615	10.25
MGI:2135601	Slc1a4	#N/A	10.7326	#N/A	9.7579453	10.25
MGI:2445121	Slfn9	#N/A	8.54919	#N/A	11.544125	10.05
MGI:2684937	Lclat1	#N/A	6.50308	#N/A	13.413973	9.96
MGI:1346346	Scamp3	#N/A	9.93719	#N/A	9.8722343	9.90
MGI:1858305	Pgrmc1	#N/A	3.40926	#N/A	16.286498	9.85
MGI:105093	Cnn2	#N/A	6.91252	#N/A	12.403334	9.66
MGI:1345633	Mars	1.847	6.67663	#N/A	12.299233	9.49
MGI:2149821	Hsd17b11	#N/A	8.15733	#N/A	10.764164	9.46
MGI:109274	Trim28	#N/A	15.4827	#N/A	3.3783119	9.43
MGI:98763	Tk1	#N/A	12.3278	#N/A	6.4806242	9.40
MGI:2442040	G3bp2	#N/A	2.42086	#N/A	16.33007	9.38
MGI:1277956	Pycr2	#N/A	12.1164	#N/A	6.6010928	9.36
MGI:1890357	Igf2bp1	#N/A	10.5525	#N/A	8.0353863	9.29
MGI:1915128	Tmem33	#N/A	11.0099	#N/A	7.5049667	9.26
MGI:88516	Cryab	#N/A	10.8444	#N/A	7.6153309	9.23
MGI:1355326	Preb	#N/A	10.643	#N/A	7.7528365	9.20
MGI:106621	Myo1e	#N/A	1.81103	#N/A	16.513121	9.16
MGI:97553	Pgd	#N/A	2.97475	#N/A	15.342831	9.16
MGI:1097158	Calu	#N/A	4.33562	#N/A	13.880071	9.11
MGI:95755	Slc2a1	#N/A	7.68639	#N/A	10.376513	9.03
MGI:98884	U2af1	#N/A	11.8486	#N/A	6.2044795	9.03
MGI:104816	Hnrnpl	#N/A	9.75576	#N/A	8.2720883	9.01
MGI:1915265	Trap1	#N/A	10.9523	#N/A	6.9869266	8.97
MGI:2135610	Dync1li1	#N/A	10.0995	#N/A	7.7685561	8.93
MGI:1888921	P3h1	#N/A	7.25004	#N/A	10.477427	8.86
MGI:1914731	Alg2	#N/A	9.02805	#N/A	8.5641463	8.80
MGI:88457	Col5a1	#N/A	10.3349	#N/A	7.1488642	8.74

MGI:2384802	Eif2b1	#N/A	7.31491	#N/A	10.005258	8.66
MGI:1858232	Nudt5	#N/A	7.50457	#N/A	9.723895	8.61
MGI:103038	Stat3	#N/A	6.78333	#N/A	10.434999	8.61
MGI:108177	Dhx9	#N/A	13.897	#N/A	2.6661048	8.28
MGI:1344381	Dnajb6	#N/A	13.465	#N/A	3.0938027	8.28
MGI:95775	Gnao1	#N/A	8.54568	#N/A	7.9914069	8.27
MGI:1926081	Ncln	#N/A	9.15337	#N/A	7.271945	8.21
MGI:1913416	S100a14	#N/A	8.26675	#N/A	8.1482513	8.21
MGI:105491	Cdipt	#N/A	9.13488	#N/A	7.1791358	8.16
MGI:1920037	Ndc1	#N/A	8.17362	#N/A	8.1130168	8.14
MGI:Q5EBK8	Dynlt1	#N/A	5.76495	#N/A	10.453907	8.11
MGI:1914186	ASPH	#N/A	11.5745	#N/A	4.5023813	8.04
MGI:105968	Txlna	#N/A	6.23475	#N/A	9.6204375	7.93
MGI:2444777	Ncaph	#N/A	13.3408	#N/A	2.0163193	7.68
MGI:1919792	Pgam5	#N/A	10.2171	#N/A	5.1262987	7.67
MGI:1915059	Rmdn3	#N/A	9.08835	#N/A	6.2374895	7.66
MGI:1918816	Clmp	#N/A	7.98761	#N/A	7.3241875	7.66
MGI:1098684	Eif2a	#N/A	8.71898	#N/A	6.5857918	7.65
MGI:98180	Rrm1	#N/A	3.33806	#N/A	11.961935	7.65
MGI:98283	Srsf1	1.965	9.5242	1.875	5.7537129	7.64
MGI:106098	Etfb	#N/A	2.61673	#N/A	12.609575	7.61
MGI:1913293	Atp5d	#N/A	7.06322	#N/A	8.1536527	7.61
MGI:1913697	Mgst3	#N/A	7.60796	#N/A	7.5568204	7.58
MGI:1915851	Qars	#N/A	5.58606	#N/A	9.5499148	7.57
MGI:2450248	Tomm22	1.704	5.96383	#N/A	9.1102779	7.54
MGI:88042	Apex1	#N/A	10.3207	#N/A	4.7449224	7.53
MGI:894681	Usp9x	#N/A	12.1519	#N/A	2.9131145	7.53
MGI:2149728	Impa2	1.605	6.68243	#N/A	8.3290187	7.51
MGI:1913677	Cyb5b	#N/A	10.5242	#N/A	4.4515781	7.49
MGI:1915517	Slc25a22	#N/A	7.62207	#N/A	7.3279486	7.48
MGI:1914291	Oxct1	#N/A	3.83201	#N/A	11.067135	7.45
MGI:2384308	Pdk3	#N/A	10.7505	#N/A	4.1469464	7.45
MGI:97831	Ppa1	#N/A	3.53529	#N/A	11.320262	7.43
MGI:3642386	Gm9774	#N/A	8.69951	#N/A	6.1229546	7.41
MGI:1913607	Ostc	#N/A	7.25055	#N/A	7.5643501	7.41
MGI:1343176	Timm17b	#N/A	11.8314	#N/A	2.9457388	7.39
MGI:1915401	Wls	#N/A	10.5261	#N/A	4.2397423	7.38
MGI:1913944	Uqcrfs1	#N/A	8.63938	#N/A	5.9267465	7.28
MGI:106908	Srpk1	#N/A	5.75057	#N/A	8.6752357	7.21
MGI:88084	Asl	#N/A	7.47373	#N/A	6.8510528	7.16
MGI:1917403	2210016F16Rik	#N/A	6.95973	#N/A	7.3263346	7.14
MGI:108074	Sptlc2	#N/A	7.30537	#N/A	6.9770787	7.14
MGI:96795	Lmnb1	#N/A	9.94048	#N/A	4.1926384	7.07
MGI:1341044	Alyref	#N/A	7.36706	#N/A	6.6468022	7.01
MGI:1913348	Chchd6	#N/A	7.0134	#N/A	6.969213	6.99
MGI:893586	Snu13	#N/A	8.46421	#N/A	5.406503	6.94
MGI:95773	Gnai3	#N/A	8.89904	#N/A	4.9654984	6.93
MGI:104669	Man2a1	#N/A	4.17202	#N/A	9.5284185	6.85
MGI:95777	Gnas	#N/A	9.15485	#N/A	4.529574	6.84
MGI:87870	Acat1	#N/A	5.12086	#N/A	8.5574539	6.84
MGI:1298205	Slc7a5	#N/A	8.93357	#N/A	4.5822787	6.76
MGI:1913335	Eif3f	#N/A	6.85379	#N/A	6.6167381	6.74
MGI:88357	Cdk4	#N/A	4.90497	#N/A	8.5058897	6.71
MGI:1924015	Mlec	#N/A	2.79892	#N/A	10.372079	6.59

MGI:104810	Plaa	0	4.69464	#N/A	8.4741626	6.58
MGI:1099786	Dhx15	#N/A	10.697	#N/A	2.4175763	6.56
MGI:107252	Nsun2	#N/A	8.47992	#N/A	4.4294343	6.45
MGI:98287	Srsf5	#N/A	6.59135	#N/A	6.2450067	6.42
MGI:1097667	Ganab	#N/A	2.00482	#N/A	10.756454	6.38
MGI:1306799	D17H6S56E-5	#N/A	7.14978	#N/A	5.6013715	6.38
MGI:1913309	Krtcap2	2.384	6.11602	#N/A	6.4999115	6.31
MGI:1919055	Nup93	#N/A	5.42188	#N/A	7.0909708	6.26
MGI:1926178	Pigt	#N/A	8.42709	#N/A	4.0778345	6.25
MGI:99526	Ddx19a	#N/A	3.42818	#N/A	9.0652918	6.25
MGI:1915013	Prpsap1	#N/A	1.83867	#N/A	10.647794	6.24
MGI:1929084	Fbxo3	#N/A	9.31508	#N/A	3.0872171	6.20
MGI:2387194	Qsox2	#N/A	5.13457	#N/A	7.1567452	6.15
MGI:1343463	Bub3	#N/A	9.50662	#N/A	2.7046585	6.11
MGI:1915069	Derl1	1.949	6.84363	#N/A	5.3181163	6.08
MGI:1913863	Pigk	#N/A	7.57308	#N/A	4.5604818	6.07
MGI:2135962	Gorasp2	#N/A	9.12769	#N/A	2.8774669	6.00
MGI:1924348	Colgalt1	#N/A	7.29067	1.748	4.6044681	5.95
MGI:1927468	Samhd1	#N/A	5.7361	#N/A	5.9561874	5.85
MGI:1858964	Actr1a	#N/A	5.80169	#N/A	5.8872023	5.84
MGI:2139207	Sec16a	#N/A	1.82808	#N/A	9.8456113	5.84
MGI:1098259	Capg	#N/A	2.69975	#N/A	8.9286997	5.81
MGI:1924059	Bri3bp	#N/A	4.42198	#N/A	7.197279	5.81
MGI:97776	Prps2	#N/A	7.67298	#N/A	3.8613111	5.77
MGI:103232	Grb10	#N/A	4.21012	#N/A	7.2371647	5.72
MGI:107450	Dld	2.555	8.87535	#N/A	2.5624924	5.72
MGI:Q3THL1		#N/A	5.62688	2	5.7415476	5.68
MGI:1913789	Xpo5	#N/A	5.61876	#N/A	5.7279077	5.67
MGI:1306775	Sucla2	#N/A	3.9967	#N/A	7.1601822	5.58
MGI:1917349	Smc4	#N/A	7.5094	#N/A	3.6122009	5.56
MGI:1201685	Ctbp1	#N/A	6.04574	#N/A	4.9994071	5.52
MGI:1915469	Nudt21	#N/A	5.64702	#N/A	5.344135	5.50
MGI:99926	ATP8	#N/A	5.55025	#N/A	5.4219551	5.49
MGI:107795	Hnrnpc	#N/A	8.36133	#N/A	2.5825799	5.47
MGI:87867	Acadm	#N/A	2.28531	#N/A	8.5852633	5.44
MGI:2180203	Tmlhe	#N/A	1.94891	1.991	8.8836002	5.42
MGI:107738	Dync1li2	#N/A	6.18852	#N/A	4.4458236	5.32
MGI:1914247	Psmd12	#N/A	2.0067	#N/A	8.5929849	5.30
MGI:1861776	Rbms2	#N/A	3.77394	#N/A	6.7604916	5.27
MGI:1347045	Psmb2	2.736	7.27337	#N/A	3.1906407	5.23
MGI:1888908	Aldh18a1	#N/A	4.13661	#N/A	6.2974931	5.22
MGI:108077	Nptn	#N/A	4.33227	#N/A	6.0404298	5.19
MGI:1351352	Atic	1.986	5.22871	#N/A	5.1207175	5.17
MGI:108117	Emd	#N/A	4.52479	#N/A	5.7973657	5.16
MGI:87866	Acadl	#N/A	2.96364	#N/A	7.338145	5.15
MGI:1919305	Slc38a10	#N/A	7.70818	#N/A	2.4263661	5.07
MGI:2442174	Mic13	#N/A	4.96199	#N/A	5.1702509	5.07
MGI:894689	Ywhae	#N/A	2.77799	#N/A	7.3436368	5.06
MGI:99425	Rab11b	#N/A	2.04455	#N/A	7.9065201	4.98
MGI:87868	Acads	#N/A	4.27507	#N/A	5.5973459	4.94
MGI:1918732	Rdh13	#N/A	4.05021	#N/A	5.7921588	4.92
MGI:1913687	Fis1	#N/A	4.79412	#N/A	5.0126234	4.90
MGI:1860267	Set	#N/A	4.94162	#N/A	4.7609632	4.85
MGI:1914208	Tmx2	#N/A	3.96702	#N/A	5.7293228	4.85

MGI:893579	Khdrbs1	#N/A	5.70429	#N/A	3.959846	4.83
MGI:1919214	Atad3	#N/A	5.53073	#N/A	4.1183848	4.82
MGI:1925201	Cyp20a1	#N/A	6.66273	#N/A	2.9426308	4.80
MGI:1345622	Slc35a1	#N/A	7.41964	#N/A	2.147866	4.78
MGI:1347002	Angptl2	#N/A	4.84201	#N/A	4.6639009	4.75
MGI:2146571	Rfc4	#N/A	3.4468	#N/A	5.9781554	4.71
MGI:1915295	RTRAF	#N/A	4.77994	#N/A	4.6400081	4.71
MGI:1929763	Cdc42ep1	#N/A	5.04121	#N/A	4.3574967	4.70
MGI:98973	Xdh	#N/A	3.07983	#N/A	6.3035948	4.69
MGI:104559	Rcn1	#N/A	6.47788	#N/A	2.8215599	4.65
MGI:1913498	Alg5	#N/A	2.05745	#N/A	7.2182196	4.64
MGI:2384568	Kank2	#N/A	3.57796	#N/A	5.6807268	4.63
MGI:1351597	Atp5l	#N/A	4.48216	#N/A	4.7749233	4.63
MGI:1913370	Fkbp11	#N/A	6.85137	#N/A	2.3824589	4.62
MGI:1353586	Lmo7	#N/A	2.99834	#N/A	6.1737643	4.59
MGI:2384309	Polr2h	#N/A	6.42766	#N/A	2.6624756	4.55
MGI:104837	Amz2	#N/A	3.40414	#N/A	5.6398735	4.52
MGI:1345192	Psmd13	#N/A	4.87378	#N/A	4.1514549	4.51
MGI:1333879	Ap3b1	#N/A	3.57827	#N/A	5.27764	4.43
MGI:1860763	Eif3i	#N/A	4.60596	#N/A	4.1449766	4.38
MGI:1935173	Pcdhgb4	#N/A	3.40848	#N/A	5.3032379	4.36
MGI:107741	Pvr	#N/A	6.64718	#N/A	2.0210884	4.33
MGI:101924	Slc12a2	#N/A	4.41696	#N/A	4.1930479	4.31
MGI:1913618	Rtca	2.179	5.94837	#N/A	2.6462243	4.30
MGI:1855692	Nono	#N/A	4.4123	#N/A	3.9972551	4.20
MGI:3032636	Ugt1a7c	#N/A	4.31351	#N/A	4.063611	4.19
MGI:1859652	Mtx2	#N/A	6.41613	#N/A	1.8681649	4.14
MGI:1933527	Srrt	#N/A	2.8906	#N/A	5.3861775	4.14
MGI:1914430	Yipf5	#N/A	2.57729	#N/A	5.6011066	4.09
MGI:2141989	Grwd1	#N/A	5.59872	#N/A	2.5670791	4.08
MGI:94900	Dlk1	#N/A	4.3495	#N/A	3.7298747	4.04
MGI:88108	Atp1b1	#N/A	4.05943	#N/A	4.0196122	4.04
MGI:1914461	Armc10	#N/A	5.36961	#N/A	2.6889765	4.03
MGI:1916604	Slc38a4	#N/A	6.12846	#N/A	1.8485763	3.99
MGI:2151483	Derl2	#N/A	5.09549	#N/A	2.8597722	3.98
MGI:2443003	Pcid2	#N/A	5.19385	#N/A	2.7063682	3.95
MGI:1338762	Fhl2	#N/A	5.64367	#N/A	2.1487257	3.90
MGI:1930187	Maged1	#N/A	4.24851	#N/A	3.518503	3.88
MGI:1915722	Tmem126b	#N/A	5.8469	#N/A	1.8394936	3.84
MGI:2443300	Cpped1	#N/A	4.37465	#N/A	3.2062593	3.79
MGI:98284	Srsf2	#N/A	3.83321	#N/A	3.7389851	3.79
MGI:88208	Bsg	#N/A	5.61743	#N/A	1.9115185	3.76
MGI:88338	Cd44	#N/A	4.48836	#N/A	3.0341201	3.76
MGI:1915490	Rpa3	#N/A	3.75545	#N/A	3.7421052	3.75
MGI:1891017	Zfpl1	#N/A	3.59639	#N/A	3.8030989	3.70
MGI:2443225	Gatad2b	#N/A	4.89856	#N/A	2.4967318	3.70
MGI:1913521	Tmem126a	#N/A	3.47591	#N/A	3.9034078	3.69
MGI:1919135	Faap100	#N/A	5.51461	#N/A	1.7967571	3.66
MGI:894688	Serpinb6b	#N/A	3.36983	#N/A	3.9080458	3.64
MGI:1915209	Puf60	#N/A	2.62664	#N/A	4.5194304	3.57
MGI:1930076	Rps6ka4	#N/A	4.30378	#N/A	2.7990813	3.55
MGI:2384902	Rnpep	#N/A	2.28374	#N/A	4.779907	3.53
MGI:1338850	Mthfd2	#N/A	4.83506	#N/A	2.2220187	3.53
MGI:88548	Csnk2b	#N/A	4.85898	#N/A	2.0749073	3.47

MGI:88529	Cs	#N/A	1.93146	#N/A	4.967726	3.45
MGI:1915731	Mpzl1	#N/A	2.24582	#N/A	4.5861082	3.42
MGI:2140998	Ube3c	#N/A	4.31019	#N/A	2.5213253	3.42
MGI:1298388	Umps	#N/A	4.49451	#N/A	2.3172529	3.41
MGI:1917498	Dazap1	#N/A	3.40726	#N/A	3.3741896	3.39
MGI:1917173	Agk	#N/A	3.17571	#N/A	3.6005452	3.39
MGI:1099460	Rbm3	#N/A	2.20899	#N/A	4.4345925	3.32
MGI:106201	Tmed1	#N/A	1.96209	#N/A	4.5871731	3.27
MGI:1891396	Kirrel1	#N/A	3.62417	#N/A	2.9171703	3.27
MGI:1917560	Plscr3	#N/A	3.60535	#N/A	2.9110892	3.26
MGI:1261845	Esyt2	#N/A	2.83213	#N/A	3.6654708	3.25
MGI:1914549	Dock7	#N/A	4.32108	#N/A	2.1510723	3.24
MGI:2442418	Tmx3	#N/A	4.5808	#N/A	1.8234996	3.20
MGI:2142581	Nsd3	#N/A	4.29511	#N/A	2.0743549	3.18
MGI:104995	Gclm	#N/A	3.98418	#N/A	2.3465319	3.17
MGI:1914262	Tm9sf3	#N/A	2.207	#N/A	4.0992832	3.15
MGI:2446173	Farp1	#N/A	1.85832	#N/A	4.425341	3.14
MGI:95657	Gas2	#N/A	3.01729	#N/A	3.2349846	3.13
MGI:104968	Ppox	#N/A	2.08748	#N/A	4.1619782	3.12
MGI:1341868	Rfc2	#N/A	3.5877	#N/A	2.6400535	3.11
MGI:2139740	Ppm1l	#N/A	2.29733	#N/A	3.8846871	3.09
MGI:106227	Capza1	#N/A	3.05083	#N/A	3.089349	3.07
MGI:1927155	Clptm1	#N/A	4.29757	#N/A	1.8148376	3.06
MGI:1915525	Rpa1	#N/A	4.45312	#N/A	1.6074085	3.03
MGI:98822	Tfrc	#N/A	2.32503	#N/A	3.6844199	3.00
MGI:1915789	Tmem109	#N/A	2.80758	#N/A	3.1750157	2.99
MGI:1859607	Praf2	#N/A	2.87862	#N/A	3.1017535	2.99
MGI:1099431	Sptlc1	#N/A	4.22975	#N/A	1.7315688	2.98
MGI:106442	Vkorc1	#N/A	2.22438	#N/A	3.654271	2.94
MGI:3612472	Pisd-ps2	#N/A	2.9368	#N/A	2.9381042	2.94
MGI:1929955	Akr1a1	0	1.74547	#N/A	4.0309879	2.89
MGI:108081	Sypl	#N/A	3.61995	#N/A	2.1441932	2.88
MGI:1858416	Stk39	#N/A	2.00187	#N/A	3.7359602	2.87
MGI:107745	Dctn1	#N/A	1.64122	#N/A	4.0545701	2.85
MGI:1915814	Nufip2	#N/A	2.88388	#N/A	2.7821162	2.83
MGI:Q9CWA4		#N/A	2.51506	#N/A	3.1303179	2.82
MGI:2135760	Sgpp1	#N/A	1.76588	#N/A	3.8764387	2.82
MGI:1196314	Dhrs1	#N/A	2.86111	#N/A	2.7727644	2.82
MGI:2444773	Mavs	#N/A	2.81157	#N/A	2.816664	2.81
MGI:1920374	Golim4	#N/A	2.67802	#N/A	2.9391689	2.81
MGI:1352748	Dpf1	#N/A	1.64364	#N/A	3.9720048	2.81
MGI:2446632	Ago2	#N/A	3.45121	#N/A	2.1187823	2.78
MGI:2685515	Arhgef40	#N/A	2.75082	#N/A	2.8106649	2.78
MGI:1914132	Bzw1	#N/A	3.3263	#N/A	2.234849	2.78
MGI:1351477	Cars	#N/A	3.72239	#N/A	1.7618079	2.74
MGI:1276111	Pfdn2	#N/A	2.87479	#N/A	2.5939567	2.73
MGI:1195263	Lims1	#N/A	2.76002	#N/A	2.7039845	2.73
MGI:1098234	Adprh	#N/A	2.80203	#N/A	2.6037536	2.70
MGI:2135756	Hspb8	#N/A	3.57294	#N/A	1.830843	2.70
MGI:1917678	Polr3b	#N/A	1.78276	#N/A	3.578292	2.68
MGI:3769724	Tomt	#N/A	2.86554	0	2.4791481	2.67
MGI:3036255	Tmtc3	#N/A	1.83326	#N/A	3.3586601	2.60
MGI:96270	Trmt2a	#N/A	1.70594	#N/A	3.4731709	2.59
MGI:2442402	Cnot1	#N/A	2.60051	#N/A	2.5518944	2.58

MGI:106247	Prpf19	#N/A	2.60975	#N/A	2.4677794	2.54
MGI:1889008	Atp2c1	#N/A	2.50049	#N/A	2.5653045	2.53
MGI:1928139	Mrps10	#N/A	2.30017	#N/A	2.7442386	2.52
MGI:2149842	Sdf2l1	#N/A	2.69445	#N/A	2.3312778	2.51
MGI:2179381	Prpf8	#N/A	2.93212	#N/A	2.0578794	2.49
MGI:1923001	Ipo4	#N/A	2.21488	#N/A	2.7615514	2.49
MGI:2446242	Atxn2l	#N/A	2.24027	#N/A	2.7306087	2.49
MGI:96013	Hat1	#N/A	2.48403	#N/A	2.4584374	2.47
MGI:1918611	Aifm2	#N/A	2.93815	#N/A	2.0014279	2.47
MGI:1913302	Sdhc	#N/A	2.46904	#N/A	2.333426	2.40
MGI:97748	Ctsa	#N/A	2.66474	#N/A	2.0962808	2.38
MGI:2149961	Pawr	#N/A	2.29993	#N/A	2.4593174	2.38
MGI:1914523	Ndufa10	#N/A	2.34506	#N/A	2.3992455	2.37
MGI:1196294	Fubp1	#N/A	1.8857	#N/A	2.6922457	2.29
MGI:1202066	Sec61g	#N/A	2.04847	#N/A	2.5187383	2.28
MGI:98731	Tgm2	#N/A	2.69969	#N/A	1.867045	2.28
MGI:1915339	Arpc4	#N/A	2.3957	#N/A	2.1653366	2.28
MGI:1914498	Rpl39	#N/A	2.48729	#N/A	2.0686016	2.28
MGI:95546	Foxs1	#N/A	2.71581	#N/A	1.8389947	2.28
MGI:1915387	Kdelr1	#N/A	2.42942	#N/A	2.0694947	2.25
MGI:1920908	Spns1	#N/A	2.16132	#N/A	2.3240244	2.24
MGI:1925905	Eif3j	#N/A	2.24112	#N/A	2.2334073	2.24
MGI:1933181	Eif3d	#N/A	2.26138	#N/A	2.1971622	2.23
MGI:1354175	Txnrd1	#N/A	1.78181	#N/A	2.6758986	2.23
MGI:1922169	Slc35f6	#N/A	2.4029	#N/A	2.0427229	2.22
MGI:1196412	Tnpo3	#N/A	2.30691	#N/A	2.0722203	2.19
MGI:107931	Sqstm1	#N/A	2.02073	#N/A	2.347188	2.18
MGI:1918007	Hacd2	#N/A	2.38252	#N/A	1.9703074	2.18
MGI:1931526	Hist1h1c	#N/A	2.31609	#N/A	2.0064974	2.16
MGI:104967	Glg1	#N/A	1.79576	#N/A	2.4353209	2.12
MGI:87881	Acp1	#N/A	2.07044	#N/A	2.130636	2.10
MGI:1195345	Zbtb14	#N/A	1.98678	#N/A	2.2024357	2.09
MGI:1889341	Hacd3	#N/A	2.12251	#N/A	2.0629721	2.09
MGI:88137	Bckdhb	#N/A	2.06918	#N/A	2.1004722	2.08
MGI:97890	Rad51	#N/A	1.9568	#N/A	2.1307352	2.04
MGI:1931013	Abhd1	#N/A	1.89773	#N/A	2.08337	1.99
MGI:2448481	Mgst2	#N/A	1.95735	#N/A	2.0235405	1.99
MGI:1201789	Rpl36a	#N/A	2.06562	0	1.8573108	1.96
MGI:2685862	Cd101	#N/A	1.72023	#N/A	2.1703033	1.95
MGI:1196217	Tcaim	#N/A	1.99061	#N/A	1.8703039	1.93
MGI:103264	Arhgef2	#N/A	1.73912	#N/A	2.1006429	1.92
MGI:96745	Lamp1	#N/A	1.73038	#N/A	2.0985465	1.91
MGI:1914497	37316	#N/A	1.63205	#N/A	2.1795893	1.91
MGI:1914401	Psmd9	#N/A	1.87182	#N/A	1.9216247	1.90
MGI:1916043	Rab3gap2	#N/A	2.00594	#N/A	1.7770663	1.89
MGI:106014	Nudc	#N/A	1.79489	#N/A	1.9698772	1.88
MGI:1095403	Sf1	#N/A	1.9977	#N/A	1.7602582	1.88
MGI:1346017	Clpx	#N/A	2.00927	#N/A	1.7102872	1.86
MGI:108089	Erh	#N/A	1.93533	#N/A	1.7825304	1.86
MGI:97538	Rhox5	#N/A	1.71018	#N/A	1.9915472	1.85
MGI:1278332	Bcl6b	#N/A	1.92513	#N/A	1.7397888	1.83
MGI:2145953	Kdelr3	#N/A	1.71516	#N/A	1.9460511	1.83
MGI:1100535	Myt1	#N/A	1.73689	#N/A	1.9142752	1.83
MGI:99476	Abhd16a	#N/A	1.90285	#N/A	1.7451849	1.82

MGI:108409	Rgs4	#N/A	1.66862	#N/A	1.9703896	1.82
MGI:1344351	Dlg2	#N/A	1.8223	#N/A	1.8020025	1.81
MGI:1916330	Gmppa	#N/A	1.7839	#N/A	1.8142556	1.80
MGI:3609260	Chrna10	#N/A	1.69101	#N/A	1.903821	1.80
MGI:97370	Enpp1	#N/A	1.6999	#N/A	1.8263299	1.76
MGI:1860494	Ddx21	#N/A	1.71662	#N/A	1.7175374	1.72
MGI:1914324	Mon2	#N/A	1.79565	#N/A	1.6257255	1.71
MGI:104885	Psma2	#N/A	1.69393	#N/A	1.7136288	1.70
MGI:2179717	Glcci1	#N/A	1.64179	#N/A	1.743886	1.69

7. References

Aherne, A., Kennan, A., Kenna, P. F., McNally, N., Lloyd, D. G., Alberts, I. L., Kiang, A. S., Humphries, M. M., Ayuso, C., Engel, P. C., et al. (2004). On the molecular pathology of neurodegeneration in IMPDH1-based retinitis pigmentosa. *Hum. Mol. Genet.*

Ahmed, S. M., Nishida-Fukuda, H., Li, Y., McDonald, W. H., Gradinaru, C. C. and Macara, I. G. (2018). Exocyst dynamics during vesicle tethering and fusion. *Nat. Commun.* **9**, 1–17.

Amodeo, A. A. and Skotheim, J. M. (2016). Cell-size control. *Cold Spring Harb. Perspect. Biol.* **8**,.

Anvarian, Z., Mykytyn, K., Mukhopadhyay, S., Pedersen, L. B. and Christensen, S. T. (2019). Cellular signalling by primary cilia in development, organ function and disease. *Nat. Rev. Nephrol.* **15**, 199–219.

Aughey, G. N., Grice, S. J., Shen, Q.-J., Xu, Y., Chang, C.-C., Azzam, G., Wang, P.-Y., Freeman-Mills, L., Pai, L.-M., Sung, L.-Y., et al. (2014). Nucleotide synthesis is regulated by cytoophidium formation during neurodevelopment and adaptive metabolism. *Biol. Open* **3**, 1045–56.

Azzam, G. and Liu, J. L. (2013). Only One Isoform of Drosophila melanogaster CTP Synthase Forms the Cytoophidium. *PLoS Genet.*

Badano, J. L., Mitsuma, N., Beales, P. L. and Katsanis, N. (2006). The Ciliopathies: An Emerging Class of Human Genetic Disorders. *Annu. Rev. Genomics Hum. Genet.* **7**, 125–148.

Baek, K., Knödler, A., Lee, S. H., Zhang, X., Orlando, K., Zhang, J., Foskett, T. J., Guo, W. and Dominguez, R. (2010). Structure-function study of the N-terminal domain of exocyst subunit Sec3. *J. Biol. Chem.* **285**, 10424–10433.

Barry, R. M., Bitbol, A. F., Lorestani, A., Charles, E. J., Habrian, C. H., Hansen, J. M., Li, H. J., Baldwin, E. P., Wingreen, N. S., Kollman, J. M., et al. (2014). Large-scale filament formation inhibits the activity of CTP synthetase. *Elife*.

Blankenship, J. T., Fuller, M. T. and Zallen, J. A. (2007). The Drosophila homolog of the Exo84 exocyst subunit promotes apical epithelial identity. *J. Cell Sci.* **120**, 3099–3110.

Bloom, G. S. and Goldstein, L. S. (1998). Cruising along microtubule highways: how membranes move through the secretory pathway. *J. Cell Biol.* **140**, 1277–1280.

Bodemann, B. O., Orvedahl, A., Cheng, T., Ram, R. R., Ou, Y. H., Formstecher, E., Maiti, M., Hazelett, C. C., Wauson, E. M., Balakireva, M., et al. (2011). RalB and the exocyst mediate the cellular starvation response by direct activation of autophagosome assembly. *Cell* **144**, 253–267.

Boucrot, E. and Kirchhausen, T. (2007). Endosomal recycling controls plasma membrane area during mitosis. *Proc. Natl. Acad. Sci. U. S. A.* **104**, 7939–

7944.

Bowne, S. J., Sullivan, L. S., Blanton, S. H., Cepko, C. L., Blackshaw, S., Birch, D. G., Hughbanks-Wheaton, D., Heckenlively, J. R. and Daiger, S. P. (2002). Mutations in the inosine monophosphate dehydrogenase 1 gene (IMPDH1) cause the RP10 form of autosomal dominant retinitis pigmentosa. *Hum. Mol. Genet.* **11**, 559–568.

Bowne, S. J., Sullivan, L. S., Mortimer, S. E., Hedstrom, L., Zhu, J., Spellicy, C. J., Gire, A. I., Hughbanks-Wheaton, D., Birch, D. G., Lewis, R. A., et al. (2006). Spectrum and frequency of mutations in IMPDH1 associated with autosomal dominant retinitis pigmentosa and leber congenital amaurosis. *Investig. Ophthalmol. Vis. Sci.*

Boyd, C., Hughes, T., Pypaert, M. and Novick, P. (2004). Vesicles carry most exocyst subunits to exocytic sites marked by the remaining two subunits, Sec3p and Exo70p. *J. Cell Biol.* **167**, 889–901.

Brancati, F., Dallapiccola, B. and Valente, E. M. (2010). Joubert Syndrome and related disorders. *Orphanet J. Rare Dis.* **5**, 1–10.

Bröcker, C., Engelbrecht-Vandré, S. and Ungermann, C. (2010). Multisubunit tethering complexes and their role in membrane fusion. *Curr. Biol.* **20**, R943–R952.

Bronner, M. E. (2012). Formation and migration of neural crest cells in the vertebrate embryo. *Histochem. Cell Biol.* **138**, 179–186.

Brunet, S. and Sacher, M. (2014). Are All Multisubunit Tethering Complexes Bona Fide Tethers? *Traffic* **15**, 1282–1287.

Bulgakova, N. A. and Knust, E. (2009). The Crumbs complex: From epithelial-cell polarity to retinal degeneration. *J. Cell Sci.* **122**, 2587–2596.

Caballero-Lima, D. and Sudbery, P. E. (2014). In Candida albicans, phosphorylation of Exo84 by Cdk1-Hgc1 is necessary for efficient hyphal extension. *Mol. Biol. Cell* **25**, 1097–1110.

Calise, S. J., Carcamo, W. C., Krueger, C., Yin, J. D., Purich, D. L. and Chan, E. K. L. (2014). Glutamine deprivation initiates reversible assembly of mammalian rods and rings. *Cell. Mol. Life Sci.* **71**, 2963–2973.

Calise, S. J., Keppeke, G. D., Andrade, L. E. C. and Chan, E. K. L. (2015). Anti-Rods/Rings: A Human Model of Drug-Induced Autoantibody Generation. *Front. Immunol.* **6**, 41.

Calise, S. J., Purich, D. L., Nguyen, T., Saleem, D. A., Krueger, C., Yin, J. D. and Chan, E. K. L. (2016). “Rod and ring” formation from IMP dehydrogenase is regulated through the one-carbon metabolic pathway. *J. Cell Sci.* **129**, 3042–52.

Cam, S. F., Papp, E., Wu, J. C. and Natsumedas, Y. (1993). *THE JOURNAL OF BIOLOGICAL CHEMISTRY Characterization of Human Type I and Type I1 IMP Dehydrogenases**.

Carcamo, W. C., Satoh, M., Kasahara, H., Terada, N., Hamazaki, T., Chan, J. Y. F., Yao, B., Tamayo, S., Covini, G., von Mühlen, C. A., et al. (2011). Induction of cytoplasmic rods and rings structures by inhibition of the CTP

and GTP synthetic pathway in mammalian cells. *PLoS One* **6**,.

Carcamo, W. C., Calise, S. J., von Mühlen, C. A., Satoh, M. and Chan, E. K. L. (2014). Molecular cell biology and immunobiology of mammalian rod/ring structures. In *International Review of Cell and Molecular Biology*, pp. 35–74. Elsevier Inc.

Carr, S. F., Papp, E., Wu, J. C. and Natsumeda, Y. (1993). Characterization of human type I and type II IMP dehydrogenases. *J. Biol. Chem.*

Cascone, I., Selimoglu, R., Ozdemir, C., Del Nery, E., Yeaman, C., White, M. and Camonis, J. (2008). Distinct roles of RalA and RalB in the progression of cytokinesis are supported by distinct RalGEFs. *EMBO J.* **27**, 2375–2387.

Chadha, A., Volland, S., Baliaouri, N. V., Tran, E. M. and Williams, D. S. (2019). The route of the visual receptor rhodopsin along the cilium. *J. Cell Sci.*

Chang, J., Seo, S. G., Lee, K. H., Nagashima, K., Bang, J. K., Kim, B. Y., Erikson, R. L., Lee, K. W., Lee, H. J., Park, J. E., et al. (2013). Essential role of Cenexin1, but not Odf2, in ciliogenesis. *Cell Cycle* **12**, 655–662.

Chang, C.-C., Lin, W.-C., Pai, L.-M., Lee, H.-S., Wu, S.-C., Ding, S.-T., Liu, J.-L. and Sung, L.-Y. (2015). Cytoophidium assembly reflects upregulation of IMPDH activity. *J. Cell Sci.* **128**, 3550–5.

Chang, C.-C., Jeng, Y.-M., Peng, M., Keppeke, G. D., Sung, L.-Y. and Liu, J.-L. (2017). CTP synthase forms the cytoophidium in human hepatocellular carcinoma. *Exp. Cell Res.* **361**, 292–299.

Chang, C., Keppeke, G. D., Sung, L. and Liu, J. (2018). Interfilament interaction between IMPDH and CTPS cytoophidia. *FEBS J.* **285**, 3753–3768.

Chen, Y. A. and Scheller, R. H. (2001). Snare-mediated membrane fusion. *Nat. Rev. Mol. Cell Biol.* **2**, 98–106.

Chen, J. and Zhang, M. (2013). The Par3/Par6/aPKC complex and epithelial cell polarity. *Exp. Cell Res.* **319**, 1357–1364.

Chen, X. W., Inoue, M., Hsu, S. C. and Saltiel, A. R. (2006). RalA-exocyst-dependent recycling endosome trafficking is required for the completion of cytokinesis. *J. Biol. Chem.* **281**, 38609–38616.

Chen, K., Zhang, J., Tastan, Ö. Y., Deussen, Z. A., Siswick, M. Y.-Y. and Liu, J.-L. (2011). Glutamine analogs promote cytoophidium assembly in human and Drosophila cells. *J. Genet. Genomics* **38**, 391–402.

Chen, J., Yamagata, A., Kubota, K., Sato, Y., Goto-Ito, S. and Fukai, S. (2017). Crystal structure of Sec10, a subunit of the exocyst complex. *Sci. Rep.* **7**, 40909.

Climent, J., Morandeira, F., Castellote, J., Xiol, J., Niubó, J., Calatayud, L., Mestre, M. and Bas, J. (2016). Clinical correlates of the “rods and rings” antinuclear antibody pattern. *Autoimmunity*.

Covini, G., Carcamo, W. C., Bredi, E., Von Mühlen, C. A., Colombo, M. and Chan, E. K. L. (2012). Cytoplasmic rods and rings autoantibodies developed during pegylated interferon and ribavirin therapy in patients with chronic hepatitis C. *Antivir. Ther.* **17**, 805–811.

Croteau, N. J., Furgason, M. L. M., Devos, D. and Munson, M. (2009). Conservation of helical bundle structure between the exocyst subunits. *PLoS One* **4**,.

Da Silva, J. S. and Dotti, C. G. (2002). Breaking the neuronal sphere: Regulation of the actin cytoskeleton in neuritogenesis. *Nat. Rev. Neurosci.*

Das, A., Gajendra, S., Falenta, K., Oudin, M. J., Peschard, P., Feng, S., Wu, B., Marshall, C. J., Doherty, P., Guo, W., et al. (2014). RalA promotes a direct exocyst-Par6 interaction to regulate polarity in neuronal development. *J. Cell Sci.* **127**, 686–699.

Dehmelt, L. and Halpain, S. (2005). The MAP2/Tau family of microtubule-associated proteins. *Genome Biol.* **6**, 204.

Dellago, H., Löscher, M., Ajuh, P., Ryder, U., Kaisermayer, C., Grillari-Voglauer, R., Fortschegger, K., Gross, S., Gstraunthaler, A., Borth, N., et al. (2011). Exo70, a subunit of the exocyst complex, interacts with SNEV hPrp19/hPso4 and is involved in pre-mRNA splicing. *Biochem. J.* **438**, 81–91.

Deng, Y. Z., Cai, Z., Shi, S., Jiang, H., Shang, Y. R., Ma, N., Wang, J. J., Guan, D. X., Chen, T. W., Rong, Y. F., et al. (2018). Cilia loss sensitizes cells to transformation by activating the mevalonate pathway. *J. Exp. Med.*

Dittmar, G. and Winklhofer, K. F. (2020). Linear Ubiquitin Chains: Cellular Functions and Strategies for Detection and Quantification. *Front. Chem.*

Dixon-Salazar, T. J., Silhavy, J. L., Udpa, N., Schroth, J., Bielas, S., Schaffer, A. E., Olvera, J., Bafna, V., Zaki, M. S., Abdel-Salam, G. H., et al. (2012). Exome Sequencing Can Improve Diagnosis and Alter Patient Management. *Sci. Transl. Med.* **4**, 138ra78.

Dong, G., Hutagalung, A. H., Fu, C., Novick, P. and Reinisch, K. M. (2005). The structures of exocyst subunit Exo70p and the Exo84p C-terminal domains reveal a common motif. *Nat. Struct. Mol. Biol.* **12**, 1094–1100.

Duan, Y., Guo, Q., Zhang, T., Meng, Y., Sun, D., Luo, G. and Liu, Y. (2020). Cyclin-dependent kinase-mediated phosphorylation of the exocyst subunit Exo84 in late G1 phase suppresses exocytic secretion and cell growth in yeast Running Title: Exo84 suppresses exocytic secretion in late G1 phase.

Feltri, M. L., Poitelon, Y. and Previtali, S. C. (2016). How Schwann Cells Sort Axons: New concepts. *Neuroscientist* **22**, 252–265.

Fielding, A. B., Schonteich, E., Matheson, J., Wilson, G., Yu, X., Hickson, G. R. X., Srivastava, S., Baldwin, S. A., Prekeris, R. and Gould, G. W. (2005). Rab11-FIP3 and FIP4 interact with Arf6 and the Exocyst to control membrane traffic in cytokinesis. *EMBO J.* **24**, 3389–3399.

Finger, F. P. and Novick, P. (1997). Sec3p is involved in secretion and morphogenesis in Saccharomyces cerevisiae. *Mol. Biol. Cell* **8**, 647–662.

Finger, F. P., Hughes, T. E. and Novick, P. (1998). Sec3p is a spatial landmark for polarized secretion in budding yeast. *Cell*.

Foletti, D. L., Prekeris, R. and Scheller, R. H. (1999). Generation and maintenance of neuronal polarity: Mechanisms of transport and targeting.

Neuron.

Fölsch, H., Pypaert, M., Maday, S., Pelletier, L. and Mellman, I. (2003). The AP-1A and AP-1B clathrin adaptor complexes define biochemically and functionally distinct membrane domains. *J. Cell Biol.* **163**, 351–362.

Fukai, S., Matern, H. T., Jagath, J. R., Scheller, R. H. and Brunger, A. T. (2003). Structural basis of the interaction between RalA and Sec5, a subunit of the sec6/8 complex. *EMBO J.* **22**, 3267–3278.

Furukawa, M., He, Y. J., Borchers, C. and Xiong, Y. (2003). Targeting of protein ubiquitination by BTB-Cullin 3-Roc1 ubiquitin ligases. *Nat. Cell Biol.*

Ganesan, S. J., Feyder, M. J., Chemmama, I. E., Fang, F., Rout, M. P., Chait, B. T., Shi, Y., Munson, M. and Sali, A. (2020). Integrative Structure and Function of the Yeast Exocyst Complex. *Protein Sci.*

Gerber, S. H. and Südhof, T. C. (2002). Molecular determinants of regulated exocytosis. In *Diabetes*, pp. S3–S11. American Diabetes Association.

Gerdes, J. M., Davis, E. E. and Katsanis, N. (2009). The Vertebrate Primary Cilium in Development, Homeostasis, and Disease. *Cell*.

Giansanti, M. G., Vanderleest, T. E., Jewett, C. E., Sechi, S., Frappaolo, A., Fabian, L., Robinett, C. C., Brill, J. A., Loerke, D., Fuller, M. T., et al. (2015). Exocyst-Dependent Membrane Addition Is Required for Anaphase Cell Elongation and Cytokinesis in Drosophila. *PLOS Genet.* **11**, e1005632.

Gillingham, A. K. and Munro, S. (2003). Long coiled-coil proteins and membrane traffic. *Biochim. Biophys. Acta - Mol. Cell Res.* **1641**, 71–85.

Glick, D., Barth, S. and Macleod, K. F. (2010). Autophagy: Cellular and molecular mechanisms. *J. Pathol.* **221**, 3–12.

Gomez-Lopez, N., Guilbert, L. J. and Olson, D. M. (2010). Invasion of the leukocytes into the fetal-maternal interface during pregnancy. *J. Leukoc. Biol.* **88**, 625–633.

Goranov, A. I., Cook, M., Ricicova, M., Ben-Ari, G., Gonzalez, C., Hansen, C., Tyers, M. and Amon, A. (2009). The rate of cell growth is governed by cell cycle stage. *Genes Dev.* **23**, 1408–1422.

Gou, K.-M., Chang, C.-C., Shen, Q.-J., Sung, L.-Y. and Liu, J.-L. (2014). CTP synthase forms cytoophidia in the cytoplasm and nucleus. *Exp. Cell Res.* **323**, 242–253.

Grindstaff, K. K., Yeaman, C., Anandasabapathy, N., Hsu, S. C., Rodriguez-Boulan, E., Scheller, R. H. and Nelson, W. J. (1998). Sec6/8 complex is recruited to cell-cell contacts and specifies transport vesicle delivery to the basal-lateral membrane in epithelial cells. *Cell* **93**, 731–740.

Gromley, A., Yeaman, C., Rosa, J., Redick, S., Chen, C. T., Mirabelle, S., Guha, M., Sillibourne, J. and Doxsey, S. J. (2005). Centriolin anchoring of exocyst and SNARE complexes at the midbody is required for secretory-vesicle-mediated abscission. *Cell* **123**, 75–87.

Grote, E., Carr, C. M. and Novick, P. J. (2000). Ordering the final events in yeast exocytosis. *J. Cell Biol.* **151**, 439–451.

Gu, J. J., Stegmann, S., Gathy, K., Murray, R., Laliberte, J., Ayscue, L. and Mitchell, B. S. (2000). Inhibition of T lymphocyte activation in mice heterozygous for loss of the IMPDH II gene. *J. Clin. Invest.*

Guertin, D. A., Trautmann, S. and McCollum, D. (2002). Cytokinesis in Eukaryotes. *Microbiol. Mol. Biol. Rev.* **66**, 155–178.

Gumy, L. F., Katrukha, E. A., Grigoriev, I., Jaarsma, D., Kapitein, L. C., Akhmanova, A. and Hoogenraad, C. C. (2017). MAP2 Defines a Pre-axonal Filtering Zone to Regulate KIF1- versus KIF5-Dependent Cargo Transport in Sensory Neurons. *Neuron* **94**, 347–362.e7.

Gunter, J. H., Thomas, E. C., Lengefeld, N., Kruger, S. J., Worton, L., Gardiner, E. M., Jones, A., Barnett, N. L. and Whitehead, J. P. (2008). Characterisation of inosine monophosphate dehydrogenase expression during retinal development: Differences between variants and isoforms. *Int. J. Biochem. Cell Biol.*

Guo, W., Luo, G., Luca, F. C. and Zhang, J. (2013). Mitotic phosphorylation of Exo84 disrupts exocyst assembly and arrests cell growth. *J. Cell Biol.* **202**, 97–111.

Hamburger, Z. A., Hamburger, A. E., West, A. P. and Weis, W. I. (2006). Crystal structure of the S. cerevisiae exocyst component Exo70p. *J. Mol. Biol.* **356**, 9–21.

Han, J., Pluhackova, K. and Böckmann, R. A. (2017). The multifaceted role of SNARE proteins in membrane fusion. *Front. Physiol.* **8**, 5.

Hayward, D., Kouznetsova, V. L., Pierson, H. E., Hasan, N. M., Guzman, E. R., Tsigelny, I. F. and Lutsenko, S. (2019). ANKRD9 is a metabolically-controlled regulator of IMPDH2 abundance and macro-assembly. *J. Biol. Chem.*

Hazelett, C. C. and Yeaman, C. (2012). Sec5 and Exo84 mediate distinct aspects of rala-dependent cell polarization. *PLoS One* **7**,.

Hazelett, C. C., Sheff, D. and Yeaman, C. (2011). RalA and RalB differentially regulate development of epithelial tight junctions. *Mol. Biol. Cell* **22**, 4787–4800.

He, Q., Wang, G., Dasgupta, S., Dinkins, M., Zhu, G. and Bieberich, E. (2012). Characterization of an apical ceramide-enriched compartment regulating ciliogenesis. *Mol. Biol. Cell* **23**, 3156–3166.

Hedstrom, L. (2009). IMP dehydrogenase: Structure, mechanism, and inhibition. *Chem. Rev.* **109**, 2903–2928.

Heider, M. R. and Munson, M. (2012). Exorcising the exocyst complex. *Traffic* **13**, 898–907.

Heider, M. R., Gu, M., Duffy, C. M., Mirza, A. M., Marcotte, L. L., Walls, A. C., Farrall, N., Hakhverdyan, Z., Field, M. C., Rout, M. P., et al. (2016). Subunit connectivity, assembly determinants and architecture of the yeast exocyst complex. *Nat. Struct. Mol. Biol.* **23**, 59–66.

Hofer, A., Steverding, D., Chabes, A., Brun, R. and Thelander, L. (2001). Trypanosoma brucei CTP synthetase: A target for the treatment of African

sleeping sickness. *Proc. Natl. Acad. Sci. U. S. A.*

Hsu, S. C., Hazuka, C. D., Roth, R., Foletti, D. L., Heuser, J. and Scheller, R. H. (1998). Subunit composition, protein interactions, and structures of the mammalian brain sec6/8 complex and septin filaments. *Neuron* **20**, 1111–1122.

Humbert, P., Russell, S. and Richardson, H. (2003). Dlg, scribble and Lgl in cell polarity, cell proliferation and cancer. *BioEssays*.

Inamdar, S. M., Hsu, S.-C. and Yeaman, C. (2016). Probing Functional Changes in Exocyst Configuration with Monoclonal Antibodies. *Front. Cell Dev. Biol.*

Ingerson-Mahar, M., Briegel, A., Werner, J. N., Jensen, G. J. and Gitai, Z. (2010). The metabolic enzyme CTP synthase forms cytoskeletal filaments. *Nat. Cell Biol.* **12**, 739–746.

Issaq, S. H., Lim, K. H. and Counter, C. M. (2010). Sec5 and Exo84 foster oncogenic ras-mediated tumorigenesis. *Mol. Cancer Res.* **8**, 223–231.

Jahn, R. and Scheller, R. H. (2006). SNAREs - Engines for membrane fusion. *Nat. Rev. Mol. Cell Biol.* **7**, 631–643.

Jahn, R. and Südhof, T. C. (1999). Membrane Fusion and Exocytosis. *Annu. Rev. Biochem.* **68**, 863–911.

Ji, Y. S., Gu, J. J., Makhov, A. M., Griffith, J. D. and Mitchell, B. S. (2006). Regulation of the interaction of inosine monophosphate dehydrogenase with mycophenolic acid by GTP. *J. Biol. Chem.* **281**, 206–212.

Jin, R., Junutula, J. R., Matern, H. T., Ervin, K. E., Scheller, R. H. and Brunger, A. T. (2005). Exo84 and Sec5 are competitive regulatory Sec6/8 effectors to the RalA GTPase. *EMBO J.* **24**, 2064–2074.

Joberty, G., Petersen, C., Gao, L. and Macara, I. G. (2000). The cell-polarity protein Par6 links Par3 and atypical protein kinase C to Cdc42. *Nat. Cell Biol.* **2**, 531–539.

Joffre, C., Dupont, N., Hoa, L., Gomez, V., Pardo, R., Gonçalves-Pimentel, C., Achard, P., Bettoun, A., Meunier, B., Bauvy, C., et al. (2015). The pro-apoptotic STK38 kinase is a new Beclin1 Partner positively regulating autophagy. *Curr. Biol.* **25**, 2479–2492.

Jorgensen, P. and Tyers, M. (2004). How cells coordinate growth and division. *Curr. Biol.* **14**, R1014–R1027.

Juda, P., Šmigová, J., Kováčik, L., Bártová, E. and Raška, I. (2014). Ultrastructure of Cytoplasmic and Nuclear Inosine-5'-Monophosphate Dehydrogenase 2 "Rods and Rings" Inclusions. *J. Histochem. Cytochem.* **62**, 739–750.

Keppeke, G. D., Calise, S. J., Chan, E. K. L. and Andrade, L. E. C. (2015). Assembly of IMPDH2-Based, CTPS-Based, and Mixed Rod/Ring Structures Is Dependent on Cell Type and Conditions of Induction. *J. Genet. Genomics* **42**, 287–299.

Keppeke, G. D., Chang, C. C., Peng, M., Chen, L.-Y., Lin, W.-C., Pai, L.-M., Andrade, L. E. C., Sung, L.-Y. and Liu, J.-L. (2018). IMP/GTP balance modulates cytoophidium assembly and IMPDH activity. *Cell Div.* **13**, 5.

Keppeke, G. D., Calise, S. J., Chan, E. K. L. and Andrade, L. E. C. (2019). Ribavirin induces widespread accumulation of IMP dehydrogenase into rods/rings structures in multiple major mouse organs. *Antiviral Res.* **162**, 130–135.

Keppeke, G. D., Barcelos, D., Fernandes, M., Comodo, A. N., Guimarães, D. P., Cardili, L., Carapeto, F. C. L., Andrade, L. E. C. and Landman, G. (2020). IMP dehydrogenase rod/ring structures in acral melanomas. *Pigment Cell Melanoma Res.*

Kim, S.-M. and Kim, J.-S. (2017). A Review of Mechanisms of Implantation. *Dev. Reprod.* **21**, 351–359.

Kizaki, H., Williams, J. C., Morris, H. P. and Weber, G. (1980). Increased Cytidine 5'-Triphosphate Synthetase Activity in Rat and Human Tumors. *Cancer Res.*

Kowal, T. J. and Falk, M. M. (2015). Primary cilia found on HeLa and other cancer cells. *Cell Biol. Int.* **39**, 1341–1347.

Kumar, H., Pushpa, K., Kumari, A., Verma, K., Pergu, R. and Mylavarapu, S. V. S. (2019). The exocyst complex and Rab5 are required for abscission by localizing ESCRT III subunits to the cytokinetic bridge. *J. Cell Sci.* **132**,.

Kursula, P., Flodin, S., Ehn, M., Hammarström, M., Schüler, H., Nordlund, P. and Stenmark, P. (2006). Structure of the synthetase domain of human CTP synthetase, a target for anticancer therapy. *Acta Crystallogr. Sect. F Struct. Biol. Cryst. Commun.*

Labesse, G., Alexandre, T., Vaupré, L., Salard-Arnaud, I., Him, J. L. K., Raynal, B., Bron, P. and Munier-Lehmann, H. (2013). MgATP regulates allostery and fiber formation in IMPDHs. *Structure* **21**, 975–985.

Lalli, G. (2009). RalA and the exocyst complex influence neuronal polarity through PAR-3 and aPKC. *J. Cell Sci.* **122**, 1499–1506.

Lee, Y., Lim, B., Lee, S. W., Lee, W. R., Kim, Y. I., Kim, M., Ju, H., Kim, M. Y., Kang, S. J., Song, J. J., et al. (2018). ANKRD9 is associated with tumor suppression as a substrate receptor subunit of ubiquitin ligase. *Biochim. Biophys. Acta - Mol. Basis Dis.*

Lepore, D. M., Martínez-Núñez, L. and Munson, M. (2018). Exposing the Elusive Exocyst Structure. *Trends Biochem. Sci.* **43**, 714–725.

Letinic, K., Sebastian, R., Toomre, D. and Rakic, P. (2009). Exocyst is involved in polarized cell migration and cerebral cortical development. *Proc. Natl. Acad. Sci. U. S. A.*

Li, Q., Li, N., Liu, C.-Y., Xu, R., Kolosov, V. P., Perelman, J. M. and Zhou, X.-D. (2015). Ezrin/Exocyst Complex Regulates Mucin 5AC Secretion Induced by Neutrophil Elastase in Human Airway Epithelial Cells. *Cell. Physiol. Biochem.* **35**, 326–338.

Lim, K. H., Baines, A. T., Fiordalisi, J. J., Shipitsin, M., Feig, L. A., Cox, A. D., Der, C. J. and Counter, C. M. (2005). Activation of RalA is critical for Ras-induced tumorigenesis of human cells. *Cancer Cell* **7**, 533–545.

Lin, D., Edwards, A. S., Fawcett, J. P., Mbamalu, G., Scott, J. D. and Pawson,

T. (2000). A mammalian PAR-3-PAR-6 complex implicated in Cdc42/Rac1 and aPKC signalling and cell polarity. *Nat. Cell Biol.* **2**, 540–547.

Lipschutz, J. H. (2019). The role of the exocyst in renal ciliogenesis, cystogenesis, tubulogenesis, and development. *Kidney Res. Clin. Pract.* **38**, 260–266.

Liu, J.-L. (2010). Intracellular compartmentation of CTP synthase in Drosophila. *J. Genet. Genomics* **37**, 281–296.

Liu, J.-L. (2011). The enigmatic cytoophidium: Compartmentation of CTP synthase via filament formation. *BioEssays* **33**, 159–164.

Liu, J.-L. (2016). The Cytoophidium and Its Kind: Filamentation and Compartmentation of Metabolic Enzymes. *Annu. Rev. Cell Dev. Biol.* **32**, 349–372.

Liu, J. and Guo, W. (2012). The exocyst complex in exocytosis and cell migration. *Protoplasma* **249**, 587–597.

Long, C. W. and Pardee, A. B. (1967). Cytidine triphosphate synthetase of Escherichia coli B. I. Purification and kinetics. *J. Biol. Chem.*

López-Colomé, A. M., Lee-Rivera, I., Benavides-Hidalgo, R. and López, E. (2017). Paxillin: A crossroad in pathological cell migration. *J. Hematol. Oncol.* **10**, 1–15.

Lynch, E. M., Hicks, D. R., Shepherd, M., Endrizzi, J. A., Maker, A., Hansen, J. M., Barry, R. M., Gitai, Z., Baldwin, E. P. and Kollman, J. M. (2017). Human CTP synthase filament structure reveals the active enzyme conformation. *Nat. Struct. Mol. Biol.* **24**, 507–514.

Ma, W., Wang, Y., Yao, X., Xu, Z., An, L. and Yin, M. (2016). The role of Exo70 in vascular smooth muscle cell migration. *Cell. Mol. Biol. Lett.* **21**, 20.

Martín-Cuadrado, A. B., Morrell, J. L., Konomi, M., An, H., Petit, C., Osumi, M., Balasubramanian, M., Gould, K. L., Del Rey, F. and Vázquez De Aldana, C. R. (2005). Role of septins and the exocyst complex in the function of hydrolytic enzymes responsible for fission yeast cell separation. *Mol. Biol. Cell* **16**, 4867–4881.

Martin, T. D., Samuel, J. C., Routh, E. D., Der, C. J. and Yeh, J. J. (2011). Activation and involvement of Ral GTPases in colorectal cancer. *Cancer Res.*

Matern, H. T., Yeaman, C., Nelson, W. J. and Scheller, R. H. (2001). The Sec6/8 complex in mammalian cells: Characterization of mammalian Sec3, subunit interactions, and expression of subunits in polarized cells. *Proc. Natl. Acad. Sci. U. S. A.* **98**, 9648–9653.

McCusker, D. and Kellogg, D. R. (2012). Plasma membrane growth during the cell cycle: Unsolved mysteries and recent progress. *Curr. Opin. Cell Biol.* **24**, 845–851.

McGrew, D. A. and Hedstrom, L. (2012). Towards a pathological mechanism for IMPDH1-Linked retinitis pigmentosa. In *Advances in Experimental Medicine and Biology*, .

Mei, K., Li, Y., Wang, S., Shao, G., Wang, J., Ding, Y., Luo, G., Yue, P., Liu,

J. J., Wang, X., et al. (2018). Cryo-EM structure of the exocyst complex. *Nat. Struct. Mol. Biol.* **25**, 139–146.

Miao, Y., Wu, J. and Abraham, S. N. (2016). Ubiquitination of Innate Immune Regulator TRAF3 Orchestrates Expulsion of Intracellular Bacteria by Exocyst Complex. *Immunity* **45**, 94–105.

Miettinen, T. P., Kang, J. H., Yang, L. F. and Manalis, S. R. (2019). Mammalian cell growth dynamics in mitosis. *Elife* **8**,.

Moore, B. A., Robinson, H. H. and Xu, Z. (2007). The Crystal Structure of Mouse Exo70 Reveals Unique Features of the Mammalian Exocyst. *J. Mol. Biol.* **371**, 410–421.

Morgera, F., Sallah, M. R., Dubuke, M. L., Gandhi, P., Brewer, D. N., Carr, C. M. and Munson, M. (2012). Regulation of exocytosis by the exocyst subunit Sec6 and the SM protein Sec1. *Mol. Biol. Cell* **23**, 337–346.

Morin, A., Cordelières, F. P., Cherfils, J. and Olofsson, B. (2010). RhoGDI3 and RhoG: Vesicular trafficking and interactions with the Sec3 Exocyst subunit. *Small GTPases* **1**, 142–156.

Moskalenko, S., Henry, D. O., Rosse, C., Mirey, G., Camonis, J. H. and White, M. A. (2002). The exocyst is a Ral effector complex. *Nat. Cell Biol.* **4**, 66–72.

Moskalenko, S., Tong, C., Rosse, C., Mirey, G., Formstecher, E., Daviet, L., Camonis, J. and White, M. A. (2003). Ral GTPases Regulate Exocyst Assembly through Dual Subunit Interactions. *J. Biol. Chem.* **278**, 51743–51748.

Mott, H. R., Nietlispach, D., Hopkins, L. J., Mirey, G., Camonis, J. H. and Owen, D. (2003). Structure of the GTPase-binding Domain of Sec5 and Elucidation of its Ral Binding Site*.

Munson, M. and Novick, P. (2006). The exocyst defrocked, a framework of rods revealed. *Nat. Struct. Mol. Biol.* **13**, 577–581.

Naegeli, K. M., Hastie, E., Garde, A., Wang, Z., Keeley, D. P., Gordon, K. L., Pani, A. M., Kelley, L. C., Morrissey, M. A., Chi, Q., et al. (2017). Cell Invasion In Vivo via Rapid Exocytosis of a Transient Lysosome-Derived Membrane Domain. *Dev. Cell* **43**, 403–417.e10.

Nag, C., Ghosh, M., Das, K. and Ghosh, T. (2013). Joubert syndrome: The molar tooth sign of the mid-brain. *Ann. Med. Health Sci. Res.*

Neto, H., Balmer, G. and Gould, G. (2013). Exocyst proteins in cytokinesis. *Commun. Integr. Biol.* **6**, e27635.

Noble, J. W., Hunter, D. V., Roskelley, C. D., Chan, E. K. L. and Mills, J. (2016). Loukoumasomes are distinct subcellular structures from rods and rings and are structurally associated with MAP2 and the nuclear envelope in retinal cells. *PLoS One* **11**,.

Nola, S., Sebbagh, M., Marchetto, S., Osmani, N., Nourry, C., Audebert, S., Navarro, C., Rachel, R., Montcouquiol, M., Sans, N., et al. (2008). Scrib regulates PAK activity during the cell migration process. *Hum. Mol. Genet.*

Noree, C., Sato, B. K., Broyer, R. M. and Wilhelm, J. E. (2010). Identification of novel filament-forming proteins in Saccharomyces cerevisiae and

Drosophila melanogaster. *J. Cell Biol.* **190**, 541–551.

Noree, C., Monfort, E., Shiau, A. K. and Wilhelm, J. E. (2014). Common regulatory control of CTP synthase enzyme activity and filament formation. *Mol. Biol. Cell*.

Novick, P., Field, C. and Schekman, R. (1980). Identification of 23 complementation groups required for post-translational events in the yeast secretory pathway. *Cell* **21**, 205–215.

Ohta, Y., Suzuki, N., Nakamura, S., Hartwig, J. H. and Stossel, T. P. (1999). The small GTPase RalA targets filamin to induce filopodia. *Proc. Natl. Acad. Sci. U. S. A.* **96**, 2122–2128.

Ommer, A., Figlia, G., Pereira, J. A., Datwyler, A. L., Gerber, J., DeGeer, J., Lalli, G. and Suter, U. (2019). Ral GTPases in schwann cells promote radial axonal sorting in the peripheral nervous system. *J. Cell Biol.* **218**, 2350–2369.

Oztan, A., Silvis, M., Weisz, O. A., Bradbury, N. A., Hsu, S. C., Goldenring, J. R., Yeaman, C. and Apodaca, G. (2007). Exocyst requirement for endocytic traffic directed toward the apical and basolateral poles of polarized MDCK cells. *Mol. Biol. Cell* **18**, 3978–3992.

Pai, L.-M., Wang, P.-Y., Lin, W.-C., Chakraborty, A., Yeh, C.-T. and Lin, Y.-H. (2016). Ubiquitination and filamentous structure of cytidine triphosphate synthase. *Fly (Austin).* **10**, 108–114.

Park, C. K. and Horton, N. C. (2019). Structures, functions, and mechanisms of filament forming enzymes: a renaissance of enzyme filamentation. *Biophys. Rev.*

Parrini, M. C., Sadou-Dubourgnoux, A., Aoki, K., Kunida, K., Biondini, M., Hatzoglou, A., Poullet, P., Formstecher, E., Yeaman, C., Matsuda, M., et al. (2011). SH3BP1, an Exocyst-Associated RhoGAP, Inactivates Rac1 at the Front to Drive Cell Motility. *Mol. Cell* **42**, 650–661.

Petit, M. M. R., Meulemans, S. M. P., Alen, P., Ayoubi, T. A. Y., Jansen, E. and Van de Ven, W. J. M. (2005). The tumor suppressor Scrib interacts with the zyxin-related protein LPP, which shuttles between cell adhesion sites and the nucleus. *BMC Cell Biol.*

Pfeffer, S. R. (1999). Transport-vesicle targeting: Tethers before SNAREs. *Nat. Cell Biol.* **1**, E17–E22.

Picco, A., Irastorza-Azcarate, I., Specht, T., Böke, D., Pazos, I., Rivier-Cordey, A. S., Devos, D. P., Kaksonen, M. and Gallego, O. (2017). The In Vivo Architecture of the Exocyst Provides Structural Basis for Exocytosis. *Cell* **168**, 400–412.e18.

Pickett, J. A. and Edwardson, J. M. (2006). Compound exocytosis: Mechanisms and functional significance. *Traffic*.

Polgar, N. and Fogelgren, B. (2018). Regulation of cell polarity by exocyst-mediated trafficking. *Cold Spring Harb. Perspect. Biol.* **10**,.

Porat-Shliom, N., Milberg, O., Masedunskas, A. and Weigert, R. (2013). Multiple roles for the actin cytoskeleton during regulated exocytosis. *Cell.*

Mol. Life Sci. **70**, 2099–2121.

Probst, C., Radzimski, C., Blöcker, I. M., Teegen, B., Bogdanos, D. P., Stöcker, W. and Komorowski, L. (2013). Development of a recombinant cell-based indirect immunofluorescence assay (RC-IFA) for the determination of autoantibodies against “rings and rods”-associated inosine-5’-monophosphate dehydrogenase 2 in viral hepatitis C. *Clin. Chim. Acta* **418**, 91–96.

Ramer, M. S., Cabrera, M. A. C., Alan, N., Scott, A. L. M. and Inskip, J. A. (2010). A new organellar complex in rat sympathetic neurons. *PLoS One* **5**,.

Reiter, J. F. and Leroux, M. R. (2017). Genes and molecular pathways underpinning ciliopathies. *Nat. Rev. Mol. Cell Biol.*

Riefler, G. M., Balasingam, G., Lucas, K. G., Wang, S., Hsu, S. C. and Firestein, B. L. (2003). Exocyst complex subunit sec8 binds to postsynaptic density protein-95 (PSD-95): A novel interaction regulated by cypin (cytosolic PSD-95 interactor). *Biochem. J.* **373**, 49–55.

Rochette, S., Gagnon-Arsenault, I., Diss, G. and Landry, C. R. (2014). Modulation of the yeast protein interactome in response to DNA damage. *J. Proteomics* **100**, 25–36.

Rosse, C., Formstecher, E., Boeckeler, K., Zhao, Y., Kremerskothen, J., White, M. D., Camonis, J. H. and Parker, P. J. (2009). An aPKC-Exocyst Complex Controls Paxillin Phosphorylation and Migration through Localised JNK1 Activation. *PLoS Biol.* **7**, e1000235.

Ruan, H., Song, Z., Cao, Q., Ni, D., Xu, T., Wang, K., Bao, L., Tong, J., Xiao, H., Xiao, W., et al. (2020). IMPDH1/YB-1 Positive Feedback Loop Assembles Cytoophidia and Represents a Therapeutic Target in Metastatic Tumors. *Mol. Ther.*

Salzer, J. L. (2015). Schwann cell myelination. *Cold Spring Harb. Perspect. Biol.* **7**,.

Satir, P., Pedersen, L. B. and Christensen, S. T. (2010). The primary cilium at a glance. *J. Cell Sci.* **123**, 499–503.

Schiavon, C. R., Griffin, M. E., Pirozzi, M., Parashuraman, R., Zhou, W., Jinnah, H. A., Reines, D. and Kahn, R. A. (2018). Compositional complexity of rods and rings. *Mol. Biol. Cell* **29**, 2303–2316.

Schiel, J. A. and Prekeris, R. (2013). Membrane dynamics during cytokinesis. *Curr. Opin. Cell Biol.* **25**, 92–98.

Schmoranzer, J. and Simon, S. M. (2003). Role of microtubules in fusion of post-Golgi vesicles to the plasma membrane. *Mol. Biol. Cell* **14**, 1558–1569.

Serini, G., Sigismund, S. and Lanzetti, L. (2012). Endocytosis and Exocytosis in Signal Transduction and in Cell Migration. In *Crosstalk and Integration of Membrane Trafficking Pathways*, p. InTech.

Shen, Q.-J., Kassim, H., Huang, Y., Li, H., Zhang, J., Li, G., Wang, P.-Y., Yan, J., Ye, F. and Liu, J.-L. (2016). Filamentation of Metabolic Enzymes in Saccharomyces cerevisiae. *J. Genet. Genomics* **43**, 393–404.

Sherwood, D. R. and Plastino, J. (2018). Invading, leading and navigating cells

in caenorhabditis elegans: Insights into cell movement in vivo. *Genetics* **208**, 53–78.

Shi, S. H., Jan, L. Y. and Jan, Y. N. (2003). Hippocampal neuronal polarity specified by spatially localized mPar3/mPar6 and PI 3-kinase activity. *Cell* **112**, 63–75.

Simicek, M., Lievens, S., Laga, M., Guzenko, D., Aushev, V. N., Kalev, P., Baietti, M. F., Strelkov, S. V., Gevaert, K., Tavernier, J., et al. (2013). The deubiquitylase USP33 discriminates between RALB functions in autophagy and innate immune response. *Nat. Cell Biol.* **15**, 1220–1230.

Sivaram, M. V. S., Furgason, M. L. M., Brewer, D. N. and Munson, M. (2006). The structure of the exocyst subunit Sec6p defines a conserved architecture with diverse roles. *Nat. Struct. Mol. Biol.* **13**, 555–556.

Song, D. K., Choi, J. H. and Kim, M. S. (2018). Primary cilia as a signaling platform for control of energy metabolism. *Diabetes Metab. J.*

Songer, J. A. and Munson, M. (2009). Sec6p anchors the assembled exocyst complex at sites of secretion. *Mol. Biol. Cell* **20**, 973–982.

Spiczka, K. S. and Yeaman, C. (2008). Ral-regulated interaction between Sec5 and paxillin targets Exocyst to focal complexes during cell migration. *J. Cell Sci.* **121**, 2880–2891.

Spiegelman, N. A., Zhang, X., Jing, H., Cao, J., Kotliar, I. B., Aramsangtienchai, P., Wang, M., Tong, Z., Rosch, K. M. and Lin, H. (2019). SIRT2 and Lysine Fatty Acylation Regulate the Activity of RalB and Cell Migration. *ACS Chem. Biol.* **14**, 2014–2023.

Spiliotis, E. T. and Nelson, W. J. (2003). Spatial control of exocytosis. *Curr. Opin. Cell Biol.* **15**, 430.

Strochlic, T. I., Stavrides, K. P., Thomas, S. V, Nicolas, E., O'Reilly, A. M. and Peterson, J. R. (2014). Ack kinase regulates CTP synthase filaments during Drosophila oogenesis . *EMBO Rep.*

Sugihara, K., Asano, S., Tanaka, K., Iwamatsu, A., Okawa, K. and Ohta, Y. (2002). The exocyst complex binds the small GTPase RalA to mediate filopodia formation. *Nat. Cell Biol.* **4**, 73–78.

Sun, Z. and Liu, J.-L. (2019). Forming cytoophidia prolongs the half-life of CTP synthase. *Cell Discov.* **5**, 32.

Synek, L., Sekereš, J. and Žárský, V. (2014). The exocyst at the interface between cytoskeleton and membranes in eukaryotic cells. *Front. Plant Sci.* **4**, 543.

Takahashi, S., Kubo, K., Waguri, S., Yabashi, A., Shin, H. W., Katoh, Y. and Nakayama, K. (2012). Rab11 regulates exocytosis of recycling vesicles at the plasma membrane. *J. Cell Sci.* **125**, 4049–4057.

Takeuchi, H., Furuta, N., Morisaki, I. and Amano, A. (2011). Exit of intracellular Porphyromonas gingivalis from gingival epithelial cells is mediated by endocytic recycling pathway. *Cell. Microbiol.* **13**, 677–691.

Tanaka, T., Iino, M. and Goto, K. (2014). Knockdown of Sec8 enhances the binding affinity of c-Jun N-terminal kinase (JNK)-interacting protein 4 for

mitogen-activated protein kinase kinase 4 (MKK4) and suppresses the phosphorylation of MKK4, p38, and JNK, thereby inhibiting apoptosis. *FEBS J.* **281**, 5237–5250.

Tanaka, T., Kikuchi, N., Goto, K. and Iino, M. (2016). Sec6/8 regulates Bcl-2 and Mcl-1, but not Bcl-xl, in malignant peripheral nerve sheath tumor cells. *Apoptosis* **21**, 594–608.

Tanaka, T., Goto, K. and Iino, M. (2017). Diverse Functions and Signal Transduction of the Exocyst Complex in Tumor Cells. *J. Cell. Physiol.* **232**, 939–957.

Tastan, Ö. Y. and Liu, J. L. (2015). CTP Synthase Is Required for Optic Lobe Homeostasis in Drosophila. *J. Genet. Genomics* **42**, 261–274.

TerBush, D. R. and Novick, P. (1995). Sec6, Sec8, and Sec15 are components of a multisubunit complex which localizes to small bud tips in Saccharomyces cerevisiae. *J. Cell Biol.* **130**, 299–312.

TerBush, D. R., Maurice, T., Roth, D. and Novick, P. (1996). The Exocyst is a multiprotein complex required for exocytosis in Saccharomyces cerevisiae. *EMBO J.* **15**, 6483–6494.

Thapa, N., Sun, Y., Schramp, M., Choi, S., Ling, K. and Anderson, R. A. (2012). Phosphoinositide Signaling Regulates the Exocyst Complex and Polarized Integrin Trafficking in Directionally Migrating Cells. *Dev. Cell* **22**, 116–130.

Thomas, E. C., Gunter, J. H., Webster, J. A., Schieber, N. L., Oorschot, V., Parton, R. G. and Whitehead, J. P. (2012). Different Characteristics and Nucleotide Binding Properties of Inosine Monophosphate Dehydrogenase (IMPDH) Isoforms. *PLoS One* **7**, e51096.

Thul, P. J., Akesson, L., Wiking, M., Mahdessian, D., Geladaki, A., Ait Blal, H., Alm, T., Asplund, A., Björk, L., Breckels, L. M., et al. (2017). A subcellular map of the human proteome. *Science (80-.).*

Torres, M. J., Pandita, R. K., Kulak, O., Kumar, R., Formstecher, E., Horikoshi, N., Mujoo, K., Hunt, C. R., Zhao, Y., Lum, L., et al. (2015). Role of the Exocyst Complex Component Sec6/8 in Genomic Stability. *Mol. Cell. Biol.* **35**, 3633–3645.

Van Kuilenburg, A. B. P., Meinsma, R., Vreken, P., Waterham, H. R. and Van Gennip, A. H. (2000). Identification of a cDNA encoding an isoform of human CTP synthetase. *Biochim. Biophys. Acta - Gene Struct. Expr.*

Verhage, M. and Sørensen, J. B. (2008). Vesicle Docking in Regulated Exocytosis. *Traffic* **9**, 1414–1424.

Wada, Y., Sandberg, M. A., McGee, T. L., Stillberger, M. A., Berson, E. L. and Dryja, T. P. (2005). Screen of the IMPDH1 gene among patients with dominant retinitis pigmentosa and clinical features associated with the most common mutation, Asp226Asn. *Investig. Ophthalmol. Vis. Sci.*

Wang, S., Liu, Y., Adamson, C. L., Valdez, G., Guo, W. and Hsu, S. C. (2004). The mammalian exocyst, a complex required for exocytosis, inhibits tubulin polymerization. *J. Biol. Chem.* **279**, 35958–35966.

Wang, G., Krishnamurthy, K. and Bieberich, E. (2009). Regulation of primary cilia formation by ceramide. *J. Lipid Res.* **50**, 2103–2110.

Wang, P. Y., Lin, W. C., Tsai, Y. C., Cheng, M. L., Lin, Y. H., Tseng, S. H., Chakraborty, A. and Pai, L. M. (2015). Regulation of CTP synthase filament formation during DNA endoreplication in Drosophila. *Genetics*.

Wang, H., Qiu, Z., Xu, Z., Chen, S. J., Luo, J., Wang, X. and Chen, J. (2018). aPKC is a key polarity determinant in coordinating the function of three distinct cell polarities during collective migration. *Dev.* **145**,.

Wang, B., Stanford, K. R. and Kundu, M. (2020). ER-to-Golgi Trafficking and Its Implication in Neurological Diseases. *Cells* **9**, 408.

Weng, M. and Zalkin, H. (1987). *Structural Role for a Conserved Region in the CTP Synthetase Glutamine Amide Transfer Domaint*.

Wheway, G., Nazlamova, L. and Hancock, J. T. (2018). Signaling through the primary cilium. *Front. Cell Dev. Biol.* **6**, 8.

Whyte, J. R. C. and Munro, S. (2002). Vesicle tethering complexes in membrane traffic. *J. Cell Sci.*

Wolfrum, U. and Schmitt, A. (2000). Rhodopsin transport in the membrane of the connecting cilium of mammalian photoreceptor cells. *Cell Motil. Cytoskeleton*.

Wu, B. and Guo, W. (2015). The exocyst at a glance. *J. Cell Sci.* **128**, 2957–2964.

Wu, S., Mehta, S. Q., Pichaud, F., Bellen, H. J. and Quiocho, F. a (2005). Sec15 interacts with Rab11 via a novel domain and affects Rab11 localization in vivo. *Nat. Struct. Mol. Biol.* **12**, 879–85.

Yamashita, M., Kurokawa, K., Sato, Y., Yamagata, A., Mimura, H., Yoshikawa, A., Sato, K., Nakano, A. and Fukai, S. (2010). Structural basis for the Rho- and phosphoinositide-dependent localization of the exocyst subunit Sec3. *Nat. Struct. Mol. Biol.* **17**, 180–186.

Yu, I.-M. and Hughson, F. M. (2010). Tethering Factors as Organizers of Intracellular Vesicular Traffic. *Annu. Rev. Cell Dev. Biol* **26**, 137–156.

Yue, P., Zhang, Y., Mei, K., Wang, S., Lesigang, J., Zhu, Y., Dong, G. and Guo, W. (2017). Sec3 promotes the initial binary t-SNARE complex assembly and membrane fusion. *Nat. Commun.* **8**, 1–12.

Zago, G., Biondini, M., Camonis, J. and Parrini, M. C. (2019). A family affair: A Ral-exocyst-centered network links Ras, Rac, Rho signaling to control cell migration. *Small GTPases* **10**, 323–330.

Zhang, X., Wang, P., Gangar, A., Zhang, J., Brennwald, P., TerBush, D. and Guo, W. (2005). Lethal giant larvae proteins interact with the exocyst complex and are involved in polarized exocytosis. *J. Cell Biol.* **170**, 273–283.

Zhang, J., Hulme, L. and Liu, J.-L. (2014). Asymmetric inheritance of cytoophidia in Schizosaccharomyces pombe. *Biol. Open* **3**, 1092–7.

Zhang, C., Brown, M. Q., Ven, W. van de, Zhang, Z.-M., Wu, B., Young, M. C., Synek, L., Borchardt, D., Harrison, R., Pan, S., et al. (2015). Endosidin2

targets conserved exocyst complex subunit EXO70 to inhibit exocytosis. *Proc. Natl. Acad. Sci.* 201521248.

Zhang, L., Zhai, J., Wang, L., Huang, Z., Hu, J., Li, L., Zhang, J., Tang, H., Yang, M. and Wu, Y. (2020). The value of anti-rods and rings antibodies in Western China population: A retrospective study. *Scand. J. Immunol.*

Zhao, Y., Liu, J., Yang, C., Capraro, B. R., Baumgart, T., Bradley, R. P., Ramakrishnan, N., Xu, X., Radhakrishnan, R., Svitkina, T., et al. (2013). Exo70 generates membrane curvature for morphogenesis and cell migration. *Dev. Cell* **26**, 266–278.

Zihni, C., Mills, C., Matter, K. and Balda, M. S. (2016). Tight junctions: From simple barriers to multifunctional molecular gates. *Nat. Rev. Mol. Cell Biol.*

Zuo, X., Zhang, J., Zhang, Y., Hsu, S. C., Zhou, D. and Guo, W. (2006). Exo70 interacts with the Arp2/3 complex and regulates cell migration. *Nat. Cell Biol.* **8**, 1383–1388.

Zuo, X., Guo, W. and Lipschutz, J. H. (2009). The exocyst protein Sec10 is necessary for primary ciliogenesis and cystogenesis in vitro. *Mol. Biol. Cell* **20**, 2522–2529.